Thermal and material characterisation of coated lightweight disc brake rotor

Jafar Hussain

Submitted in accordance with the requirements for the degree of Doctor of Philosophy

The University of Leeds
School of Mechanical Engineering

April, 2018

.

The candidate confirms that the work submitted is his/her own and that appropriate credit has been given where reference has been made to the work of others.

This copy has been supplied on the understanding that it is copyright material and that no quotation from the thesis may be published without proper acknowledgement.

The right of Jafar Hussain to be identified as Author of this work has been asserted by him in accordance with the Copyright, Designs and Patents Act 1988.

© 2018 The University of Leeds and Jafar Hussain

Acknowledgements

First and foremost, all praise be to Almighty God, Who gave me strength and ability to undertake this project. Without His blessings, this achievement would not have been possible.

I would like to thank my supervisors, *Prof. David C. Barton* and *Dr. Peter C. Brooks*, for their support, devotion, encouragement, and guidance during my thesis and the preparation of this thesis. I am also indebted to the technical staffs, Mr. Tony Weise and Mr. Graham Brown for their technical and laboratory support. I am also grateful for the help and support from the colleagues in Room 535 research office.

I am very grateful to *University of Engineering and Technology (Lahore)* for the financial support and study leave. I wish to acknowledge all my colleagues at University of Engineering and Technology for encouraging me for higher studies.

Specials thanks to my parents *Mr. & Mrs. Riaz Hussain* for their tiring efforts to educate me. Without their help and prayers, I would not have done it. My siblings *Azhaar Hussain*, *Afkar Hussain, Sajida Naseer* and late *Bushra Fatima* helped me to their best in times of need.

I would especially like to mention my lovely daughter *Hajra Sabaha* for making my stay in Leeds beautiful.

Last but not the least, I would also like to show my deepest appreciation to my wife *Muflaha Jafar* for her patience, encouragement and moral support during this period.

Thanks to everyone that keep me smile and happy throughout my period of study in Leeds.

Abstract

Environmental concerns linked to CO_2 emissions have placed the automotive industry under considerable pressure to reduce the carbon footprint of the vehicles that they produce. One way forward involves the use of alternative lightweight materials. The use of aluminium alloy in a brake rotor has the potential to save around 20kg in unsprung mass on a medium sized passenger car. A full scale prototype lightweight coated ventilated aluminium alloy (6082) brake rotor was manufactured to investigate the thermal performance under drag brake test conditions. The brake rotor's rubbing surface was coated with alumina layer using a plasma electrolytic oxidation (PEO) process. The ventilated brake rotor geometry contributes to the ability of the structure to dissipate heat through the inclusion of an array of appropriately configured vents and so has further bearing on the ability of the rotor to run cool. It is also feasible to explore the impact of vane design on the cooling of the rotor since the vented section of the rotor can be easily reconfigured using the current prototype. Experiments were conducted using a brake dynamometer. Brake rotor rubbing surface temperature, hydraulic pressure, rotational speed and brake torque were monitored during the test. The coefficient of friction was found to be around 0.5. Abaqus software was used to generate a three dimensional finite element model of a section of the coated brake rotor. The simulation results were found to be in good agreement with the experimental results when a heat transfer coefficient of 30 W/m^2K was specified on all free surfaces. It was shown that coating thickness has a minimum effect on the substrate temperature. In parallel, a wear analysis has also been carried out using a pin-on-disc experimental setup. The mass of the friction material and the small discs were measured before and after the test. The wear coefficient for both conventional grey cast iron (GCI) and coated aluminium alloy were also measured and compared. It was found that wear rate of the PEO coated disc is about 15 times lower than the GCI. The wear rate of the friction material when run against the PEO coating was about 5 times less than when the same material was run against cast iron, even though the friction coefficient was on average higher (0.6 of 0.5)

KEYWORDS: Lightweight disc brake rotor, Plasma Electrolytic Oxidation (PEO) process**,** Dynamometer Test, Wear coefficient.

Table of Contents

List of Figures

List of Tables

Abbreviations

3D	Three-dimensional
Al	Aluminium
AMC	Aluminium matrix composite
CAE	Computer aided engineering
CFD	Computational fluid dynamics
CO_2	Carbon dioxide
CoF	Coefficient of Friction
CP	Circular pillar
DECC	Department of energy and climate change
DP	Diamond pillar
EU	European Union
FE	Finite element
FEM	Finite element model
GCI	Grey cast iron
GUI	Graphical user interface
HC	Hydrocarbon
MMC	Metal matrix composite
MPC	Multi point constraint
MSS	Mesh sensitivity study
MTR	Modified taper radial
NaCl	Sodium chloride
NO_X	Nitrix oxide
NVH	Noise Vibration Harshness

OD	Oxygen diffused
PoD	Pin-on-disc
PEO	Plasma electrolytic oxidation
SAE	Society of automotive engineers
SEM	Scanning electron microscope
SMMT	Society of motor manufacturers and traders
SSTR	Single stop temperature rise

Chapter 1
Introduction

1.1 Background

Automobile braking systems provides the means of either to decelerate the vehicle or completely stop it. The kinetic energy of a moving vehicle is converted to heat energy using the friction force between the brake pads and the brake rotor. The most common material used for the rotor in a disc brake system is grey cast iron and is one of the factors contributing towards higher fuel consumption of the vehicle due to its high density. Researchers have been working on different lightweight materials for brake rotors that can be used as an alternative to conventional grey cast iron for many years.

In recent years, the idea of using aluminium as an alternative brake rotor material has become popular. The main problems associated with aluminium is its lower maximum operating temperature and high wear rate. The maximum operating temperature is the maximum temperature until which the braking system maintains its lower acceptable performance during braking event.

To address these issues, a coated ventilated aluminium alloy brake rotor is required. Plasma electrolytic oxidation (PEO) coating process gives the highest wear resistance as compared to other coating techniques (Yerokhin et al., 1999). Also, the substrate's surface is converted to alumina (oxide layer) during the process instead of deposition of a foreign material which provides a good adhesion strength. A vented disc brake rotor enhances the brake performance by giving rise to rapid cooling of the rotor (Chi, 2008).

In the current study, experimental and numerical analysis was carried for determining the thermal and tribology performance of a full scale PEO coated ventilated Al-6082 alloy brake rotor. A pin-on-disc (PoD) experimental setup was also used to compare the wear rate of coated Al-6082 and grey cast iron while running against the same friction material.

1.2 Motivation for research

Ever growing industrialization and population and changing life styles have increased global energy consumption which has become a major environmental issue. To counteract the problem of environmental deterioration, research has been going on for developing new technologies (use of clean energy resources i.e. renewable energy resources) and besides that the most important task is to make the existing technologies more efficient than ever before.

According to the report of DECC (2012), in UK 13.4% of total CO_2 emission exhausted to the environmental came from cars and total contribution of all kinds of road traffic vehicles towards CO_2 emission was 24.6%. Figure 1-1 shows the overall distribution of CO_2 emission from different sources in UK:

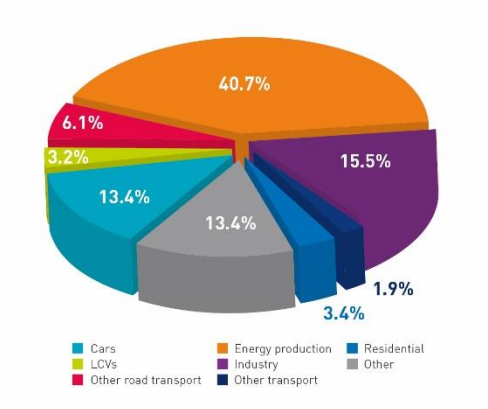

Figure 1-1: CO_2 emission from different sources in UK (DECC, 2012)

In order to reduce the CO_2 emission from automobiles, EU has been working on setting up the mandatory targets for the automobile manufacturers. For instance, the goal of one of the legislation being imposed is to further reduce the fleet average of 130 grams of CO_2 per kilometre achieved by 2015 and the ultimate goal is to reach an average value of 95 g/km by 2020 (EU, 2009)(EU, 2014).

Figure 1-2 shows EU targets for CO_2 emission for year 2007 to 2013.

Figure 1-2: EU targets for CO_2 emission (SMMT, 2014)

Under such circumstance, the focus of the current research is to investigate the use of lightweight materials such as aluminium in braking application in order to enhance the fuel efficiency to a level to achieve EU targets.

1.3 Research aim and objectives

The main aim of the research is to investigate the thermal performance of a full scale lightweight coated ventilated aluminium alloy (Al-6082) brake rotor along with the analysis of friction and wear. The main objectives of the research are outlined below:

1. To design and manufacture a prototype of a full scale coated ventilated brake rotor.
2. To carry out the wear and friction analysis using a pin-on-disc experimental setup for both grey cast iron and PEO coated aluminium alloy discs.
3. Setting up the brake dynamometer and to carry out experiments according to a pre-determined test matrix to access the thermal performance of the brake rotor.
4. To develop a three dimensional (3D) finite element model of the brake rotor using Abaqus software and to validate it against the experimental results.
5. To simulate the effect of different parameters on the performance of the disc brake.

1.4 Research Contributions

This thesis focuses on thermal and material characterisation of a lightweight PEO coated aluminium alloy brake rotor. The research aims at contributing towards finding the possibilities of using lightweight materials in automobile braking industry. Following contributions can be drawn from the overall findings of the research:

1. A novel method of coating only the rubbing surface of a brake rotor thus using uncoated surfaces to rapidly dissipate the heat to the surroundings.
2. Validation of a finite element model of PEO coated aluminium alloy brake rotor.
3. Coating thickness has almost no effect on the temperature of the substrate.
4. Lower wear rate of PEO coated aluminium discs indicative of lower non-exhaust vehicle emissions.
5. Coefficient of friction values are more stable than conventional brake rotor material under drag brake conditions.

1.5 Thesis structure

The rest of the thesis contains further six chapters and each of them are summarised below:

Chapter 2 presents a literature review on various disc brake systems, mechanical and thermal properties of conventional and lightweight rotor materials, geometry of rotors, coating technologies, experimental and thermal modelling techniques to evaluate the performance of disc brake system. Wear and corrosion test techniques are also discussed.

Chapter 3 describes the wear and friction behaviour of small rotating disc samples of coated aluminium and grey cast iron using a pin-on-disc experimental setup. The wear rate of both types of disc material that is grey cast iron and PEO coated aluminium alloy disc are presented and compared.

Chapter 4 presents the design of a prototype full scale PEO coated disc brake rotor. The prototype consist of three components namely inboard cheek, outboard cheek and inner ventilation ring. The procedure for preparing the disc for PEO coating is described. This chapter also discusses the development of 3D finite element model along with the mesh sensitivity analysis to determine the optimum number of finite elements.

Chapter 5 describes the experimental setup of the brake dynamometer in view of the developed test matrix according to SAE standards. The details of different equipment calibration are also presented. The experimental results and numerical results are compared to validate the finite element model.

Chapter 6 discusses the key finding of the research.

Chapter 7 presents the overall results from the experiments, numerical and wear analysis. Also, recommendations for future work are outlined in this chapter.

Chapter 2
Literature Review

2.1 Development of vehicle brakes

Conventional braking systems have undergone considerable development since their first appearance on horse driven carts through to modern car. Vehicle braking systems can be classified into different types as listed below:

1. Wagon brakes (Wooden block brakes)
2. Band Brakes
3. Drum brakes
4. Disc brakes

Wagon brakes are the oldest known vehicle brake design. They work by generating a friction force that acts on the circumference of the road wheel. A wooden block presses onto the tread of the wheel using the simple lever mechanism as shown in Figure 2-1. The driver of the wagon pulls the lever towards him to actuate the brake.

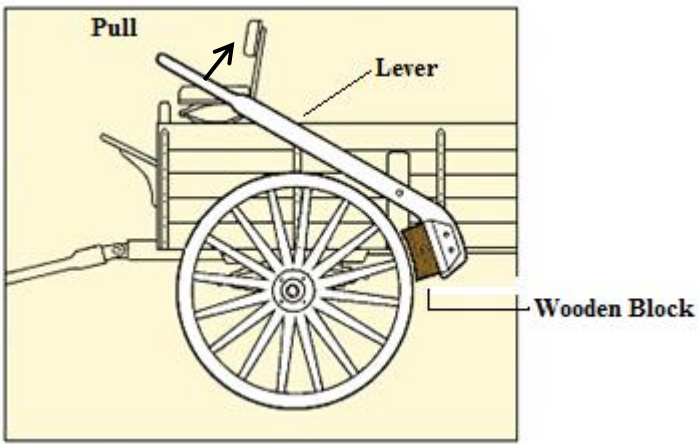

Figure 2-1: Wagon brake (Online Art. Britannica Student Encyclopædia, 2014)

Major changes began to occur with the advent of mechanically powered vehicles. In some early powered vehicles, band brakes were used. These are simple and

inexpensive brakes that work by pulling a band or rope around the wheel of the vehicle (Orthwein, 2004) as shown in Figure 2-2.

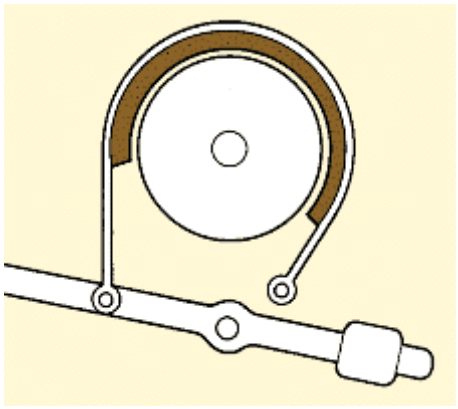

Figure 2-2: Band brake (Online Art, Britannica Student Encyclopædia, 2014)

Major development in the braking industry started at the end of 19th century when Mercedes and Renault in 1903 brought forward a new type of brake known as a drum brake (Newcomb and Spurr, 1989). In this type of brake, a brake drum was attached to the road wheel with static shoe brakes interacting with the drum inner or outer surface to apply braking. A simple drum brake is shown in Figure 2.3:

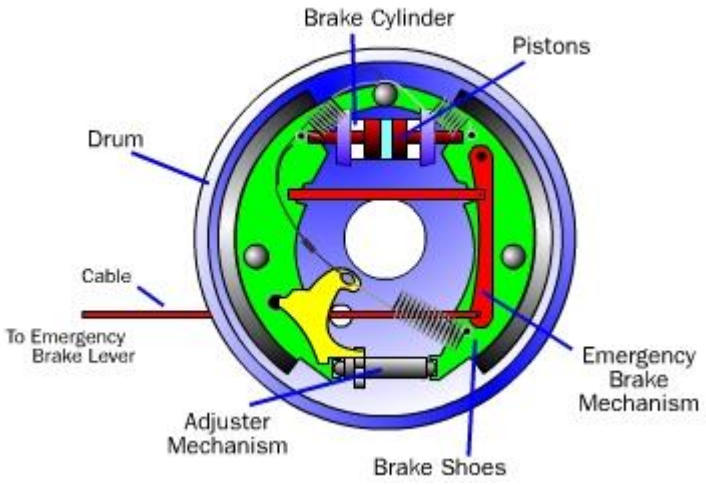

Figure 2-3: Drum brake (http://auto.howstuffworks.com/auto-parts/brakes/brake-types/drum-brake1.htm)

In the same period a British engineer Frederick William Lanchester (Lanchester, 1902) invented and patented a disc brake, which consisted of a metal disc placed within a pair of brake pads and these pads were pressed against the disc in order

to slow down the vehicle (Kinkaid et al., 2003). This simple brake disc system is shown in Figure 2-4:

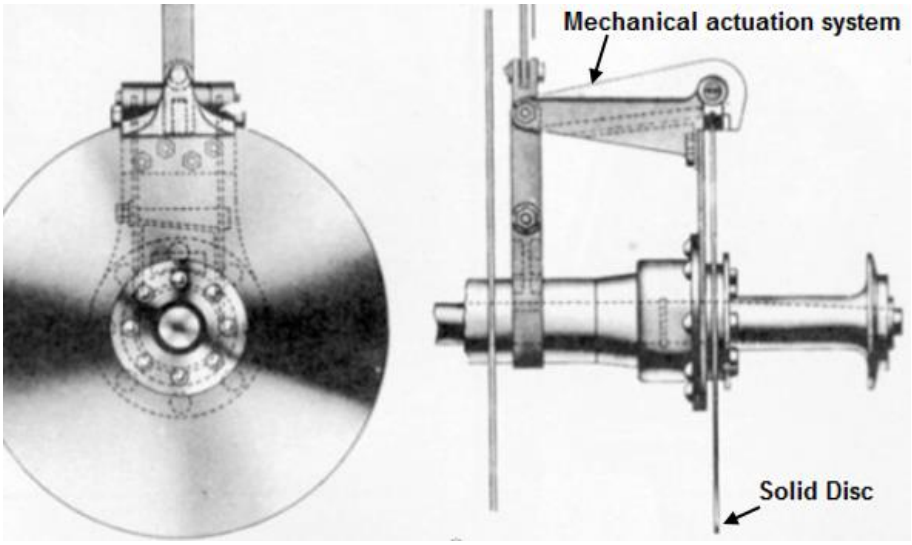

Figure 2-4: Lanchester's disc brake system (www.locarsos.com)

Brake types can be classified in a number of ways according to their configuration, design, material etc. but the most basic classification is shown in Figure 2-5.

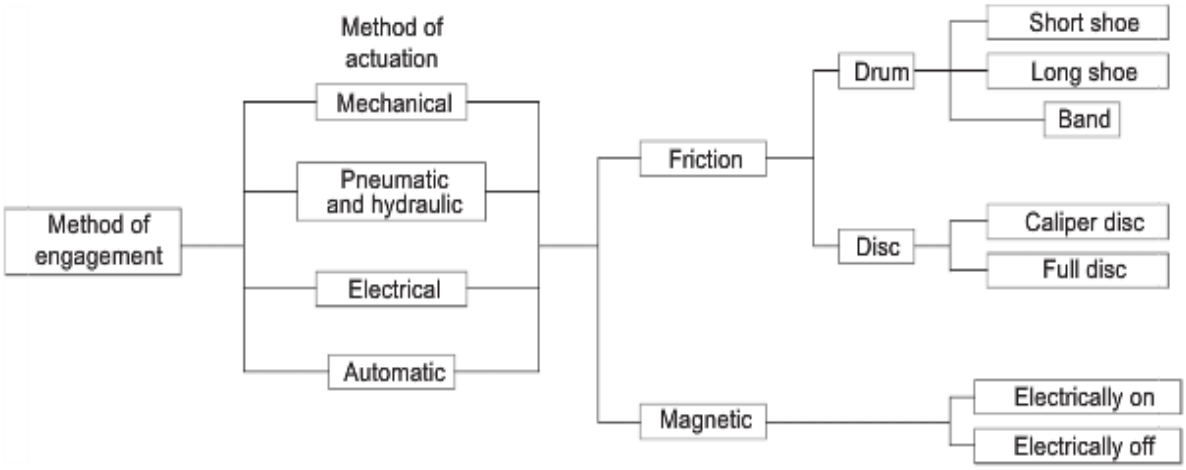

Figure 2-5: Classification of Brakes (Child, 2014)

2.2 Automotive applications

Table 2-1 lists and compares different type of brake designs on the basis of their brake performance and application:

Type of brake	Maximum operating temperat-ure	Brake factor	Stability	Dryness	Dust and dirt	Typical applications
Band Brakes	Low	High	Low	Unstable but still effective	Good	Winches, hoist, excavators, tractors
External drum brake (leading trailing edge)	Low	Medium	Medium	Unstable if humid, poor if wet	Good	Mills, elevators, winders
Internal drum brake (leading trailing edge)	Higher than external brake	Medium	Medium	Unstable if humid, ineffective if wet	Good if sealed	Vehicle (rear axles on passenger cars)
Internal drum brake (two leading shoes)	Higher than external brake	High	Low	Unstable if humid, ineffective if wet	Good if sealed	Vehicle (rear axles on passenger cars)
Internal drum brake (duo-servo)	Low	High	Low	Unstable if humid, ineffective if wet	Good if sealed	Vehicle (rear axles on passenger cars)
Caliper disc brake (Spot-type)	High	Low	High	Good	Poor	Vehicle and industrial machinery
Full disc brake (Clutch type)	High	Low	High	Good	Poor	Machine tools and r industrial machinery

Table 2-1: Brake performance comparison of different brake designs (Child, 2014)

Over the years, the vehicle brake system has undergone a lot of development. Starting with the simplest band brakes, the most recent sophisticated design of disc brakes are emerging because of using new technologies for better performance and higher standards and regulations being enforced throughout the world. For instance, before the 1970s, front wheel drum brakes were used on most vehicles running in the United States of America. Manufacturers had to replace front wheel drum brakes with disc brakes due to change in standards on brake fade, stopping distance and water resistance imposed by the the Federal Motor Vehicle Safety Standard (FMVSS No. 105, 1968 & 1976) (Kinkaid et al., 2003). The disc brake offers good fade performance and better water resistance capabilities (Halderman, et Al., 2000). Also, about 70-80 % of the braking torque is required on the front axle which makes the front wheel brake design more critical in order to satisfy FMVSS No. 105.

2.3 Brake rotor geometry

The brake rotor is an essential component of a disc brake system. Designing a rotor requires many knowledge and understanding. Besides the material properties of the rotor, geometry of rotor also has a marked effect on the performance. Curry (2012) suggested that efficient brake rotor geometry should provide:

1. Assistance in rapid cooling of the rotor
2. Ease in manufacturing
3. Reduction in cost and weight

Table 2-2 shows the performance of different rotor geometries on the basis of the single stop temperature rise (SSTR) but this should not be taken as the only criteria for designing a new rotor.

Rotor	SSTR (˚C)
Solid Disc	550
Vented Disc	600-650
Drum	350-400

Table 2-2: Single stop temperature rise for different types of cast iron rotors (Curry, 2012)

2.3.1 Solid disc rotor

A solid disc rotor has the simplest rotor geometry with both rubbing surfaces machined finished. This design is well suited for lightweight automobiles. They can't be used on heavy cars because they are less efficient in cooling the rotor as compared to vented discs. Sometimes vents are drilled through the rotor for increasing heat dissipation capability but drilling should be done carefully because such holes can reduce the frictional area and may induce cracks (Hendrickson and Burger, 2001). Figure 2-6 shows a simple solid disc brake rotor.

Figure 2-6: Solid brake Disc (Chi, 2008)

Vented discs are heavier and thicker than the solid discs and openings are provided for the flow of air through the rotors as shown in Figure 2-7. They dissipate more heat due to the higher surface area of the rotor and vanes are designed in such a way to maximise the air flow through them.

Figure 2-7: Pillar and vane type vented brake disc rotors (Chi, 2008)

Rotor vanes have different configurations according to vehicle applications and braking performance enhanced with rapid cooling of a rotor is the main factor that influence the vane design. Table 2-3 indicates some rotor design and their applications.

Rotor Vane Design	Applications
Straight, Radial or Non-Curved Rotors (Pillar or Variable vanes)	Passenger cars, Lighter in weight than curved vane rotors
Curved Rotor Vanes (Variable curved or Convergent vanes)	Racing cars, better thermal capacity due to more material and also curved vanes allows more air to flow through the rotor

Table 2-3: Rotor vane designs (http://www.cquence.net, 2012)

Many researchers have studied geometry optimisation of a brake rotor. Chi (2008) investigated the effect of vane number, inner and outer radius, vane angle and vane offset on the thermal performance of a ventilated disc rotor. He revealed that heat transfer rate can be increased by increasing the vane number but at the same time, the vane number need to be optimised as after a certain number, heat transfer rate starts decreasing as shown in Figure 2-8. This is due to the fact that vent area decreases with the addition of vanes and this narrows the air passage through the vents results in a decrease in air velocity and hence heat dissipation.

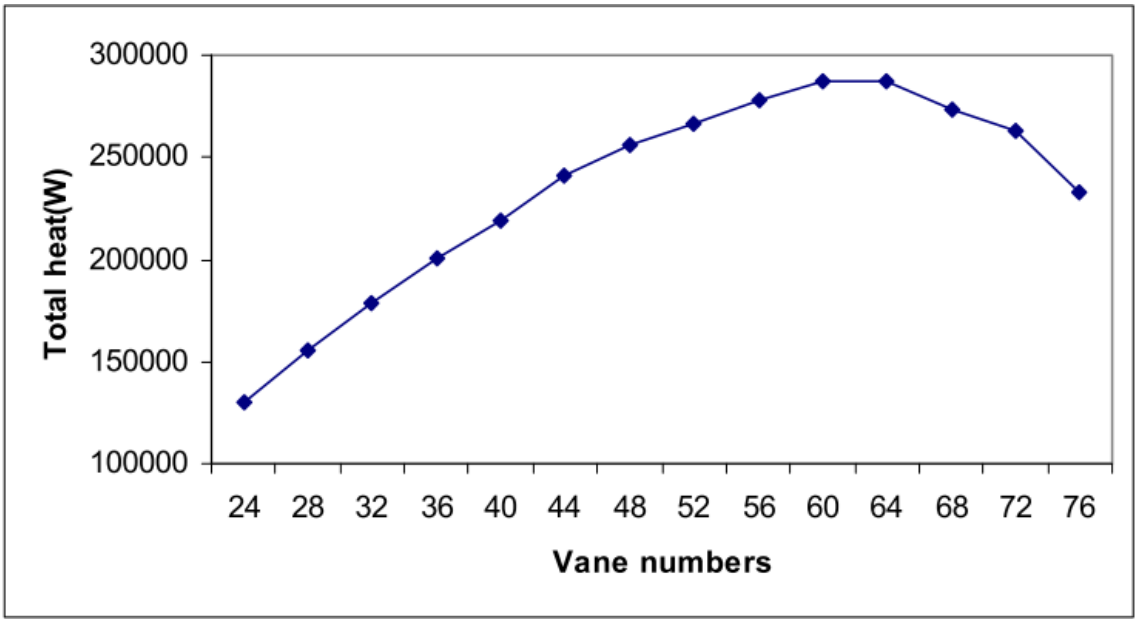

Figure 2-8: Effect of vane number on heat transfer rate (Chi, 2008)

Heat transfer rate was found to vary linearly with change in the inner radius and outer radius of the vented rotor as shown in Figure 2-9. Change in vane angle and vane offset did not show any appreciable effect on heat transfer rate. For the optimised vane numbers, heat transfer rate increases with thickness of the rotor (Chi, 2008).

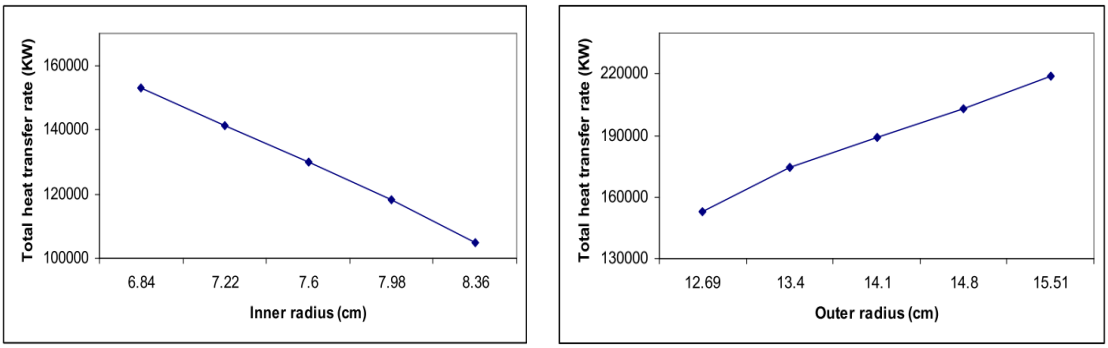

Figure 2-9: Effect of inner & outer radius on total heat transfer rate (Chi, 2008)

Raj et al. (2014) investigated the effect of fluid flow and heat transfer characterisation for three different vane types with the help of computational fluid

dynamics tool, ANSYS CFX 12. The vane types studied were circular pillar (CP), modified taper radial (MTR) and diamond pillar (DP) as shown in Figure 2-10.

Figure 2-10: Circular pillar (CP) vane, modified taper radial (MTR) vane and diamond pillar (DP) vane (Raj et al., 2014)

The simulation results were compared with results available in the literature in order to validate the results. The mass flow rate of MTR vane was around 200 % and 60 % more than CP and DP respectively as MTR vane configuration offered less resistance for the fluid flow. The rate of heat transfer for MTR and CP vane was almost the same because CP has more surface area than MTR vane. DP vane has around 25 % heat transfer rate than the other two vane configurations. Rotors not only failed due to high temperatures but also because of the uneven cooling of rotors. Raj et al. (2014) concluded that CP is the most suitable vane configuration as pressure and velocity distribution in CP is more uniform around the vanes as compared to MTR and DP vane rotors. They also concluded that uniformity in pressure and velocity distribution could be enhanced further by optimising the number and diameter of the CP vanes for further improving the mass flow rate and heat dissipation and they found that a 6 mm diameter CP with 17 vanes would provide better performance by increasing the mass flow rate by 20 % and heat dissipation by 4% as it could have at 8 mm diameter with 12 CP vane brake rotor.

Pyung & Xuan (2010) developed a 3D coupled thermo-mechanical model to study the thermoelastic instability in a vented disc brake. The objective of their work was to study the thermal performance of the ventilated brake disc during single brake application. They found that non-axisymmetric contact pressure results in a non-axisymmetric temperature distribution in the disc. This non

uniform distribution of temperature leads to uneven thermal expansion resulting in non-uniform contact pressure distribution. Initially this behaviour is more pronounced at the start of braking but later on as the heat generation rate decreases with decrease in speed of vehicle, non-axisymmetric temperature distribution shifted to nearly axisymmetric distribution. Higher convection in the vanes and disc conductivity aided in lowering the overall temperature of the disc.

2.4 Brake rotor materials

2.4.1 Physical and thermal properties of brake rotor material

Barton (2012) reviewed different materials for brake rotors and compared the properties of different brake materials. The brake rotor is the rotating part of a brake system and for the best performance of the rotor, the following should be considered before the selection of the materials:

- Stiffness of the rotor (Elasticity)
- Specific heat
- Thermal conductivity
- Maximum operating temperature
- Density
- Wear
- Cost
- Ease of manufacture

During a braking event, the brake rotor undergoes different phenomena which affects its performance for example the rise of temperature leads to the development of thermal cracks, wear, vibration and noise problems and all these problems are linked with material properties (Gigan, 2013). Figure 2-11 shows the dependency of induced thermal cracks, wear and NVH (Noise, Vibration & Harshness) of brakes on different properties of the rotor.

The rotor material must be able to withstand high temperatures (Grieve et al., 1998). Cost effectiveness, reduction in weight and the stability of the rotor must be considered during the selection of the rotor's material (Ioannidis et al., 2005).

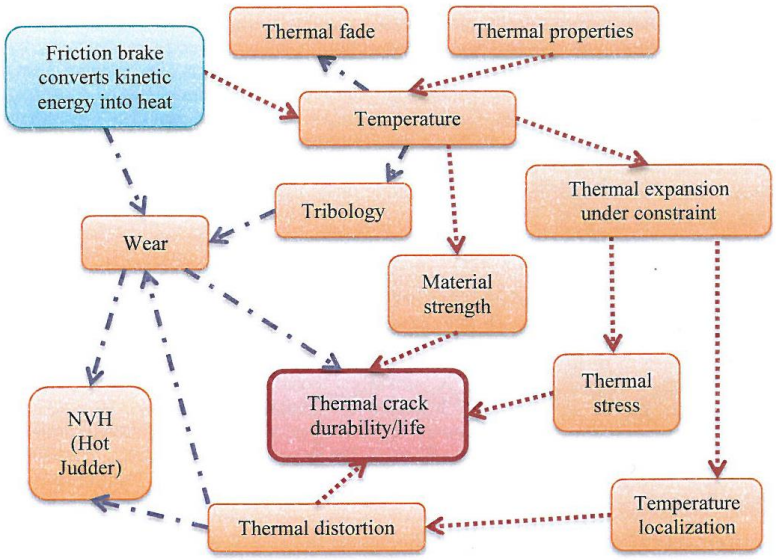

Figure 2-11: Properties of disc rotor responsible for thermal cracks, wear and NVH (Gigan, 2013)

2.4.2 Common braking materials

With the advent of steam locomotives, the initial wooden blocks were replaced with cast iron brake shoes. The major advance in the braking industry started in early 20th century with the development of automobile industry. Grey cast iron was the first material introduced in an automobile braking system as it has good mechanical and thermal properties which are suited for braking operation and most important is the ease with which it can be manufactured. The only drawback of grey cast iron is its high density and nowadays researchers are working on lightweight material for enhancing the vehicle performance in terms of better fuel economy and emission reduction.

Material selection in automobile braking systems depends on a number of mechanical and thermal properties and especially the design and material of rotor should have the ability to quickly absorb and release heat energy and withstand the thermal fatigue during repeated braking events (Jimbo et al. 1990).

During the earlier stages of development of automobiles, it was never easy to start the car with hand crank and on other hand it was never easy to stop it either. As research progressed with time, new technologies were introduced to cater for ease of driving, environmental issues, cost effectiveness and material selection. Today researchers are focusing on lightweight materials for reducing the weight

of vehicles and thereby reducing fuel consumption. However, grey cast iron is the conventional material used in the manufacturing of a brake rotor. The following Table 2-4 shows different materials for brake rotor with their advantages, disadvantages and applications. The table 2-5 below shows properties of commonly used rotor materials.

Material	Advantages	Disadvantages	Applications
Grey Cast Iron (flake graphite iron)	- Cheap - Moderate performance - Good Machinability - Good thermal capacity due to high density - Thermal Conductivity increases as increasing proportions of Carbon - MOT* = 700 °C	- Adds weight to brake assembly and in consequence increases unsprung mass - Adding carbon increases conductivity but tensile strength reduces	Passenger cars
Aluminum Metal Matrix Composite/ Aluminum Alloy	- Affordable - Thermal diffusivity is much higher so lighter rotor can be used - Weight reduction by 60-66% as compared to cast iron	- MOT = 450 °C leads to rapid pad wear	Passenger car
Titanium Alloys	- High temperature resistance - Good resistance to corrosion - Weight reduction by 37% as compared to cast iron	- High wear rate but can be reduced by using Ti composites or thermally coated Ti disks - Low thermal conductivity - Expensive	Passenger car
Carbon-Carbon Composite	- Higher Thermal Conductivity - MOT is high (> 1000) - Low coefficient of thermal expansion, leads to less distortion - Weight savings	- Low density - Low temperature friction problem	Aircraft brakes/ F1** race car
Carbon Ceramic Composite	- High thermal capacity - MOT > 900	- Expensive - Low thermal conductivity	High performance road cars
Stainless Steel	- Good resistance to corrosion	- Expensive - Low thermal conductivity	Motorcycles

Table 2-4: List of brake rotor materials with their advantages and disadvantages (Barton, 2012) (Blau et al., 2007)

*MOT= Maximum Operating Temperature ** F1 = Formula One

	Properties					
Material	**Elastic Modulus (GPA)**	**Density (Kg/m^3)**	**Specific Heat (J/kg.K)**	**Thermal Conductivity (W/m.K)**	**MOT (C)**	**Wear rate ($\times 10^{-6}$ mm^3/Nm)**
Grey Cast Iron	130	7200	649	53	700	2.36
Titanium Alloy	107-122	4420	586	6.6	800	246.3
Titanium Matrix Composite (TMC)	87 - 120	4680	510	8 - 20	-	8.19
Aluminum Alloy	70	2700	895	180	450	-
20% SiC reinforced Aluminum Matrix Composite (AMC)	-	2700	980	-	-	3.25
20% SiC reinforced Al-Cu Alloy	-	2800	920	-	-	2.91
Alumina Coating	212	3030	828	1.6	>1000	-
Carbon-Carbon Composite	-	1750	1000	40-150	>1000	-
Carbon reinforced SiC-Ceramic Matrix composite	-	2300	1000	10	>900	-

Table 2-5: Physical and thermal properties of brake rotor material (Barton, 2012) (Maleque et al., 2010) (Blau et al., 2007) (Alnaqi et al., 2014) (Curran et al., 2005)

It is important to note that different researchers have determined wear rate differently. Some of them defined it as wear mass per unit time (Kg/sec) and others used Archard's equation that can be defined as wear volume per unit load per sliding distance (mm^3/Nm). Wear rate calculated from Archard's equation is also known as specific wear rate or coefficient of wear.

2.4.3 Light weight material

Cueva at al. (2003) investigated the performance of a compact graphite iron (CGI) rotors compared with three different grey iron materials i.e. grey iron grade 250 (GI250), high carbon grey iron (GIHC) and Titanium alloyed grey iron (GI250Ti). They carried out pin-on-disc wear test and concluded that CGI wore more than the other materials under study when applied pressures were higher. Under the same friction force and under small pressures, the wear was almost same for all the grey iron materials.

Maleque et al. (2010) compared the performance of different materials for automotive disk brake rotor using digital logic method of material selection. The materials were selected initially by using Ashby's material selection chart, see Figure 2-12.

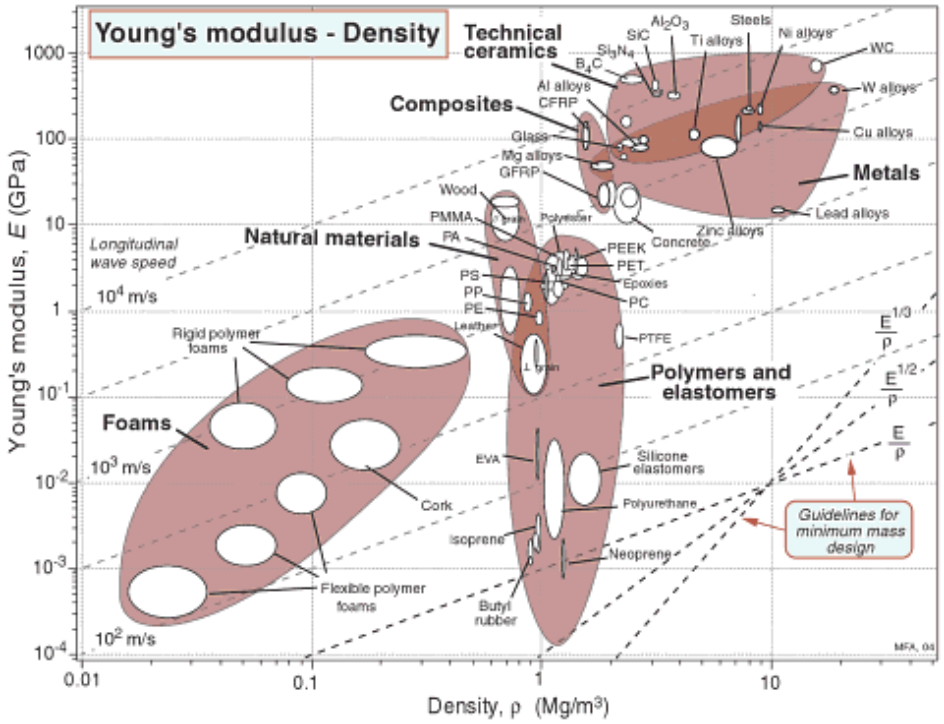

Figure 2-12: Ashby's material selection chart (Ashby, 2005)

Maleque et al. (2010) made material selection on the basis of five important brake rotor properties i.e. compressive strength, wear resistance, coefficient of friction, thermal capacity and specific gravity. Firstly, they evaluated the material performance index for five different materials based on their mechanical properties using the so called digital logic method. In the digital logic method,

certain weightage is given to materials under consideration on the basis of the importance of each material property. This weighting factor is multiplied by the numerical value of the property to evaluate the weighted property value. Then the weighted property values are added for each material to find out the performance index and materials are graded accordingly (Mahmoud, 2006). Maleque et al. (2010) also modified the index using the cost of each individual material. They concluded that aluminium matrix composite (20% SiC reinforced Al-Cu alloy) has the optimum performance followed by the conventional brake material of grey cast iron.

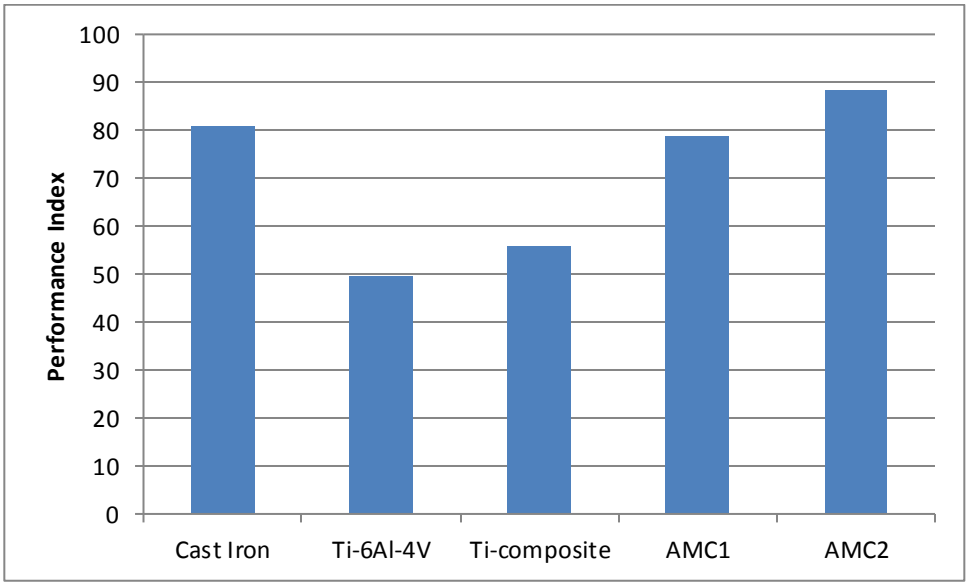

Figure 2-13: Material performance index (Maleque etal., 2010)

Metal matrix composites (MMC) have gained a lot of popularity in engineering structures as studies showed that over the years, there has been a great development in the metallurgy of MMC leading manufacturers towards producing lower cost and lighter weight materials. Adebisi et al., (2011) showed the effectiveness of aluminium matrix composite (AMC) in the field of automobile braking system. They also found that the stir casting technique for MMC production is relatively less expensive as compared to other manufacturing techniques such as squeeze casting, spray deposition, electroplating and electroforming without compromising on the quality. In stir casting, the reinforcement material is added to the molten metal by stirring. There are many

different metals used as the matrix material i.e. aluminium, copper, iron cobalt etc. Figure 2-14 shows a comparison of the relative usage of different metals used as the matrix material in MMC'S. MMCs are reinforced using many different materials to enhance the mechanical properties. The most common material used for aluminium MMCs is SiC as shown in Figure 2-15.

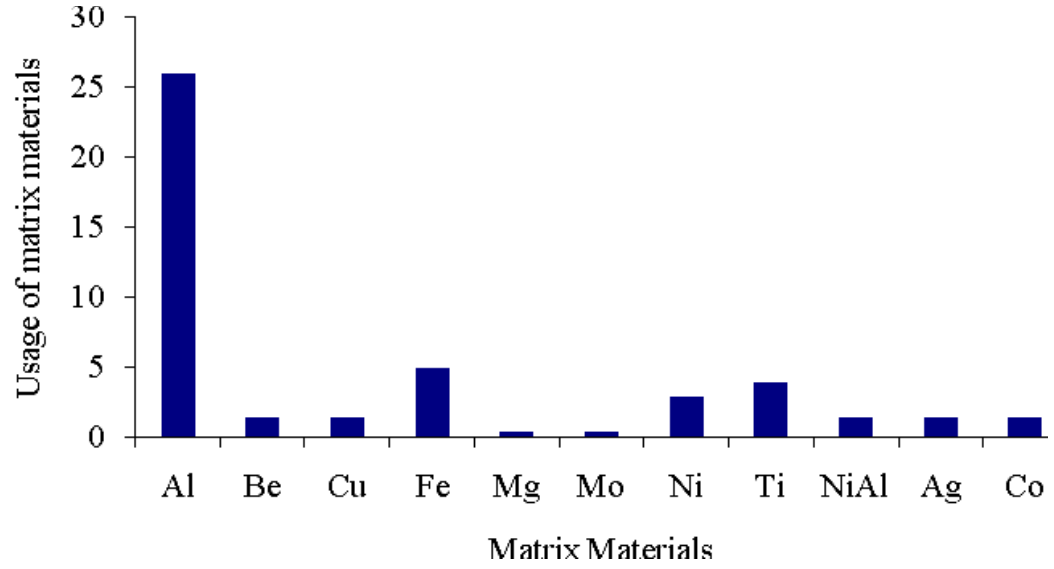

Figure 2-14: Usage of different matrix materials (Adebisi et al., 2011)

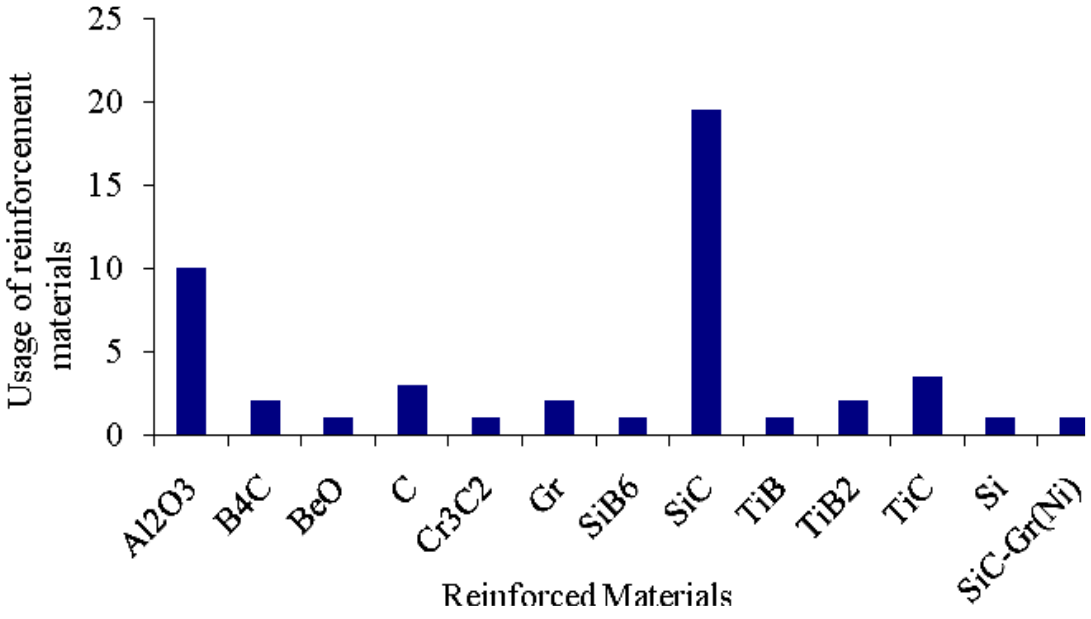

Figure 2-15: MMC reinforcement materials (Adebisi et al., 2011)

Qu et al. (2009) studied the performance of titanium rotors for automobile braking systems. They specifically focused their study on oxygen diffusion (OD) treated titanium (Ti-6Al-4V). They compared the results with titanium metal composites, ceramic particles reinforced and thermally sprayed coated titanium. An oxygen diffused layer on Ti-6Al-4V enhances the hardness and which in turns increases the wear resistance. Qu et al. concluded that OD-Ti has good fade resistance and results showed that friction coefficient remains within 0.35-0.50 under all testing conditions. Wear resistance was 40 times less than Ti based MMCs.

Grey cast iron or steel disc brakes are usually used for normal operating conditions but for high performance vehicles like racing cars, these materials are unable to withstand the high temperatures. A carbon ceramic C/C- SiC composite as alternative disc rotor material performs well at high temperatures and provides friction coefficient almost twice as high as grey cast iron which in turns increases the braking power by a factor of 2 (Kermc et al., 2005).

2.5 Brake pad friction material

The brake pad is the non-rotating part of a braking system and its main function is to rub against the brake disc rotor during braking to retard the vehicle by providing frictional braking force and hence convert kinetic energy into heat energy. Its overall structure and composition are very complex (Nicholson, 1995). Barton identified the key properties that a brake friction material must have in order to give the best performance as follows (Barton, 2012):

1. Should provide high and stable coefficient of friction with the brake rotor
2. Strong enough to withstand mechanical and temperature stresses
3. Lower thermal conductivity to avoid heating of hydraulic fluid which actuates them
4. Should wear enough to ensure smooth contact pressure distribution
5. Should have relatively lower modulus of elasticity so that it can deform accordingly to the thermally deformed rotor surface
6. Should be inexpensive and provide ease of production

In order to achieve the above properties, the brake pad material has to be a composite material and should contain the constituent components mentioned in Table 2-6.

Components	**Properties**	**Materials**
Frictional additives (Abrasive & Lubricants)	Maintains the required frictional coefficient	Lubricant: Graphite, metal sulphides, Metal oxide/silicates
		Abrasives: Zirconium oxide, Zirconium silicate, Aluminum oxide, Chromium oxide
Fillers	Reduces cost and increase manufacturability	Organic: cashew dust, rubber
		Inorganic: Barium sulphate, calcium carbonate, mica, vermiculite
Binder	Firmly binds the constituent of brake pad	Phenolic resin, silicone-modified resins
Reinforcing Fibers	Enhances mechanical strength	Glass, metallic chips, potassium nitrite, ceramic

Table 2-6: Brake pad material constituents (Eriksson et al., 1999) (Chan, 2004)

Figure 2-16 (a) & (b) show a typical composition of brake pad materials presented by different researchers. Mostly manufacturers do not reveal the actual composition of friction material and the figures below only describes the percentage of each generic component in the brake pad (Sasaki et al., 2000) (Hara et al., 2003).

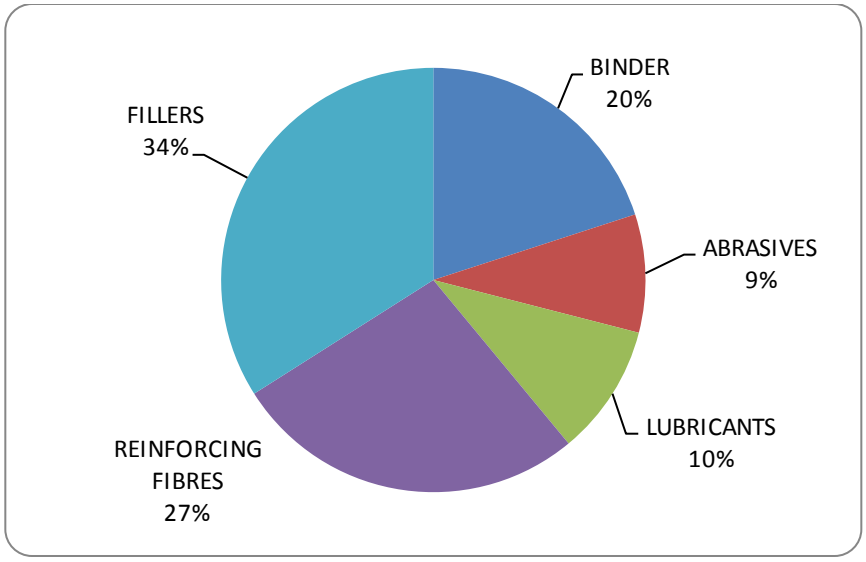

(a)(Sasaki et al., 2000)

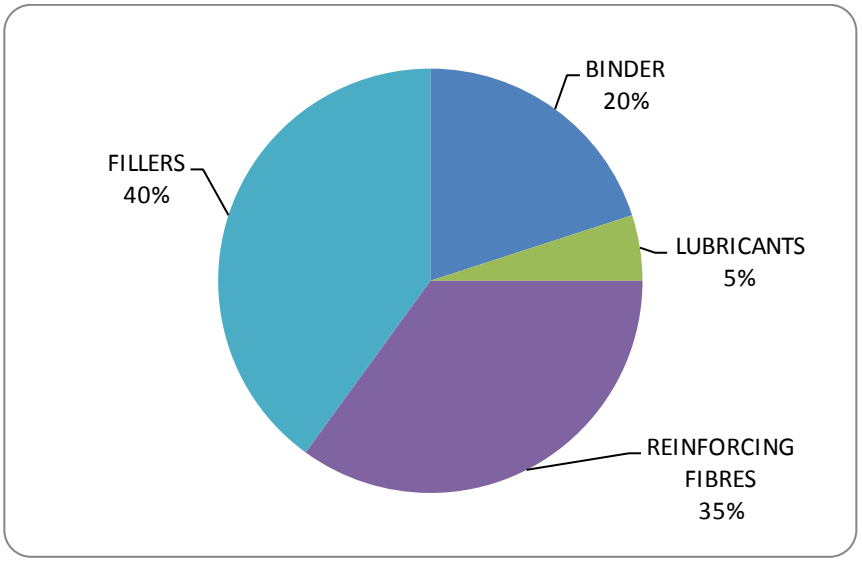

(b) (Hara et al., 2003)

Figure 2-16: Typical friction material compositions

Typical brake pad geometry consists of a friction material, substrate, adhesive, backplate and anti-noise layer. The substrate (sometime present in between pad and backplate) acts as a thermal insulator to avoid excessive flow of heat to the hydraulic fluid. The backplate is used for firmly holding the pad and for even distribution of piston force over the brake pad contact surface (Lee et al., 2003a).

A shim is often added at the back of the backplate to reduce squeal noise. A basic arrangement of the different components of a brake pad is shown in Figure 2-17.

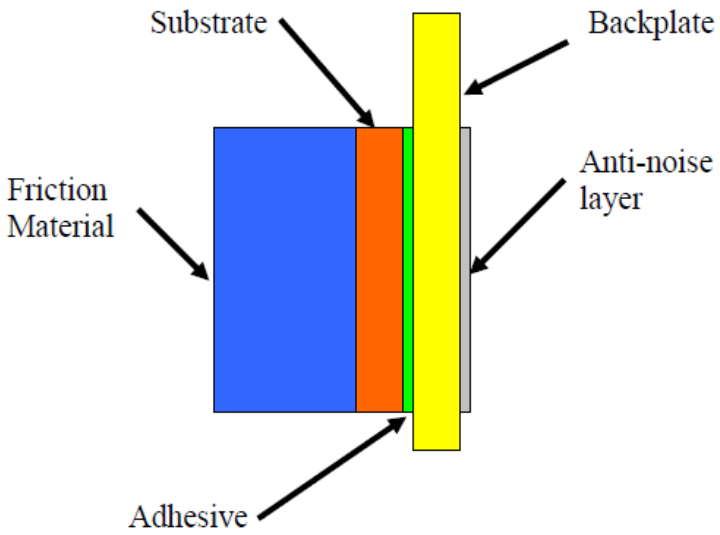

Figure 2-17: Typical disc brake pad (Nicholas, 1995)

Rovere et al. studied the effect of change in geometry of the backplate to further improve its ability to reduce the transmission of vibration produced during braking. They carried out a noise test with the conventional and the modified backplate. They concluded that modified ribbed backplates as shown in Figure 2-18 effectively lower the frequency of noise. The stiffness of the backplate was increased by introducing ribs in the backplate so for the same backplate stiffness, the weight could be reduced (Rovere et al., 2014).

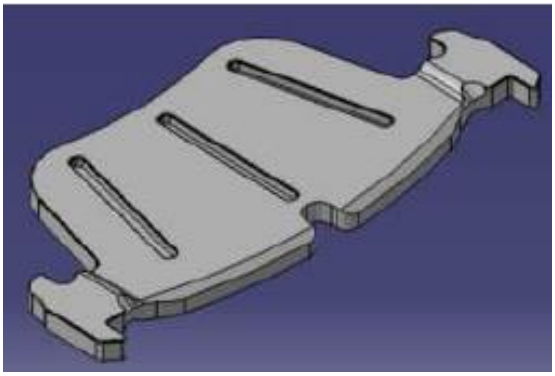

Figure 2-18: Modified ribbed backplate (Rovere et al., 2014)

2.6 Coating technologies

In recent years, automotive engineers and researchers have been focusing on the utilisation of lightweight materials due to the legislation being enforced to reduce the emissions of HC, CO_2 and NO_x from the vehicle exhaust. The conventional material used in brake disc rotor is grey cast iron which could be replaced with a lightweight material to reduce the unsprung mass of the vehicle (Grieve et al., 1998). Barton (2012) has discussed some alternative lightweight material like aluminium metal matrix composites (Al-MMC), carbon-carbon composites and carbon reinforced ceramic matrix composites. Al-MMC provides good strength to weight ratio and also have a good thermal conductivity (Ahmad et al., 2013). Al-MMC has a low maximum operating temperature (450˚C) and under severe braking conditions, temperatures in cast iron brakes may rise to above 800˚C (Jacko, 1978). Higher temperatures during braking leads to decrease in coefficient of friction and increase in wear rate that severely affect the performance of the brake system. In order to improve the thermal performance, coatings can be applied on the disc brake rotor. A well designed coating enhances wear resistance, reduces corrosion and helps in maintaining stable coefficient of friction (Batakis, 1985) (Demir et al., 2009).

Thermal spray coating and plasma electrolytic oxidation (PEO) coating are the most popular coating techniques applied in the automobile industry and details of both types of coating are given below.

2.6.1 Thermal spray coating

In thermal spray coatings, heated particles (molten, semi-molten or solid) are sprayed on the surface to be coated (substrate). Over the years, there has been a lot of development made in spraying techniques and each spraying technique provides a different bond strength, coating thickness and porosity (Pawlowski, 2008). Table 2-7 shows a comparison between various thermal spray coating techniques.

Thermal spray coating is the established coating technology and with time it has gained significant popularity in the automobile industry. For example this coating technology was used for coating of Aluminium or magnesium engine cylinders.

The coating provided better wear resistance and was also found to be very useful in enhancing the performance of the automobile by reducing the fuel consumption by about 2% (Barbezat, 2006).

Thermal Spraying Techniques	**Bond Strength (MPa)**	**Coating Thickness (µm)**	**Porosity (%)**
Flame Spraying	60-70	100 - 2500	10 - 20
Atmospheric Plasma Spraying	- 15-25 for ceramics on metals - 70 for bonding alloys	300 - 1500	1 - 7
Arc Spraying	- 10-30 for Zn & Al coatings - 70 for NiAl or NiCr+SiC	100 - 2000	10 - 20
Detonation-Gun Spraying	70 - 83	< 300	0.5 - 2
High Velocity Oxy-Fuel Spraying	90	100 - 300	< 1
Vacuum Plasma Spraying	> 80	150 - 500	1 - 2
Controlled Atmosphere Plasma Spraying	20 - 45	300 - 2000	1 - 7
Cold Gas Spraying	26-44 for Copper 33-35 for Aluminum	250 - 650	3.7 - 4.5

Table 2-7: Comparison of various thermal spraying coating techniques (Pawlowski, 2008)

Torres et al. investigated the wear resistance capabilities of an Al/$MoSi_2$ composite coating on a 6082 aluminium alloy. They used oxy-acetylene flame thermal spray coating technique. They evaluated the hardness, porosity,

reinforcement rate and wear resistance for as-sprayed coating and after cold pressed coating. Cold pressing was used to reduce the porosity and surface roughness. Results showed that porosity was reduced from 3% to 1% and hardness was increased from 30 HV to 47 HV. Wear rate were determined by using pin-on-disc test at various loads. They concluded that composite Al/$MoSi_2$ coating material offered more or less the same wear resistance when compared with Al/SiC composite coating. The wear rate of the cold pressed coating was found to be higher than the as-sprayed one (Torres et al., 2013).

Demir et al. studied and compared the performance of three cast iron brake rotors. One was tested as it was and the other two were coated. The NiCr-Cr_2C_3 coating was applied to one of them using high velocity oxygen fuel and the second one was coated with Al_2O_3-TiO_2 using plasma spray coating technique. NiCr was used as a bonding layer. An electron micrometre was used to measure thickness and an EP-20KA scale was used for measuring mass before and after the tests. Pads of coated rotors experienced higher temperature than the uncoated rotor. The NiCr-Cr_2C_3 coated rotor showed a 6% increase in coefficient of friction than the uncoated rotor. The Al_2O_3-TiO_2 rotor showed zero wear but higher pad wear occurred due to the thermal barrier effect, higher hardness of the coating and higher temperature. Because of the high temperature and coefficient of friction, wear and thickness variation of the NiCr-Cr_2C_3 coated rotor was found to be higher than the uncoated rotor. Demir et al. also suggested that the Al_2O_3-TiO_2 coated rotor could be the best option in car braking system if a more compatible pad material was found (Demir et al., 2008).

2.6.2 Plasma electrolytic oxidation (PEO) process

PEO processing is one of the surface modification technique which use an electrochemical process. The process involves the growth of an oxide layer on the metal/alloy to be coated by the generation of electric discharge (resulting in plasma) due to the high applied potential difference across two electrodes. PEO coatings are about 20-30 times more expensive than the conventional anodising process (Matykina et al., 2017). Figure 2-19 shows different plasma electrolytic deposition techniques.

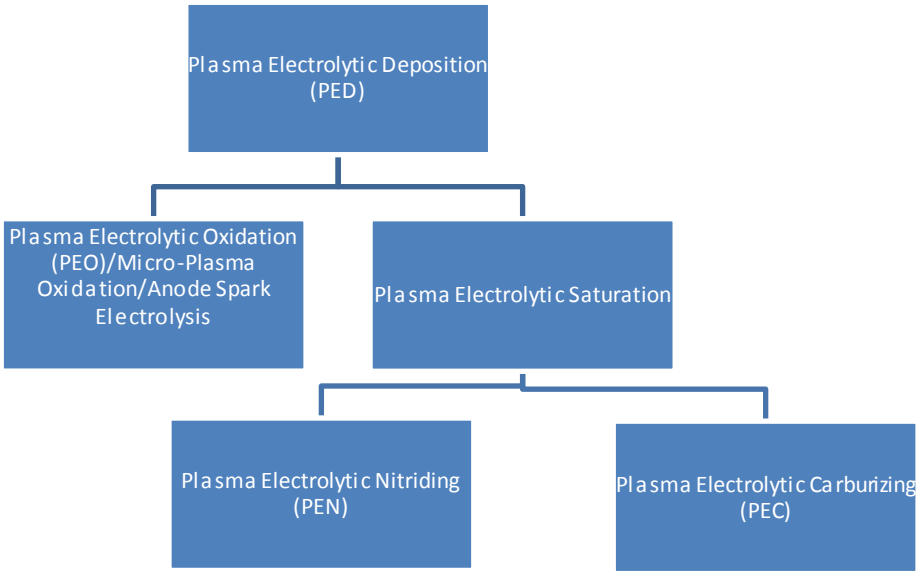

Figure 2-19: Plasma electrolytic deposition coating (Yerokhin et al., 1999)

2.6.2.1 Effect of PEO on mechanical properties

Oxide coating enhances the mechanical properties of the aluminium sheets by 100 to 200 % depending on the thickness of sheet and the depth of the oxide layer. The greater the thickness, the greater will be the adhesion of the oxide layer with the substrate. The process involves the oxidation of the substrate surface forming an alumina layer rather than deposition of any foreign material. It has been found that an adhesion strength of 350 to 380 MPa can be achieved with the oxide layer of 200 to 250 µm thick. (Yerokhin et al., 1999).

2.6.2.2 Effect of PEO on wear rate

Figure 2-20 compares the relative wear resistance (ε_w) for different materials coated using various surface modification techniques. It can be seen that PEO coating techniques offers the higher wear resistance.

Zhang et al. investigated the effect of PEO coating on the wear rate of Al 383/SiO_2. They found that the amount of reinforcement SiO_2 and the thickness of oxide film were the key elements in reducing wear rate (Zhang et al., 2010).

Cui et al. applied PEO coating on SiC_p/A356 composite and found that the specific wear was 14 times lower than the uncoated SiC_p/A356 composite and the test was carried out on a ring-on-ring wear tester (Cui et al., 2007).

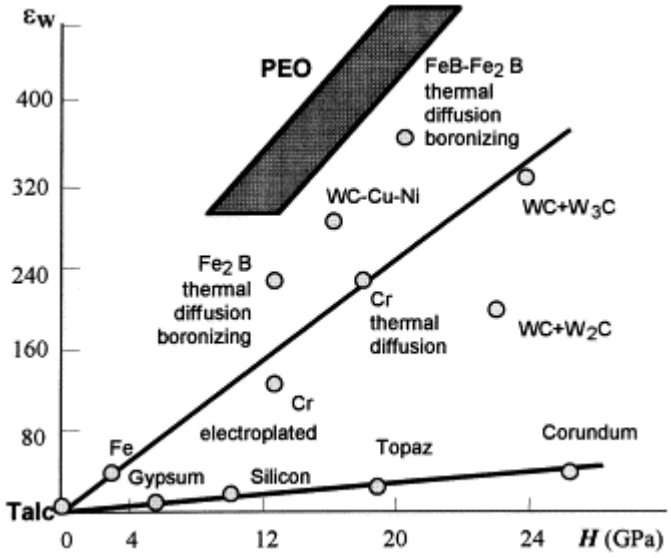

Figure 2-20: Relative wear resistance for various materials w.r.t hardness (Yerokhin et al., 1999)

2.6.2.3 Effect of PEO on Corrosion resistance

Metal matrix composites (MMC) usually have good mechanical properties and wear resistance. However, the presence of reinforcement material reduces the MMC corrosion resistance. Cui et al. investigated the corrosion behaviour of coated SiC_p/A356 and uncoated SiC_p/A356. They carried out salt spray tests and corrosion electrochemical tests. Coated SiC_p/A356 did not show any indication of corrosion until 120 hours had passed but on the other hand, corrosion started to appear on uncoated SiC_p/A356 after only 12 hours (Cui et al., 2007).

They also found that the friction coefficient of coated SiC_p/A356 against bearing steel GCr15 was 0.6 to 0.9 which was higher than for the uncoated SiC_p/A356 (0.38 to 0.5).

2.6.3 Application of PEO process in Automotive Brake Industry

Over the years, many researchers have studied lightweight materials for enhancing vehicle performance and their main focus has been on aluminium as an alternative material to reduce the weight of vehicle. Aluminium metal matrix composite (Al-MMC) and aluminium alloy provides good alternative to conventional higher density materials. They have high thermal conductivity and relative specific heat. However, they do not have good wear resistance and maximum operating conditions are low which limits their application in automobile braking system. The wear resistance and maximum operating temperature can be enhanced by using surface modification technique i.e. applying a hard coating on the alloy or MMC substrate.

Dahm et al. evaluated the roughness and friction performance of two PEO coated aluminium alloy rotor i.e. AA6082 and AA7075. Tests were carried out on a small scale dynamometer. The measured roughness of coated AA6082 was 0.46µm Ra and 0.81µm Ra for coated AA7075. Friction coefficient for coated AA6082 was found to be in the range of 0.3 to 0.33 and for the coated AA7075, it was 0.25 (Dahm et al., 2009).

Alnaqi et al. studied the braking performance of different rotor materials. The different materials analysed were grey cast iron, aluminium alloy, PEO coated aluminium alloy, Al-MMC and PEO coated Al-MMC. They concluded that out of the five rotor materials tested, coated aluminium alloy has shown the most promising results in terms of thermal stability at higher temperatures which was even greater than grey cast iron (Alnaqi et al., 2014).

2.7 Experimental Characterisation of disc brake performance

There are a number of experimental techniques used to explore the different performance parameters of lightweight coated brake rotors, such as: A few of them are listed below:

1. Full scale dynamometer testing
2. Reduced scale dynamometer testing
3. Pin-on-disc testing

Sanders et al. discussed several advantages of reduced scale testing over full scale dynamometer testing and also showed the method of designing a reduced scale dynamometer. They designed a reduced scale dynamometer for measuring the friction coefficient and compared the results obtained with the full scale dynamometer testing. There are many parameters involved in testing. First of all, parameters which are the same irrespective of the scale of the dynamometer testing are listed, for instance sliding velocity, pad pressure etc. On the other hand, scaling relations were developed for other parameters i.e. pad area, effective radius etc. The scaling methodology showed good correlation between the full scale and reduced scale dynamometer results. Small scale testing reduces set up time and cost of testing (Sanders et al., 2001).

Qu et al. performed experiment with a sub-scale brake tester to evaluate the performance of an oxygen diffused titanium rotor using a commercial brake pad. Titanium alloy has good strength, low density and better corrosion resistance. Friction and wear resistance can be enhanced by generation of an oxide layer. They compared the performance of oxygen diffused titanium alloy with untreated titanium, titanium metal matrix composite and thermal spray coated titanium alloy. Oxygen diffused titanium alloy showed stable coefficient of friction as compared to the other materials (Qu et al., 2008).

Alnaqi et al. studied the performance of PEO coated small scale Al-MMC brake rotor. The performance was measured on small as well as large scale dynamometers. All parameters of both dynamometers were controlled by LabView. Tests were carried out in accordance with the test procedure SAE J212 produced by Society of Automotive Engineers (Alnaqi et al., 2014) (SAE, 2000).

Ahmad et al. (2013) investigated the tribology properties of an alumina particle reinforced Al-MMC disc brake rotor. Wear rate was measured by pin-on-disc tests by applying loads of 25, 50, 75, and 100 N at speeds of 500, 750 and 1000 rpm. The same test was also carried out at different speeds while keeping the load constant at 25 N. The disc surface was also examined with scanning electron microscope (SEM).

Cueve et al. (2003) has also used the pin-on-disc wear testing machine for measuring the wear rate of cast iron disc brake rotor and pad. Cyclic pressures of 0.7, 2 and 4 MPa were applied with a constant rotor speed of 500rpm. Temperature was measured with an embedded thermocouple in the pin. Figure 2-21 indicates the pin-on-disc experimental set up.

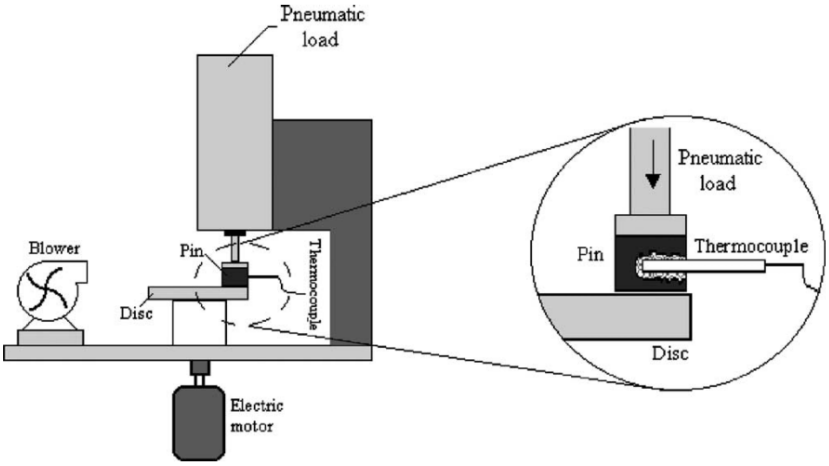

Figure 2-21: Pin-on-disc wear testing machine (Cueve et al., 2003)

Cui et al. developed an experimental set up for evaluating the corrosion and wear resistance of a PEO coated and uncoated SiCp/A356 composite. Salt spray corrosion tests and electrochemical corrosion tests were carried out. In the salt spray test, 5% by weight NaCl solution was sprayed on the composite for 120 hours at 35˚C following the GB/T 10125-1997 standard. 3.5 % by weight NaCl solution was used as electrolytic solution in the electrochemical corrosion test with platinum and saturated calomel as counter and reference electrodes respectively. SiCp/A356 samples (working electrode) were placed inside the electrolytic solution for 1 hour. Both tests revealed that the corrosion resistance capabilities of coated SiCp/A356 were far higher than that of the uncoated

material. On the other hand, wear tests were carried out on a ring-on-ring wear tester. SiCp/A356 and quenched bearing Steel GCr15 were used as lower and counter ring respectively and results are depicted in Figure 2-22 (Cui et al., 2007).

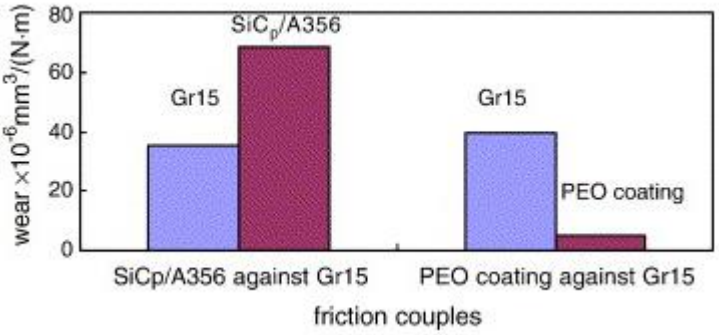

Figure 2-22: Specific wear rate of PEO coated and uncoated SiCp/A356 (Cui et al., 2007)

2.8 Numerical modelling of disc brake performance

Newcomb (1959) developed a one-dimensional thermal model to predict the temperature at the friction surface during uniform deceleration of a vehicle. He also carried out experiments and found that the predicted temperature was 15 % higher than the measured temperature. This was due to the fact that he had not incorporated any heat dissipation in his model. Newcomb (1960) then added the effect of cooling in his model. He also compared the performance of drum brake and disc brake and obtained good agreement in the results. The model could be improved further by adding the effect of radiation.

Yano and Murata investigated the flow of heat from a ventilated rotor during a braking event. Heat dissipation was considered through conduction from pad and disc flange, convective cooling from the both sides of disc rubbing surface, top hat section of the rotor and ventilating sections. They concluded that 70 % of the heat is dissipated to air from the rubbing surface. The ventilation section removes only 10% of heat. They also recommended that changes in ventilation pattern and addition of baffle plates would increase the heat flow through the ventilator section by 20% (Yano and Murata, 1993).

Macphee & Johnson conducted an experimental and analytical study to evaluate the convection of heat through the fins of a ventilated brake rotor. Heat transfer and motion of fluid over the fins of rotor were determined. Internal and external

heat transfer coefficients were measured and compared with the analytical solution. Tests were carried out at three different velocities. At a rotor speed of 342 rpm, the heat dissipation from the internal fin was around 45.5% and this was increased to 55.4% as the rotor speed was increased to 1025 rpm. The heat transfer coefficient varied linearly with the speed of the rotor. Volume flow rate through the fins was also found to hold a liner relationship with rotor speed. They also recommended that a numerical model can be generated to further explore the performance of vehicle (Macphee & Johnson, 2008).

Day et al. used a two dimensional finite element model to investigate the bulk temperature effect (i.e. drum brake expansion and disc brake coning) and the macroscopic thermal effects (i.e. hot spots, cracking). They concluded that uniform pressure distribution across the rotor could minimize above problems (Day et al., 1991).

Grieve et al. developed a three-dimensional finite element model using the ABAQUS simulation software for designing a lightweight disc brake rotor. Maximum temperature was predicted for the two brake tests involving conventional grey cast iron and lightweight Al-MMC. A Taguchi study revealed that cheek thickness, cooling rate and thermal conductivity were the most critical parameters in reducing the peak temperature. Finite element analysis combined with Taguchi study enabled the fast and economical method for optimizing the Al-MMC brake rotors (Grieve et al., 1997).

Chi investigated the effect of vane geometry on the thermal performance of a disc brake rotor. He developed the numerical model using the commercial CFD software packages, Fluent and Gambit, and analysed the model for heat flux rate, velocity of air over and through the vanes, temperature and pressure distribution in brake rotor (Chi, 2008).

2.9 Summary

In this chapter, an extensive literature review has been carried out to develop understanding of an automotive disc brake system. The main focus was to study the advancements being made to date for achieving the aims and objectives of the current project mentioned in this thesis.

It has been observed that automobile researchers are working on lightweight materials for improving the fuel efficiency which in turns also reduce the CO_2 emission. The use of lightweight materials for a disc brake rotor would also reduce the unsprung mass of the vehicle but their effect on the performance of the disc brake has not yet being fully explored.

Aluminium alloy is considered as an alternative rotor material by many researchers. Although it has certain limitations i.e. it has low maximum operating temperature and higher wear rate, its higher thermal conductivity can lead to more rapid cooling if efficiently designed ventilated rotors are used. Studies revealed that brake rotor geometry has a significant effect on the cooling of rotors and around 70% heat dissipation from the surface of brake rotor. The higher wear rate could be minimised by using coating.

The PEO coating technique shows a promising future when applied to aluminium alloy substrate. PEO processed aluminium alloy has been found to be quite promising in enhancing the thermal performance, wear resistance and corrosion resistance. Thus, the overall literature review suggests the opportunity to combine benefits linked with lightweight aluminium alloy and PEO coating along with vented rotor design concept and appropriate friction material formulation to develop novel lightweight brake rotor concept. Alnaqi et al., worked on small scale aluminium alloy brake rotor. There work was consisted of PEO coating of whole small-scale rotor. They indicated the failure of the rotor at elevated temperatures. It was found that full scale ventilated aluminium alloy brake rotor with PEO coating of only the rubbing surface could be a viable solution in both enhancing the thermal performance and reducing the cost of PEO coating.

Chapter 3

Wear and friction analysis using pin-on-disc experimental setup

3.1 Introduction

Pin-on-disc testing is a widely used tool to investigate the friction and wear behaviour of a sliding disc running over a pin cut from the pad friction material. In this chapter, the setup of a pin-on-disc equipment and the measurement of wear rate for the conventional grey cast iron (GCI) and the plasma electrolytic oxidized (PEO) aluminium alloy (Al-6082) when rubbing against a pin of the same friction material are described.

During the real braking event, brake pads come into contact with the brake rotor. Both the brake rotor and brake pads undergo wear due to the frictional sliding. It is very important to measure the wear rate in order to determine the life span of both components of a passenger car brake. Also, the wear rate affects the emissions of particulate matter into the atmosphere.

3.2 Pin-on-disc experiment setup

The pin-on-disc testing is carried out to measure the tribological characteristics such as the tangential friction force and the wear rate. The pin-on-disc test requires two components:

1. Pin – this contains samples of the friction material.
2. Disc – this represents the material of the brake disc.

Figure 3-1 shows a schematic diagram of a pin-on-disc test.

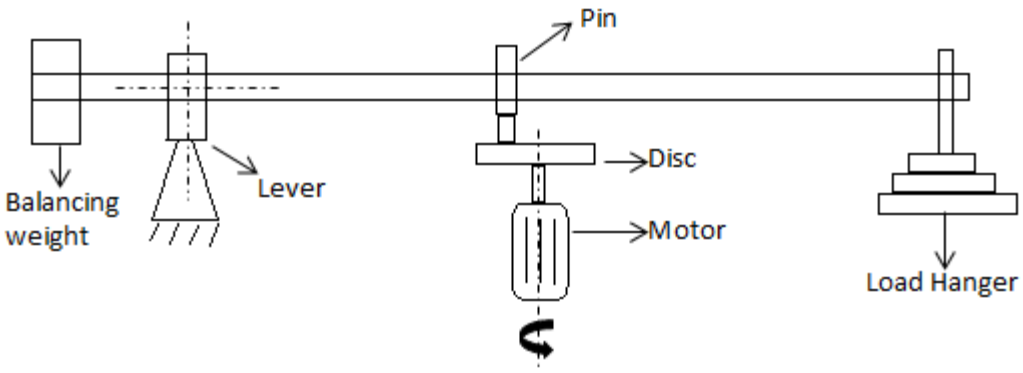

Figure 3-1: A schematic diagram of a pin-on-disc test

Figure 3-2 shows a photograph of the pin-on-disc equipment used for the tests. The load cell can measure up to 49 Newtons of tangential friction force. The maximum rotating speed can be up to 700 rpm. The pin holding the friction material is attached to the pin holder to which a normal load can be applied. The data recorded by the equipment were the mean friction force and rotating speed. Friction material was cut out from the brake pads using a laser cutter. Conventional GCI and PEO coated aluminium alloy discs were used in the experiments with the same friction material supplied by TMD Friction Inc.

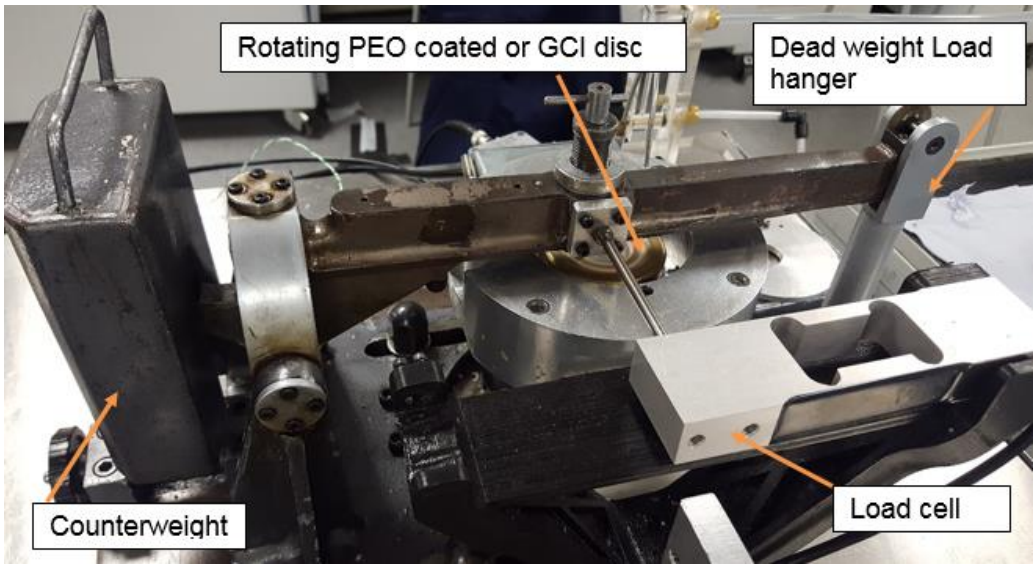

Figure 3-2: Pin-on-Disc Equipment

The normal load on the friction material is applied by adding weight to the hanger attached to one end of the loading beam. Figure 3-3 shows a stationary pin in contact with a rotating PEO aluminium disc.

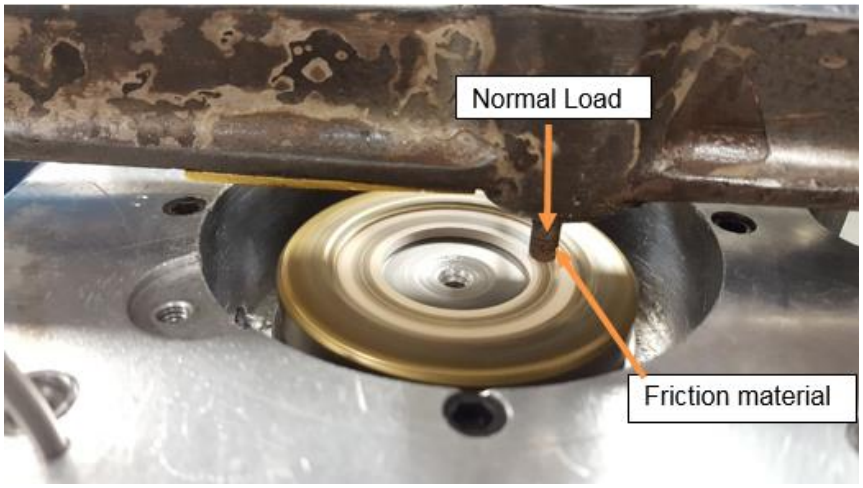

Figure 3-3: Pin-on-Disc testing

Brake pads were provided by the TMD Friction Inc and they were specifically designed to work with alumina coated aluminium alloys. Friction material was cut out from the brake pads using the SYNOVA MCS 300 water-jet guided laser cutter. The water-jet guides the laser beam for the precise cutting of the friction material. In addition to guide the laser beam, the water-jet also helps in keeping the cutting surface at low temperature during cutting and thus avoids the distortion of the sample. This laser cutter has an accuracy of ± 1µm. Each pin is of 5 ±0.1 mm diameter. The dimension of 5 mm is selected to apply a pressure mentioned in Table 3.3. Figure 3-4 shows (a) a laser cut brake pad and (b) the resulting pin which included a section of the steel back plate of the pad.

(a) Brake pad **(b) Pin (Friction material)**

Figure 3-4: Brake pad and laser cut pin

3.3 Pin holder

The pin holder is designed to accommodate the pin. The pin holder firmly holds the pin in order to avoid any failure during the testing. The pin holder and backplate of pin were bonded together using an Araldite rapid epoxy adhesive. Figure 3-5 shows an isometric view of the pin holder and its dimensions respectively.

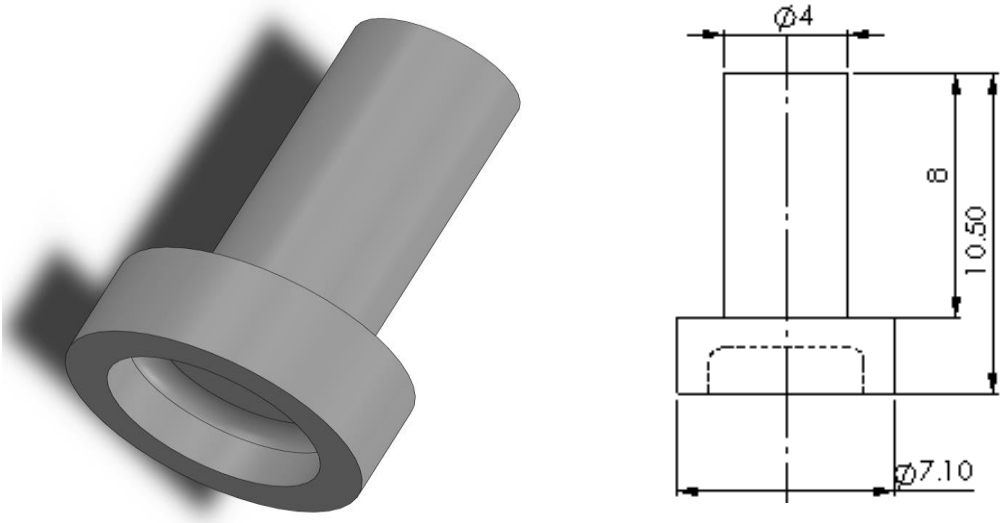

(a) Isometric view **(b) Pin holder dimensions in mm**

Figure 3-5: Pin holder

Figure 3-6 shows the pin holder bonded with the friction material sample ready for sampling.

Figure 3-6: Pin for testing

3.4 Disc for pin-on-disc Testing

Figure 3-7 shows the geometry of the discs used in the pin-on-disc testing. Two different types of disc material were used in the tests:

1. Grey cast iron disc (Grade 220)
2. PEO coated aluminium alloy (Al-6082) disc

Both types of disc were manufactured using in house facilities. The aluminium alloy discs were sent to the Keronite International Limited Company for PEO coating.

Eight discs of both type of materials were prepared. Each test was carried out using a new disc and friction material.

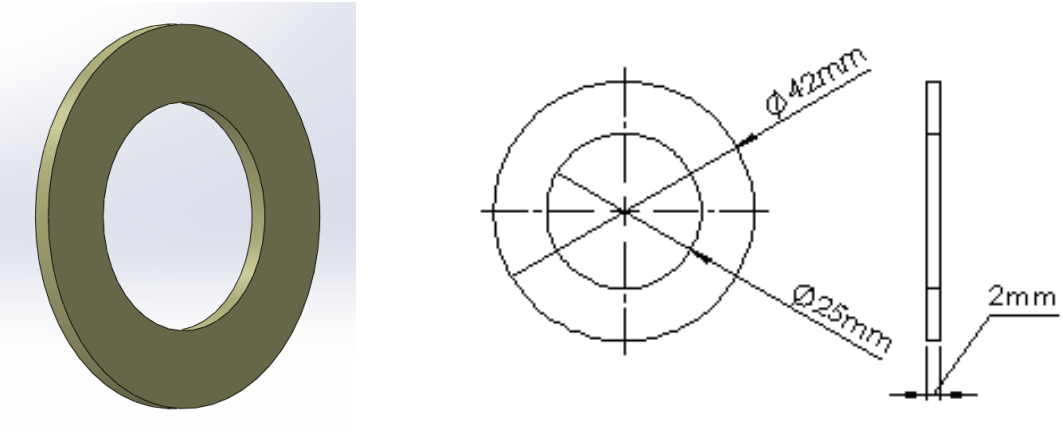

(a) Isometric view **(b) Disc Dimensions**

Figure 3-7: Disc for pin-on-disc testing

3.5 Density of friction material

The density of the pad material was measured using four different samples of friction material. The Mettler Toledo AT21 comparator was used to measure the mass of the samples. The measuring range of the AT21 comparator is from 1µg to 20 g. A digital micrometer was used to measure the dimensions of the cylindrical samples. As shown in Table 3-1, the average density of the brake pad was found to be 2.95 g/cm^3. Friction material is a blend of binder, reinforced fibers, friction additives and fillers. Mostly, copper or iron is used for reinforcement. They have a higher density as compared to other constituents of the friction material. A slight change in its composition results in change of density. Therefore, there is same variation seen in the density values shown in Table 3-1.

Table 3-1 shows the measured value of density. Each sample was measured three times.

Sample	Mass (g)	Volume			Density= Mass/Volume (g/cm^3)
		Diameter (mm)	Length (mm)	Volume (mm^3)	
1	0.233012	4.91	4.32	81.76	2.85
2	0.239129	4.89	4.11	77.15	3.10
3	0.250257	5.02	4.41	87.24	2.86
4	0.246074	4.90	4.38	82.55	2.98
Average Density					**2.95**

Table 3-1: Average density of friction material

3.6 Characterisation of PEO coated discs

3.6.1 Microscopy

Optical microscopic was used to examined the PEO coating on the Al-6082 aluminium alloy. Initially, the sample was prepared for the microscopic analysis and the following steps were carried out:

- Cutting: A small section of the specimen was cut out from a small coated disc using a abrasive cutoff machine as shown in Figure 3-8.

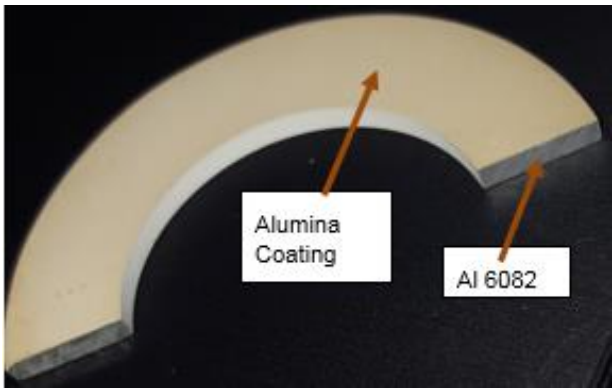

Figure 3-8: Section of a sample after cutting

- Mounting: The next process involved mounting the sample section in Bakelite. Specimen was placed in the mould and then filled out with the Bakelite powder. After applying pressure and heat for a certain time, a hard material surrounding the specimen is obtained as shown in Figure 3-9:

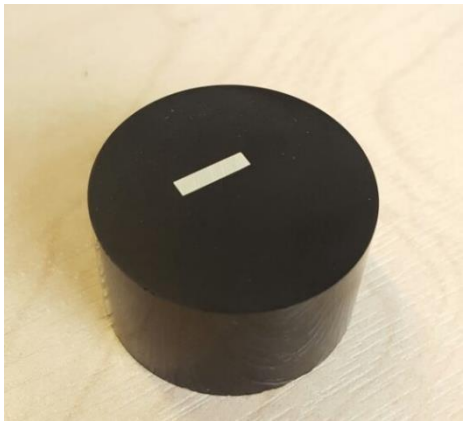

Figure 3-9: Specimen mounted in Bakelite

- Grinding: The specimen was carefully grounded on a grinding wheel to get a smooth flat surface. Different grit size papers were used starting from coarser (200) to much fine grades (1200).

The specimen was studied under the optical microscope to see the condition of the coating sandwiched between the Bakelite and the Al-6082 substrate.

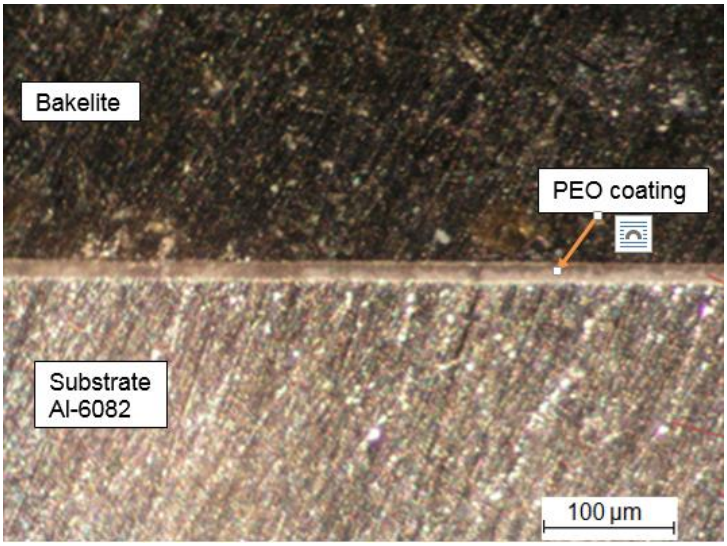

Figure 3-10: Image from microscope

3.6.2 Measurement of coating thickness

The analysis of sections of PEO coated discs was carried out using a 3D optical profilometer (Bruker NPFLEX 3D metrology system). Coating thickness was measured on both sides of the section. Figure 3-11 and Figure 3-13 shows the images taken from the profiler for both sides of the samples. Figure 3-12 and

Figure 3-14 shows the measurement of the thickness of the coating. A magnification of ×40 was used. The thickness was measured at multiple locations and the average thickness was found to be 44 microns.

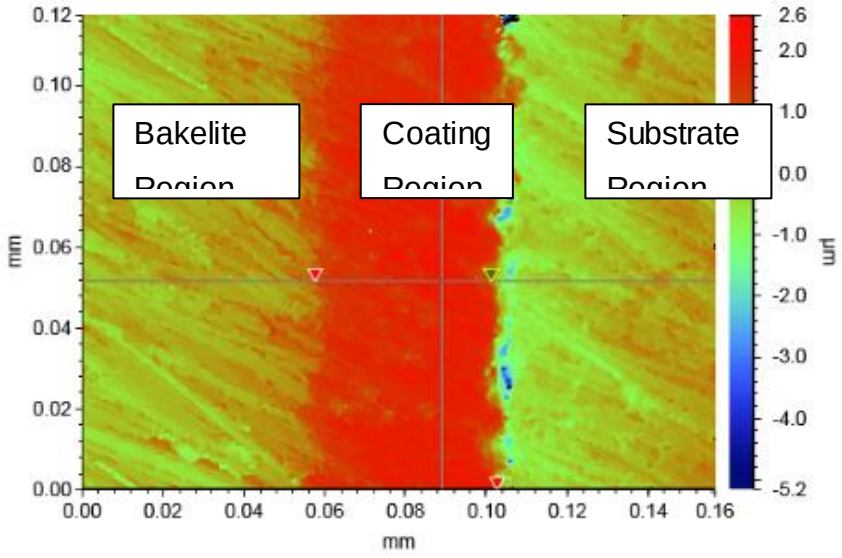

Figure 3-11: NPFLEX contour plot of PEO coated Al-6082

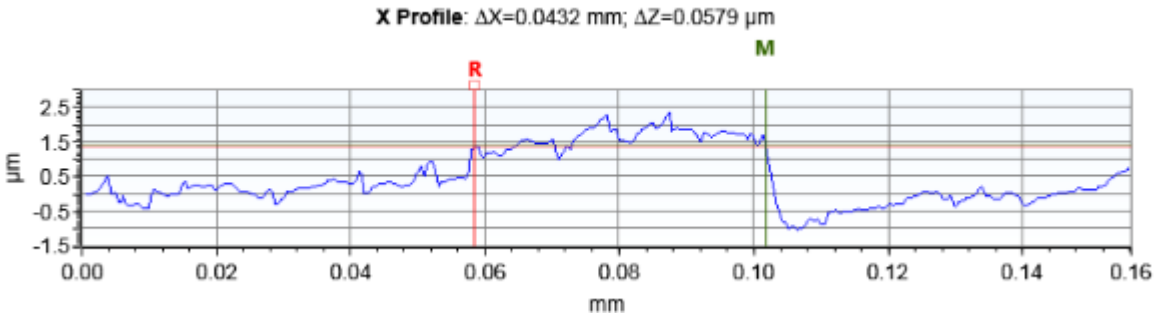

Figure 3-12: NPFLEX X Profile of PEO coated Al-6082

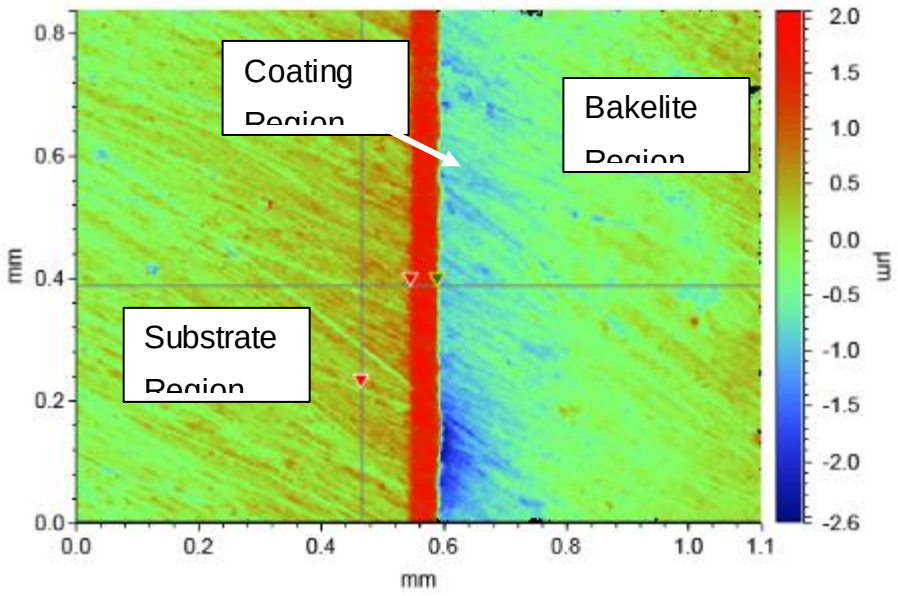

Figure 3-13: NPFLEX contour plot of PEO coated Al-6082

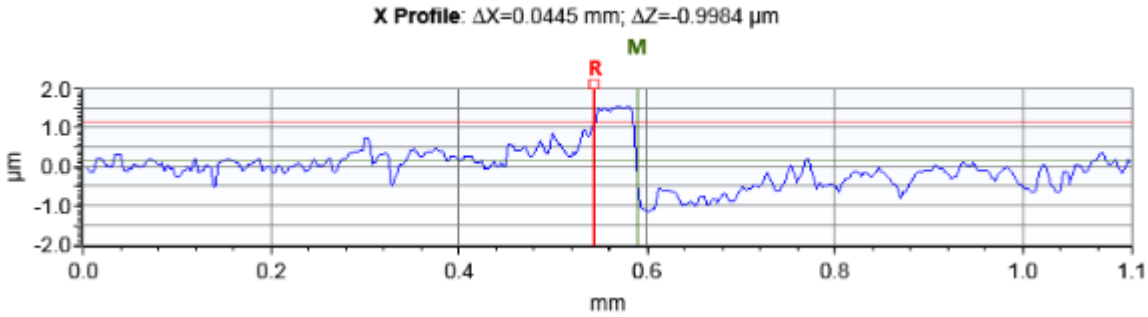

Figure 3-14: NPFLEX X Profile of PEO coated Al-6082

3.7 Test Parameters

Typically a range of contact pressures from 0.3 to 2 MPa is observed during a braking event. The lower pressure corresponds to a light braking while the higher is for a hard braking event. Also, the product of contact pressure and sliding velocity generally falls in the range of 0.3 to 20 MPa m/s (Chandra, 2015).

The load cell assembled with the pin-on-disc apparatus can measure a normal force of up to 5 kg. For these parameters, the maximum contact pressure that could be applied was found to be 2.5 MPa. However, it was found that contact

pressure above about 1 MPa caused the friction material to fail. Therefore, contact pressures of 0.5 MPa and 1.0 MPa were used for these tests.

For the disc rotating at 500 rpm and a mean wear track radius of 16.75 mm, the mean sliding velocity was found to be 0.88 m/s. This gives a range of contact pressure × sliding velocity of between 0.44 and 0.88 MPa m/s which is within the expected range for a disc brake.

Disc and pin wear were measured by recording the weight before and after each test using a Mettler Toledo AT21 comparator.

3.7.1 Preliminary test

A preliminary test for a PEO coated aluminium disc was conducted at a pressure of 0.5 MPa for one hour. Table 3-2 shows that the wear volumes for both PEO disc and friction material were quite low. Infact, the disc was found to gain rather than lose weight. This is thought to be due to the formation of a tansfer layer on the disc surface. The results show that test should be run for a longer time in order to get an appreciable amount of wear or in the case of the disc positive weight loss due to wear to counteract the weight gain due to the transfer layer. Therefore, all subsequent tests were run for a minimum of 6 hours duration. 8 separate discs were conducted for the PEO coated disc and 8 for the GCI discs. For each test, new discs and friction materials were used.

Component	**Weight before test (g)**	**Weight after test (g)**	**Specific Wear Coefficient (m^2/N)**
Disc (PEO coated Al-6082)	4.772777	4.773022	-3.09×10^{-15}
Pin (new friction material)	1.848524	1.848457	7.734×10^{-16}

Table 3-2: Preliminary test results

The calculations for the specific wear coefficients for both disc and friction material (pin) shown in Table 3-2 are given below:

- *Wear of friction material,*

$$V_{pin} = \frac{m_1 - m_2}{\rho_{pin}}$$
$$V_{pin} = \frac{1.848524 - 1.848457/1000}{2950}$$
$$= 2.271 \times 10^{-11}\ m^3$$

$$S = V \times t$$
$$= 0.88 \times 3600$$
$$= 3158\, m$$

$$K_{pin} = \frac{V_p}{S \times F}$$
$$= 7.41 \times 10^{-16}\ m^2/N$$

- *Wear of disc,*

$$V_{disc} = \frac{M_1 - M_2}{\rho_{disc}}$$
$$V_{disc} = \frac{(4.773022 - 4.772777)/1000}{2700}$$
$$= -9.074 \times 10^{-11}\ m^3$$
$$K_{disc} = \frac{V_{disc}}{S \times F}$$
$$= -2.96 \times 10^{-15}\ m^2/N$$

Note: (-) sign indicates the weight gain of the disc probably due to the transfer of friction material on the disc.

Where,

$V_{pin} = loss\ in\ volume\ of\ the\ pin\ in\ m^3$
$V_{disc} = loss\ in\ volume\ of\ the\ disc\ in\ m^3$

$$m_1, m_2 = mass\ of\ the\ pin\ before\ and\ after\ each\ test\ respectively, kg$$
$$M_1, M_2 = mass\ of\ the\ disc\ before\ and\ after\ each\ test\ respectively, kg$$
$$K_{pin}, K_{disc} = specific\ wear\ coefficient\ of the\ pin\ and\ the\ disc\ respectively, \frac{m^2}{N}$$
$$\rho_{pin}, \rho_{disc} = density\ of\ pin\ and\ disc\ respectively$$
$$S = mean\ sliding\ distance, m$$
$$F = Normal\ force\ aplied\ on\ pin, N$$

3.8 Experimental results of PEO coated Al-6082 discs

Table 3-3 summarizes all the pin-on-disc tests carried out using the PEO coated Al-6082 discs. The tests were conducted at two different contact pressures i.e. 0.5 MPa and 1 MPa. The rotating speed of the disc for all test was 500 rpm. Each test was run for 6 hours to get a measurable amount of wear.

3.8.1 Friction measurements

Figure 3-15 shows the coefficient of friction as a function of time for tests 1-4 respectively, where a contact pressure of 0.5 MPa was applied. It can be observed that the coefficient of friction starts from a value of 0.2 ±0.05 at the beginning of each test and ultimately reaches a steady state value of approximately 0.6. The variation in the value of friction in each test represents a phase in which the disc and the friction material establishes a stable contact by removing any foreign material on the pin and the disc surface. Also, due to the variation in the friction material composition, there was a significant difference in the shape of the plot of the coefficient of friction verses time for each test.

Test	Sample	Run Time (hours)	Disc Speed (RPM)	Contact Pressure (MPa)	Wear Coefficient ($\times 10^{-16}$ m²/N)		μ_{avg}*	μ_{ss}**
					Friction material	Disc		
1	PEO_01	6	500	0.5	24.8	5.05	0.55	0.62
2	PEO_02				30.0	8.78	0.63	0.67
3	PEO_03				18.5	14.9	0.39	0.56
4	PEO_04				37.8	13.2	0.48	0.59
5	PEO_05			1	47.9	10.8	0.55	0.66
6	PEO_06				28.2	16.9	0.34	0.53
7	PEO_07				54.0	29.3	0.48	0.62
8	PEO_08				44.8	25.4	0.49	0.57

Table 3-3: Pin-on-disc test results for PEO coated Al-6082

* Average coefficient of friction

** Steady state coefficient of friction

Table 3-3 shows the average values of μ_{avg} and steady state μ_{ss} for each test. μ_{ss} shows the average coefficient of friction at steady state condition during the last hour of the test. μ_{ss} was found to be approximately 0.6.

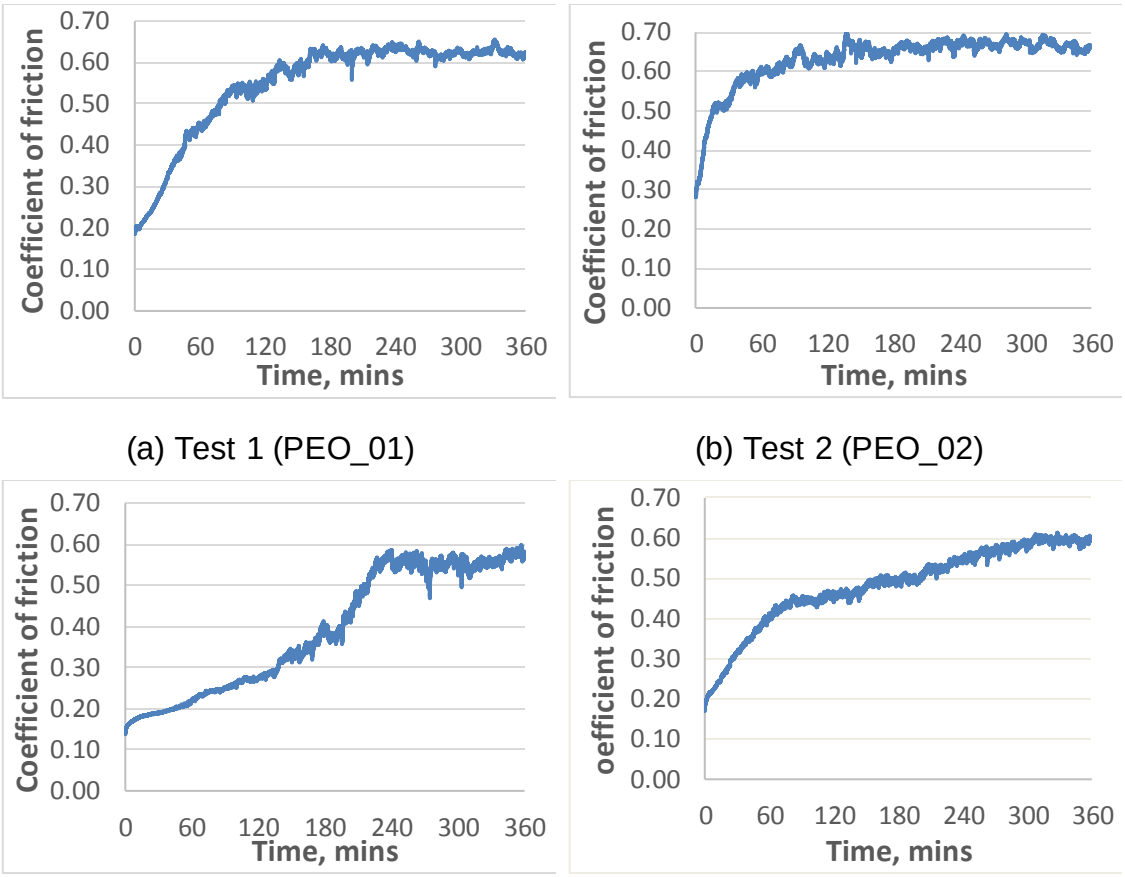

(a) Test 1 (PEO_01)

(b) Test 2 (PEO_02)

(c) Test 3 (PEO_03)

(d) Test 4 (PEO_04)

Figure 3-15: Coefficient of friction vs time graphs (0.5 MPa contact pressure)

Figure 3-16 shows the coefficient of friction as a function of time for Tests 5 - 8 respectively where s contact pressure of 1.0 MPa was applied. It can be seen that the change in contact pressure has not affected the coefficient of friction profile. Initially the coefficient of friction was 0.2 and then it ultimately attained a steady state value of approximately 0.6 as before. It can be seen that there is a variation in the profile of COF in each test and this is mainly due to the fact that the friction pin is only 5mm in x-section. Friction material is a composite material and a slight variation in composition of friction material could affect the coefficient of friction.

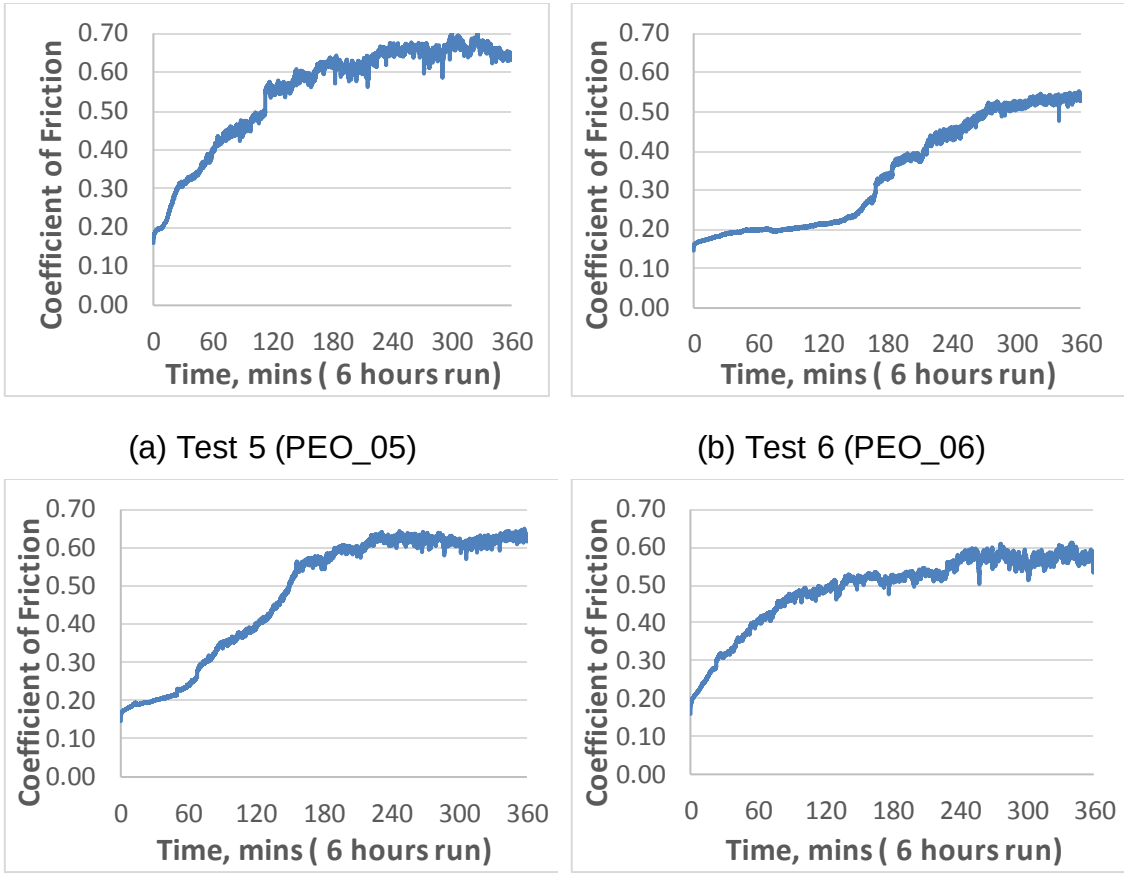

(a) Test 5 (PEO_05)

(b) Test 6 (PEO_06)

(c) Test 7 (PEO_07)

(d) Test 8 (PEO_08)

Figure 3-16: Coefficient of friction vs time graphs (1.0 MPa contact pressure)

3.8.2 Specific wear coefficients

Table 3-3 shows the measured values of specific wear coefficient for both the friction material and PEO coated aluminium alloy disc for each test. It was observed that the friction material wears more than PEO coated Al-6082 disc under both applied contact pressures i.e. 0.5 MPa and 1.0 MPa.

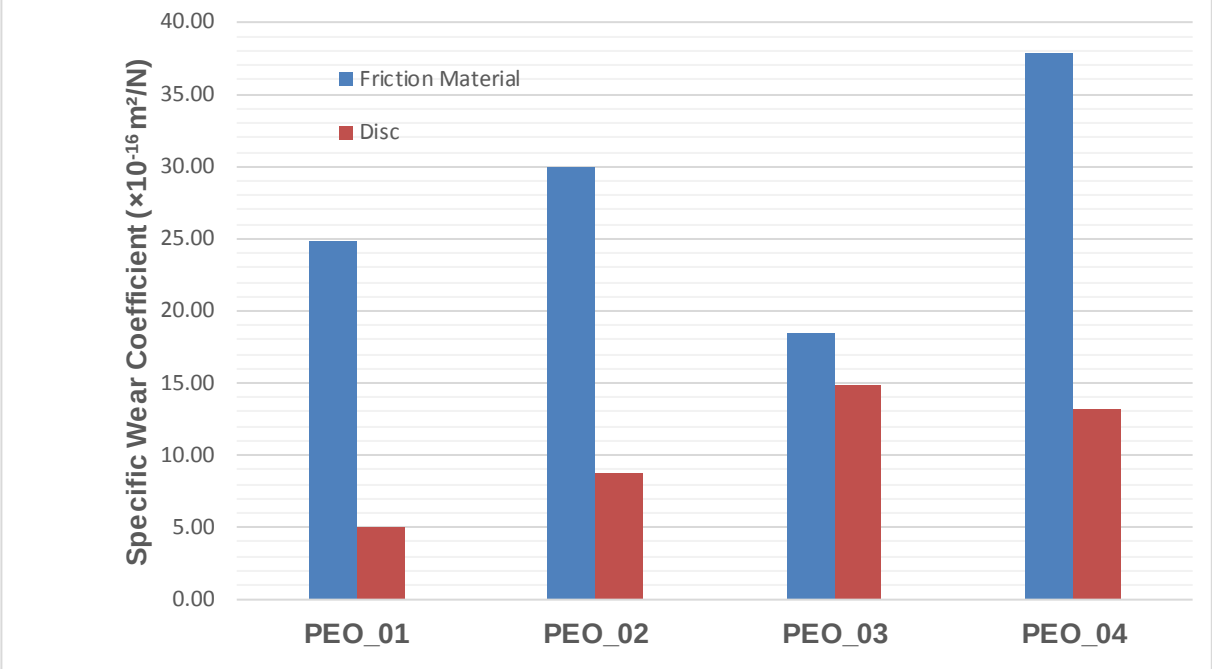

Figure 3-17: Comparison of wear coefficient (Pressure 0.5 MPa & Speed 500rpm)

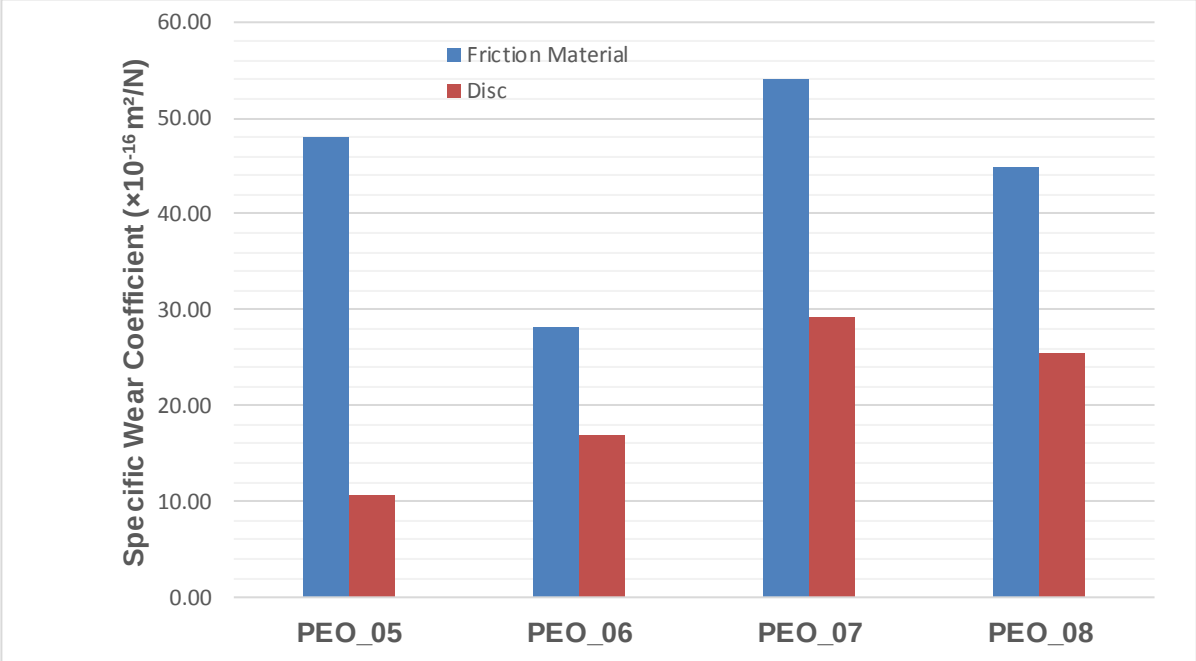

Figure 3-18: Comparison of wear coefficient (Pressure 1.0 MPa & Speed 500rpm)

Figure 3-17 and Figure 3-18 shows the specific wear coefficient for the individual tests. The PEO coated aluminium alloy discs wore consistently less than the friction material.

3.8.3 Relationship between average coefficient of friction and specific wear coefficient for PEO coated disc

The Figure 3-19 and Figure 3-20 represents the variation in measured values of specific wear coefficient of friction material and PEO coated Al 6082 disc with the average CoF. It has been observed that wear coefficient of friction material increases with the increase in average CoF for both contact pressure. On the other hand, wear coefficient for PEO coated disc has not been changed appreciably with the increase in CoF. This shows that the higher the CoF, the higher would be the transfer layer deposited on the PEO coated disc. This can be seen from the preliminary test results. In that case, there was an overall increase in the mass of the PEO coated disc after one hour of test run and the wear coefficient was found to be negative.

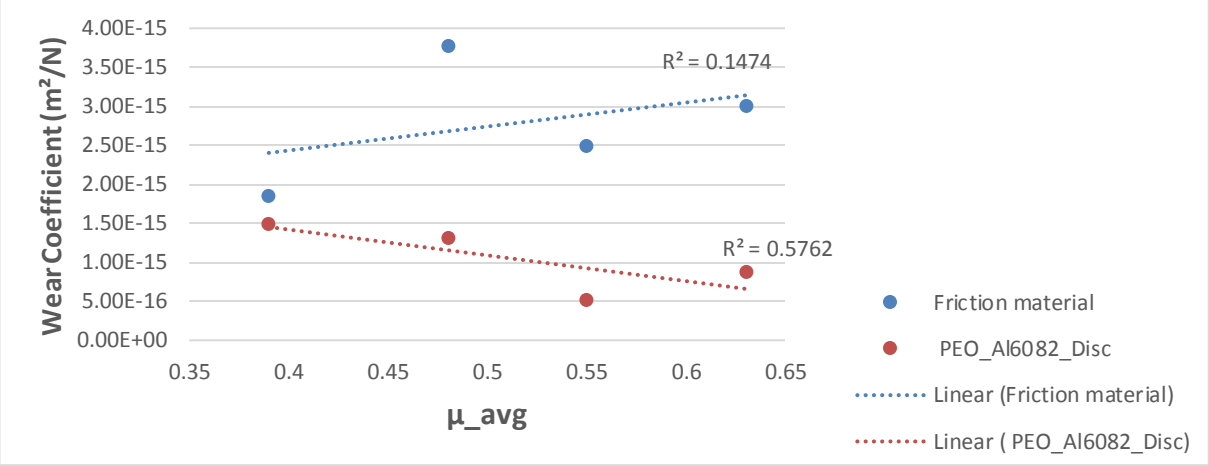

Figure 3-19: Specific wear coefficient and average CoF (Contact Pressure 0.5 MPa)

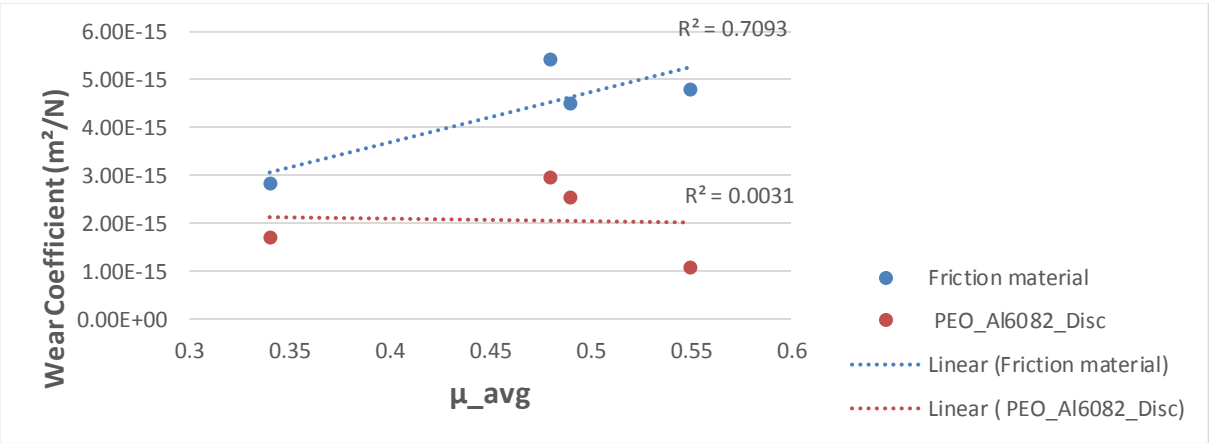

Figure 3-20: Specific Wear coefficient and average CoF (Contact Pressure 1.0 MPa)

3.9 Experimental results of GCI discs

The Table 3-4 summarises all the pin-on-disc tests carried out using the GCI discs. The tests were conducted at two different contact pressures i.e. 0.5 MPa and 1.0 MPa. The rotating speed of the disc for all test was 500 rpm. Each test was run for 6 hours to get a measurable amount of wear.

Test	Sample	Run Time (hours)	Disc Speed (RPM)	Contact Pressure (MPa)	Wear Coefficient ($\times 10^{-16}$ m²/N)		μ_{avg}	μ_{ss}
					Friction material	Disc		
9	GCI-01	6	500	0.5	190.0	571.1	0.37	0.43
10	GCI-02				203.4	949.6	0.49	0.54
11	GCI-03				125.9	449.7	0.32	0.46
12	GCI-04				124.2	414.4	0.32	0.43
13	GCI_05			1.0	135.7	508.0	0.35	0.51
14	GCI_06				200.8	861.2	0.45	0.56
15	GCI-07				201.5	820.8	0.47	0.52
16	GCI-08				157.0	606.1	0.39	0.51

Table 3-4: Pin-on-disc test results for GCI discs

The average μ_{ss} for GCI was found to be around 0.5.

Figure 3-21 shows the coefficient of friction profile against the total run time of Test 9 - 12 respectively where a contact pressure of 1.0 MPa was applied. The disc used was a GCI disc.

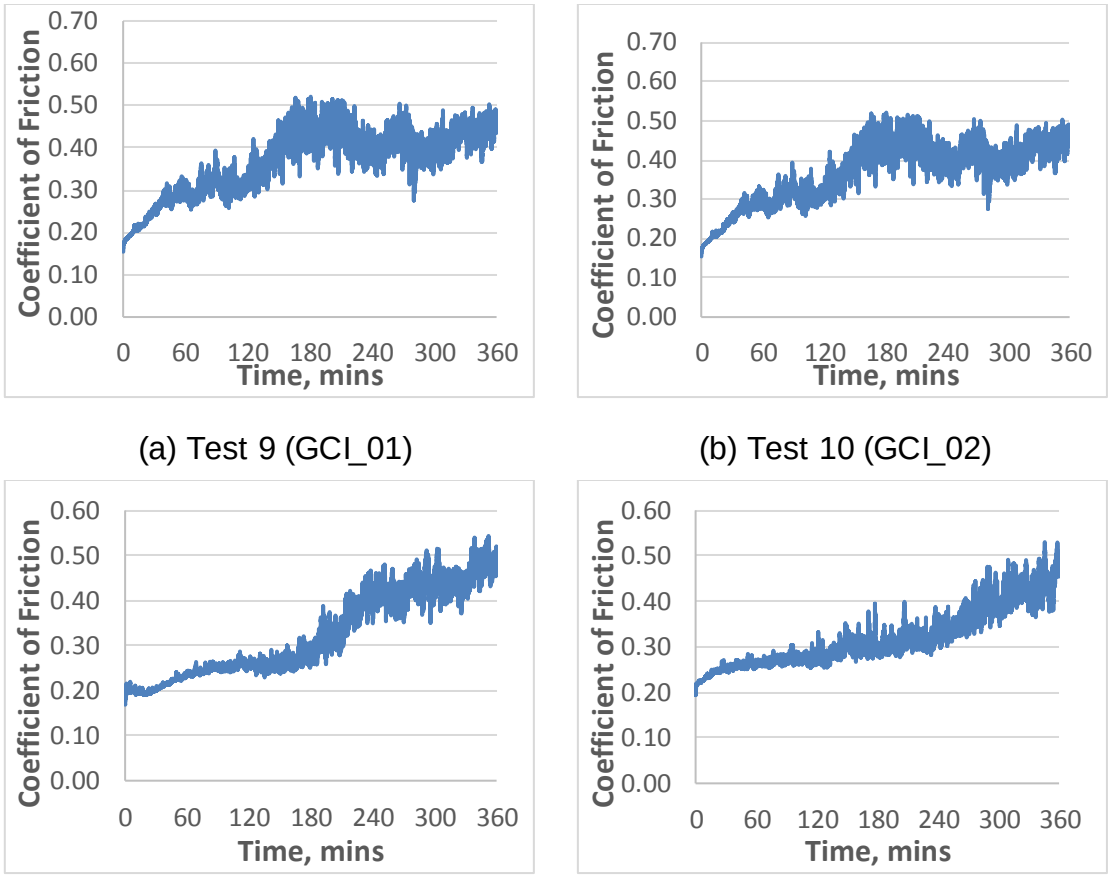

(a) Test 9 (GCI_01)

(b) Test 10 (GCI_02)

(c) Test 11 (GCI_03)

(d) Test 12 (GCI_04)

Figure 3-21: Coefficient of friction vs Time graph (0.5 MPa contact pressure)

Figure 3-22 represents the coefficient of friction profile against the total run time of Test 13 - 16 respectively where a contact pressure of 1.0 MPa was applied. The disc used was a GCI disc. Table 3-4 shows the conditions under which these tests were conducted.

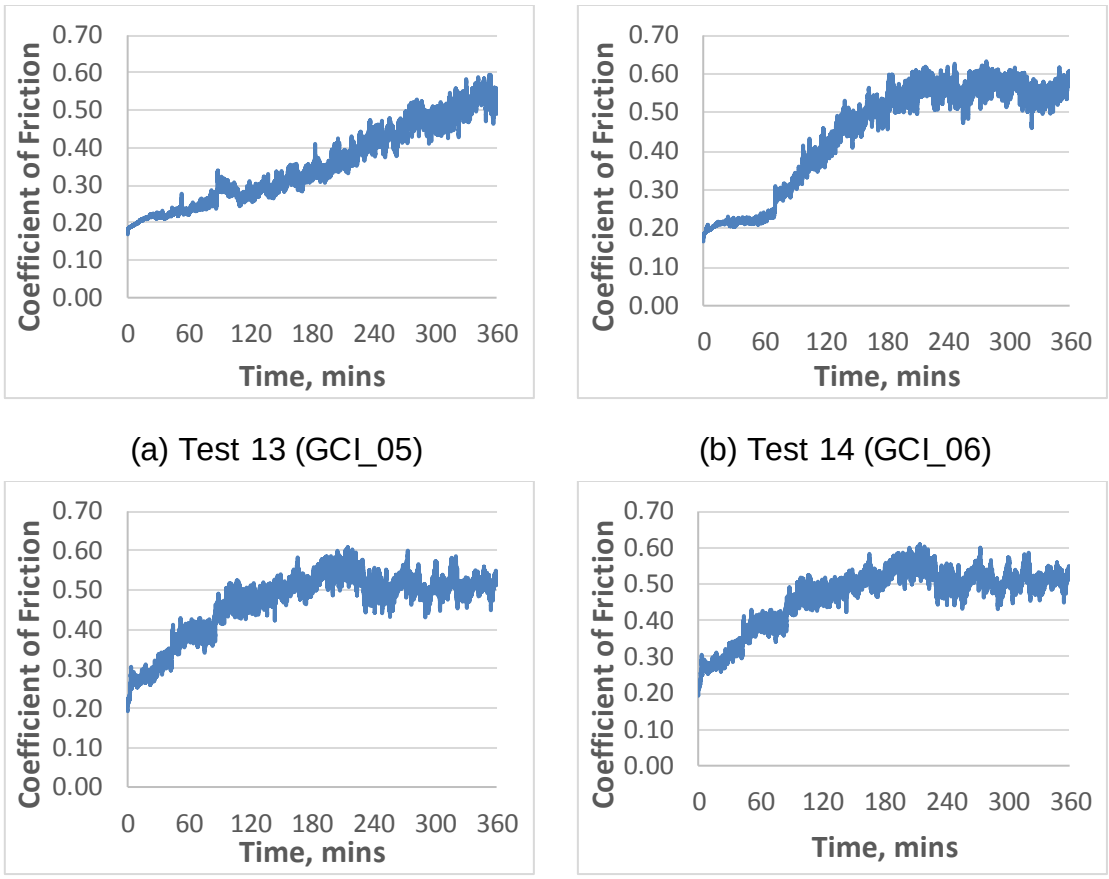

(a) Test 13 (GCI_05)

(b) Test 14 (GCI_06)

(c) Test 15 (GCI_07)

(d) Test 16 (GCI_08)

Figure 3-22: Coefficient of friction vs Time graph (1.0 MPa)

3.9.1 Specific wear coefficients

Table 3-4 shows the measured values of specific wear coefficient for both the friction material and GCI disc for each test. It was observed that the friction material wears less than the GCI disc under both applied contact pressures i.e. 0.5 MPA and 1.0 MPA.

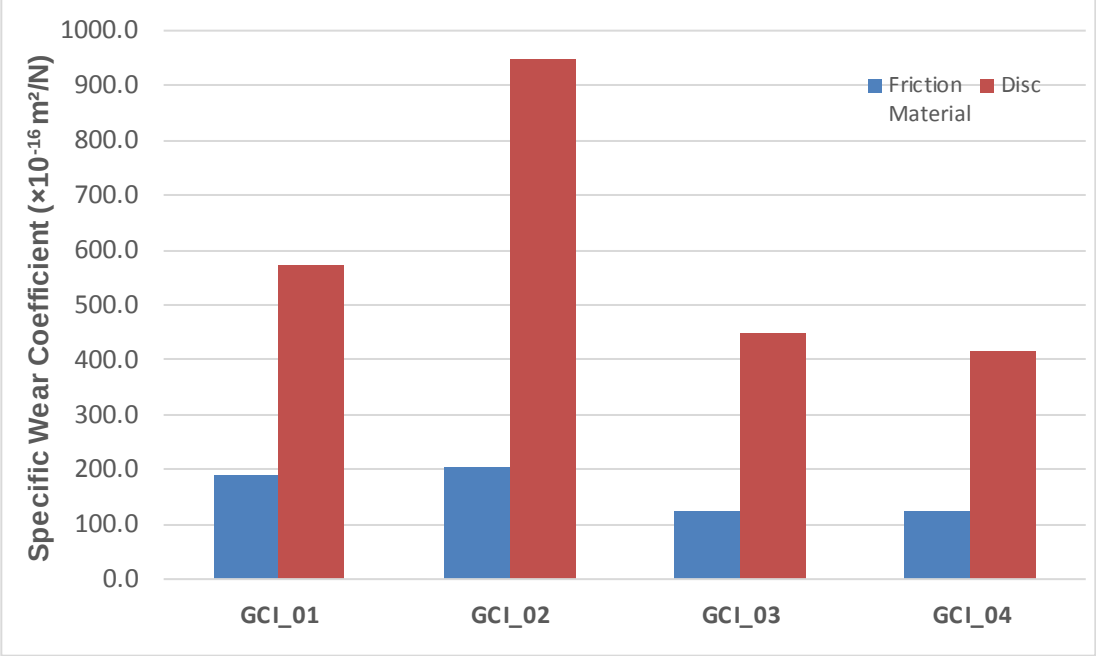

Figure 3-23: Comparison of wear coefficient (Pressure 0.5 MPa & Speed 500rpm)

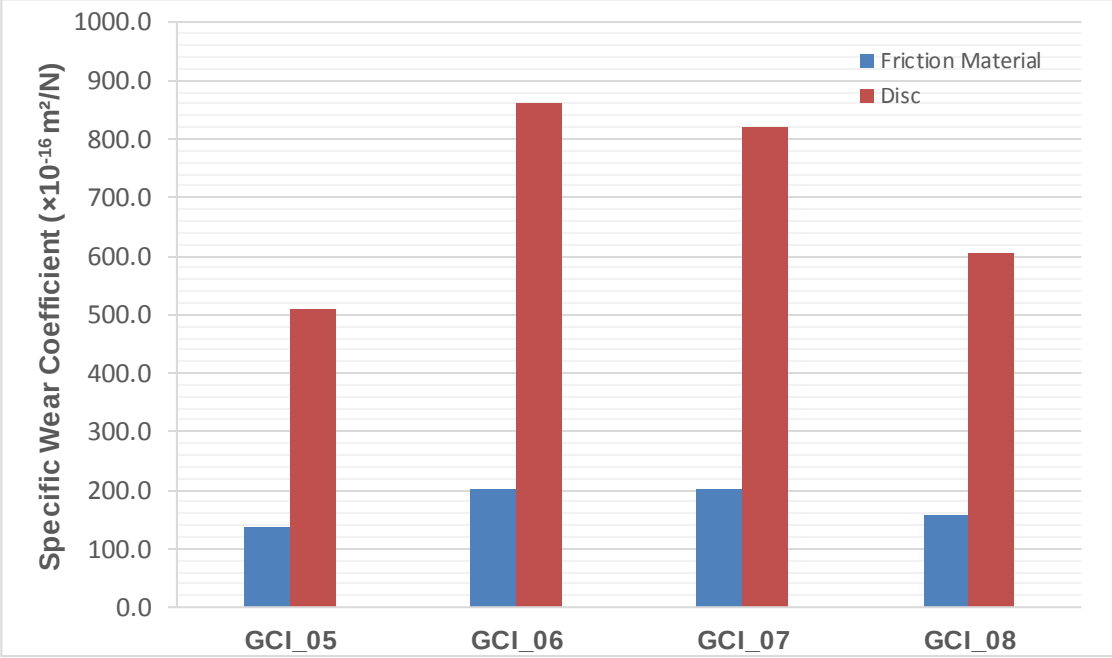

Figure 3-24: Comparison of wear coefficient (Pressure 1.0 MPa & Speed 500rpm)

Figure 3-23 and Figure 3-24 shows the specific wear coefficient for the individual test. The GCI discs wore consistently more as compared to the friction material.

3.9.2 Relationship between average coefficient of friction and specific wear coefficient for GCI disc

The Figure 3-25 and Figure 3-26 represents the variation in measured values of specific wear coefficient of friction material and GCI disc with the average CoF. It was observed that the wear coefficient of both the friction material and the disc increases with the increase in average CoF for both contact pressure.

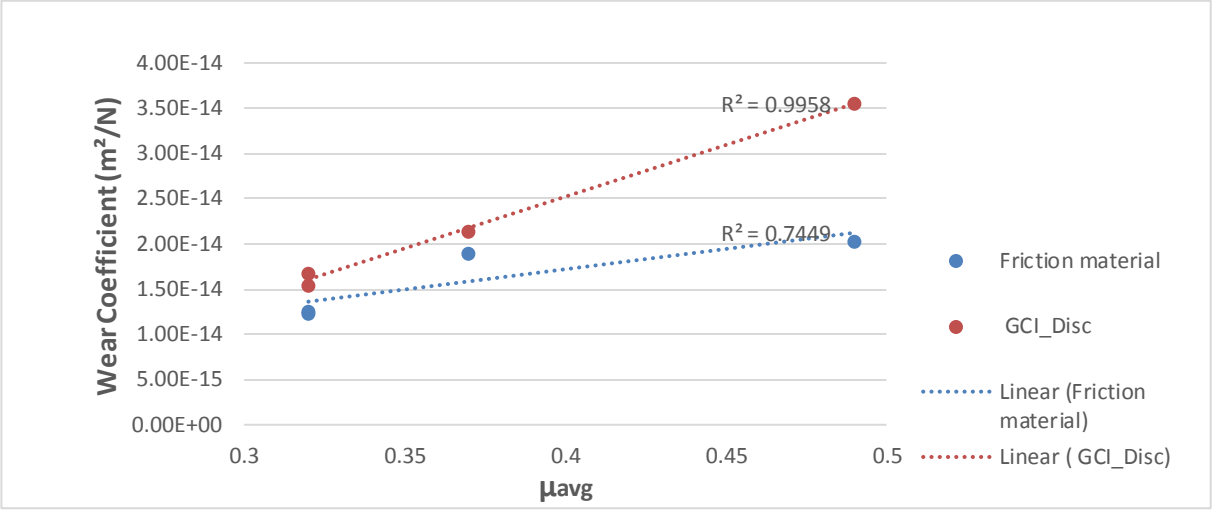

Figure 3-25: Specific wear coefficient and average CoF for GCI disc (Contact Pressure 0.5 MPa)

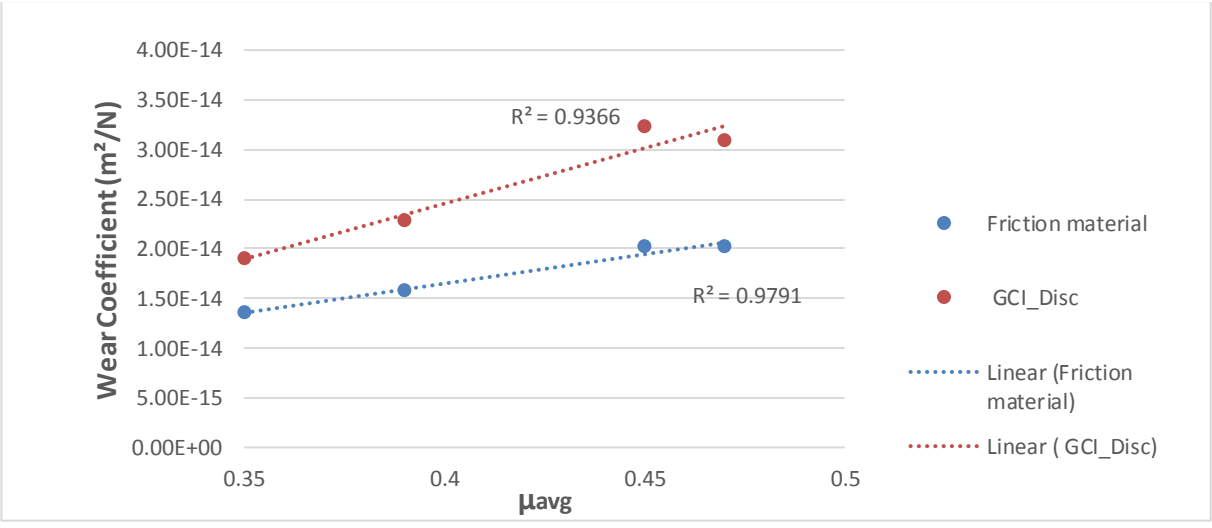

Figure 3-26: Specific wear coefficient and average CoF for GCI disc (Contact Pressure 1.0 MPa)

3.10 Comparison of wear and friction test results for PEO coated aluminium alloy and GCI discs

Both PEO coated aluminium alloy and GCI discs were tested against the same friction material. Although, the friction material was specially designed to work with PEO aluminium disc but the alteration in composition of friction material was specified in a way that new friction material exhibits the same performance as if it used with conventional friction material.

3.10.1 Specific wear coefficient

A statistical analysis was carried out to determine any significant difference between the specific wear coefficients at 0.5 MPa and 1.0 MPa for each of the two disc materials. The statistical tool used was Student T-test. The student T-test is used to determine the significant difference between two set of results. A t-value was calculated for the PEO coated and GCI discs using the following equation:

$$t = \frac{|X_1 - X_2|}{\sqrt{\frac{{S_1}^2}{n_1} + \frac{{S_2}^2}{n_2}}}$$

Where,

$X_1, X_2 = mean\ of\ data\ set\ \ 1\ and\ 2$
$S_1, S_2 = standard\ deviation\ of\ data\ set\ 1\ and\ 2$
$n_1, n_2 = number\ of\ samples\ in\ date\ set\ 1\ and\ 2$

The data sets were assumed to be independent and two tailed test technique was employed.

The critical value of t for a particular significance were calculated from the t-table. The degree of freedom was 6 $(n_1 + n_2 - 2)$.

At the 0.05 significance level, $t_{critical} = 2.45$

For the PEO coated disc, t was calculated to be 2.14 which is less than critical value.

As, $t < t_{critical}$, there is no significant difference between the two data sets.

A similar analysis was carried out on GCI test results and t value was 0.69 which was also less than $t_{critical}$ value.

It was concluded that there is no significant difference between the specific wear coefficient of friction material at 0.5 MPa and 1.0 MPa for both discs.

The average specific wear coefficients for the two disc materials are shown in Figure 3-27. The error bar represent the standard deviation of the specific wear coefficient for both PEO coated Aluminium disc and the GCI disc during the tests, which measures the amount of variation of the specific wear coefficient value during the test based on the average value. Also, the student T-test shows that there is no significant difference in results from the tests carried out at 0.5 and 1.0 MPa for each type of disc material so the results were combined. It can be seen that there is a marked difference between the specific wear coefficients for both types of disc materials. This is due to higher hardness of the PEO coating aluminium alloy as compare to GCI.

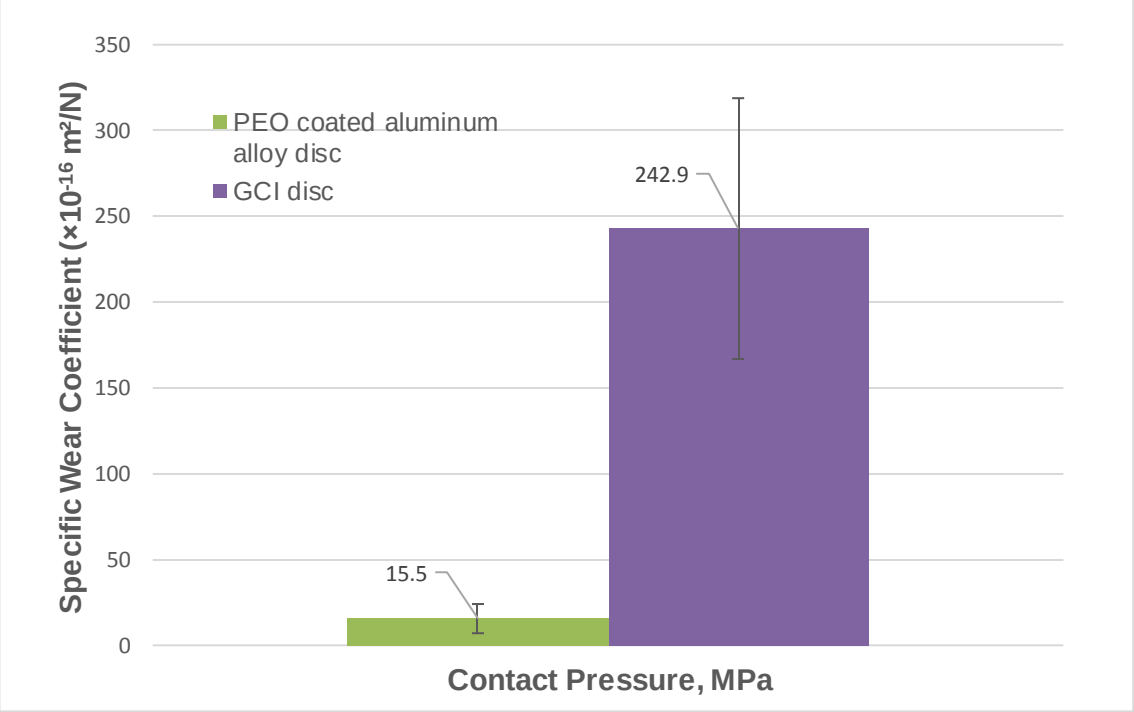

Figure 3-27: Average specific wear coefficients for the PEO coated aluminium alloy disc and GCI disc

Figure 3-28 shows the specific wear coefficient of friction material. Tests 1-8 and Tests 9-16 were performed with PEO coated aluminium alloy disc and GCI discs respectively. It can be seen that the specific wear coefficient of friction material running against the PEO coated disc is significantly lower than the friction material running against the GCI discs. Also, the Student t-test was conducted and the t value for friction material running with PEO disc and GCI discs were found to be 2.3 and 0.43 respectively. Both t values are less than the critical value of 2.45. Therefore, it was concluded that there is no significance effect of contact pressure on the specific wear rate of friction material running against PEO coated and GCI discs.

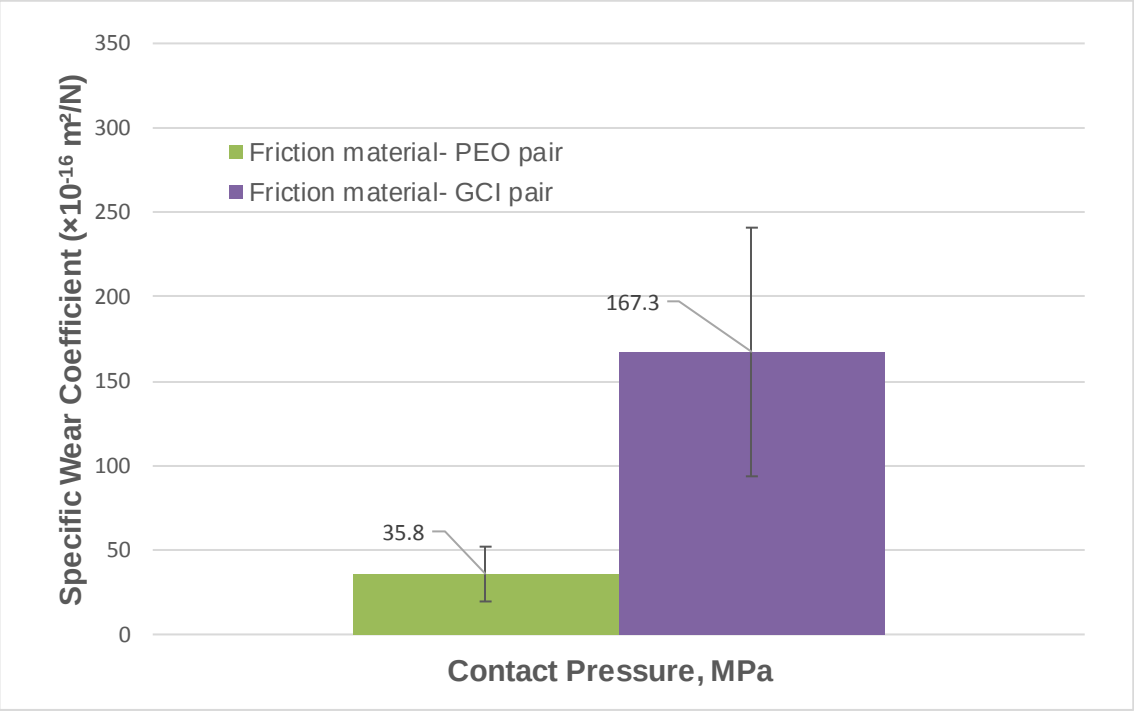

Figure 3-28: Comparison of specific wear coefficient of friction material

3.10.2 Coefficient of friction

From Figure 3-29, it can be seen that the friction material-PEO coated aluminium alloy disc pair offers a higher coefficient of friction as compared to the friction material-GCI disc pair. The error bar represents the standard deviation of the average CoF values for both types of disc material. The average CoF shown in

Figure 3-29 are the average values in last hour of the test as CoF values are much more stable during this period.

The higher value of CoF for PEO coated discs suggests that a PEO coated aluminium alloy brake rotor has the potential to be a viable alternative to a conventional GCI brake rotor.

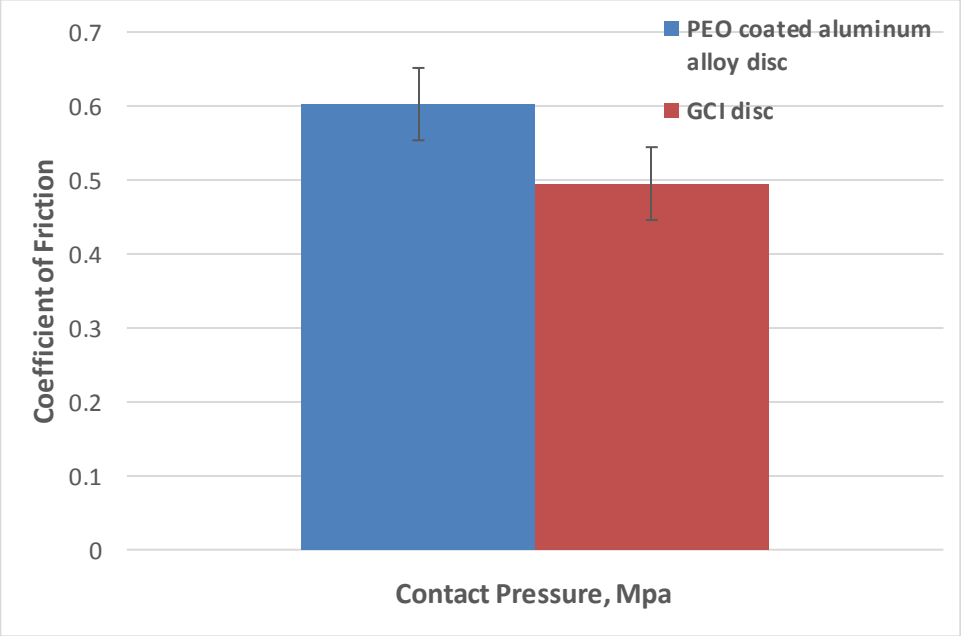

Figure 3-29: Average coefficient of friction during each test for PEO coated disc and GCI disc

3.11 Wear and non-exhaust road traffic emissions

The rate of wear effects the non-exhaust road traffic emissions. It has been found that the brakes results in contributing nearly 55% by weight of particulate matter (PM10) emissions of the total non-exhaust emissions. (Grigoratos et al., 2015). The Figure 3-30 shows the average loss of mass for both PEO coated aluminium alloy and GCI disc with their respective friction material pair. The test results shown in Figure 3-30 were conducted at a contact pressure of 0.5 MPa and 1.0 MPa respectively. Friction material 1 and friction material 2 are of same material. The only difference is that friction material 1 was used with PEO coated aluminium disc and the other one with GCI disc.

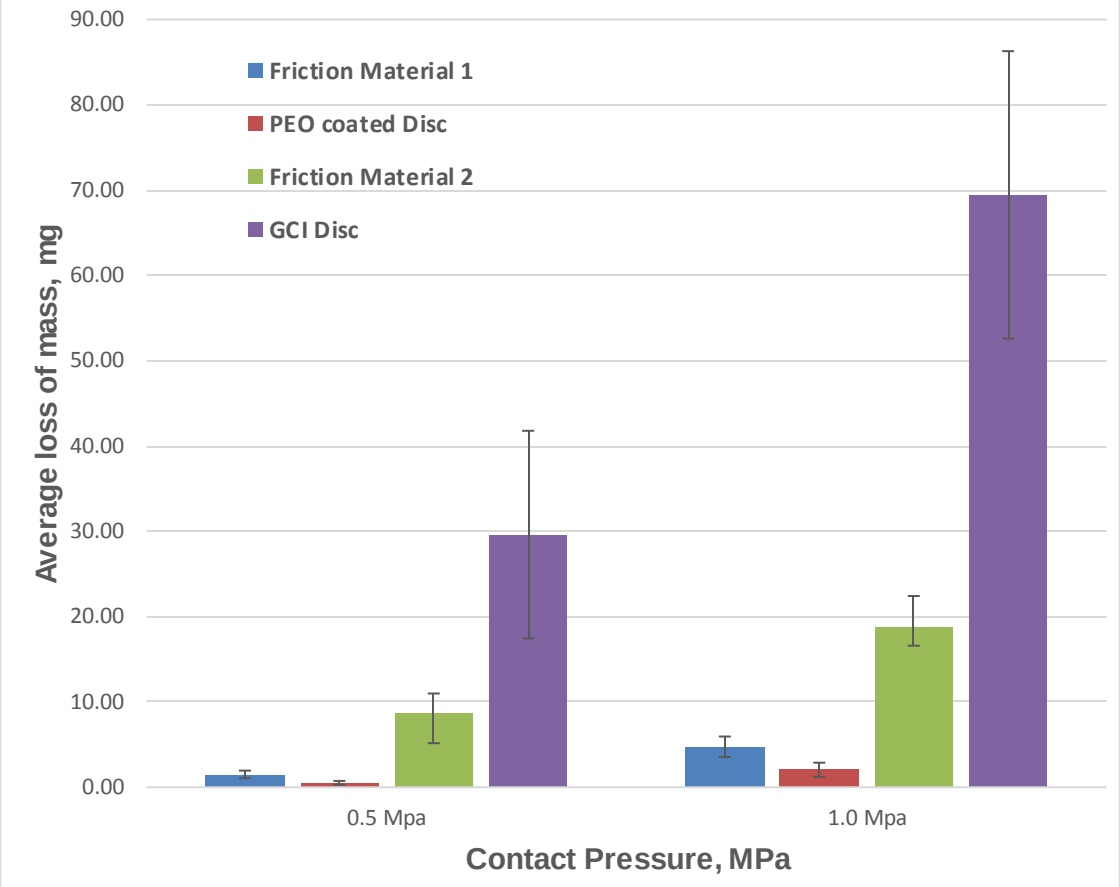

Figure 3-30: Average mass loss for PEO coated disc and GCI disc and their respective friction pairs for a contact pressure of 0.5 MPa & 1.0 MPa

The error bars in Figure 3-30 represent the standard deviation of the average loss of mass for the PEO coated aluminium alloy and the GCI disc during the tests, which measures the average amount of loss in mass value during the test based on the average value.

It can be seen that the PEO coated disc is much more environment friendly as compared to GCI disc. There is a significant difference in loss of mass for both disc against the same friction material.

3.12 Summary

In this chapter, the results from the pin-on-disc test were presented. PEO coated Al-6082 discs and conventional GCI discs were used. The same friction material was used with both discs for making the comparison. Two different sets of test parameters were used. Each test was repeated four times. PEO coated discs shows a higher coefficient of friction as compared to the GCI disc. The PEO coated disc also has low specific wear coefficient. Due to lower wear rate, the PEO coated discs exposes less particulate matter to the air. The test results are quite promising and makes the PEO coated aluminium alloy disc as a potential candidate for the future disc brake systems.

Chapter 4
Design and analysis of prototype PEO coated ventilated brake rotor

4.1 Introduction

The brake rotor of a disc brake receives about 90% of the heat dissipated during a braking event. The design and material of a brake rotor should have the capacity to offer both structural and thermal stability during the harshest braking conditions. Conventional cast iron brake rotors have high density and are therefore heavy. The fuel consumption and the exhaust emissions can be lowered if a brake rotor could be replaced with a lighter weight material. Aluminium alloy offers a lightweight alternative but has lower thermal stability. The overall weight can be reduced by 60% by replacing the conventional brake rotor material with an aluminium alloy of the same volume. However, the plain aluminium alloy and aluminium metal matrix composite rotors have been found to fail at temperatures higher than around 400℃. Alnaqi (2014) has worked on small scale PEO coated aluminium alloy and the results were quite promising. The PEO coated brake rotors worked well up to in access of 500℃. The advantages of using a PEO coating are its higher wear resistance and capability and ability to act as a thermal barrier to protect the aluminium substrate.

In the first part of this chapter, a novel design of a full scale lightweight PEO coated ventilated aluminium alloy brake rotor for a passenger car is discussed. Then, the development of a 3D finite element (FE) model of the coated brake rotor is presented in the second part. The FE model was constructed using Abaqus software and used to predict the thermal performance of the PEO aluminium rotor.

4.2 Design of brake rotor

The following key factors were considered during the design of the brake rotor:

1. Owing to the low maximum operating temperatures of the aluminium alloy, there is a need for rapid and effective heat dissipation from the rotor surfaces.
2. It should be easily manufactured in order to minimise the cost of applying the PEO coating over the rubbing surface.
3. It should be cost effective and reduce the overall weight of the rotor

In view of the first requirement above, it was decided that the brake rotor would need to be ventilated.

In order to ease the manufacturing and the coating of the brake rotor, the ventilated rotor was manufactured in three separate parts namely:

1. Inboard cheek
2. Outboard cheek
3. Inner ring containing vanes

Disc thickness variation (DTV) is a variation in the brake rotor thickness. High DTV is the cause of mechanical vibration and thermal elastic instability in vehicles. A parallelism tolerance of ±0.1mm was specified to keep the DTV as low as possible for all the components of the brake rotor. Also, a surface finish of 3.2 µm was specified on the rubbing surfaces prior to PEO treatment as indicated on the engineering drawing shown in Figure 4-2.

4.2.1 Outboard cheek

The outboard cheek include a top hat structure with four holes to assemble it with the dynamometer. A solid Al-6082 billet of 40 mm thick was used to machine the outboard cheek. The outside diameter of the rotor is 280 mm. The rubbing surface is 43 mm wide in total. The minimum thickness of the outboard cheek is 7mm but the rubbing surface is 9mm thick. For easing of applying the PEO coating

process, the thickness along the rubbing surface was kept 2 mm higher than the surrounding surface. Figure 4-1 shows a CAD model of the outboard cheek while Figure 4-2 shows the corresponding engineering drawing.

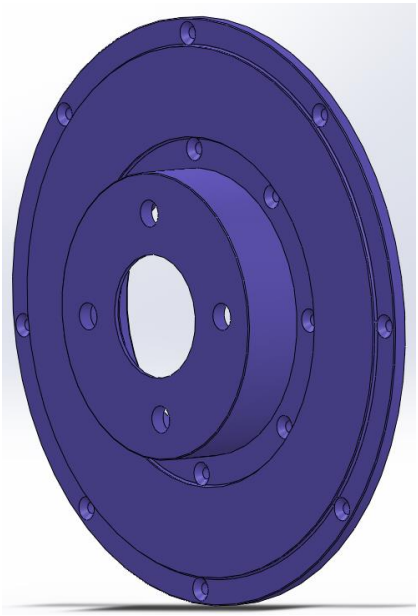

(a) Isometric view

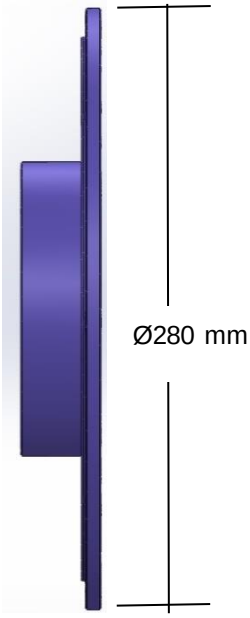

(b) Side view

(c) Elevated view

Figure 4-1: Outboard cheek

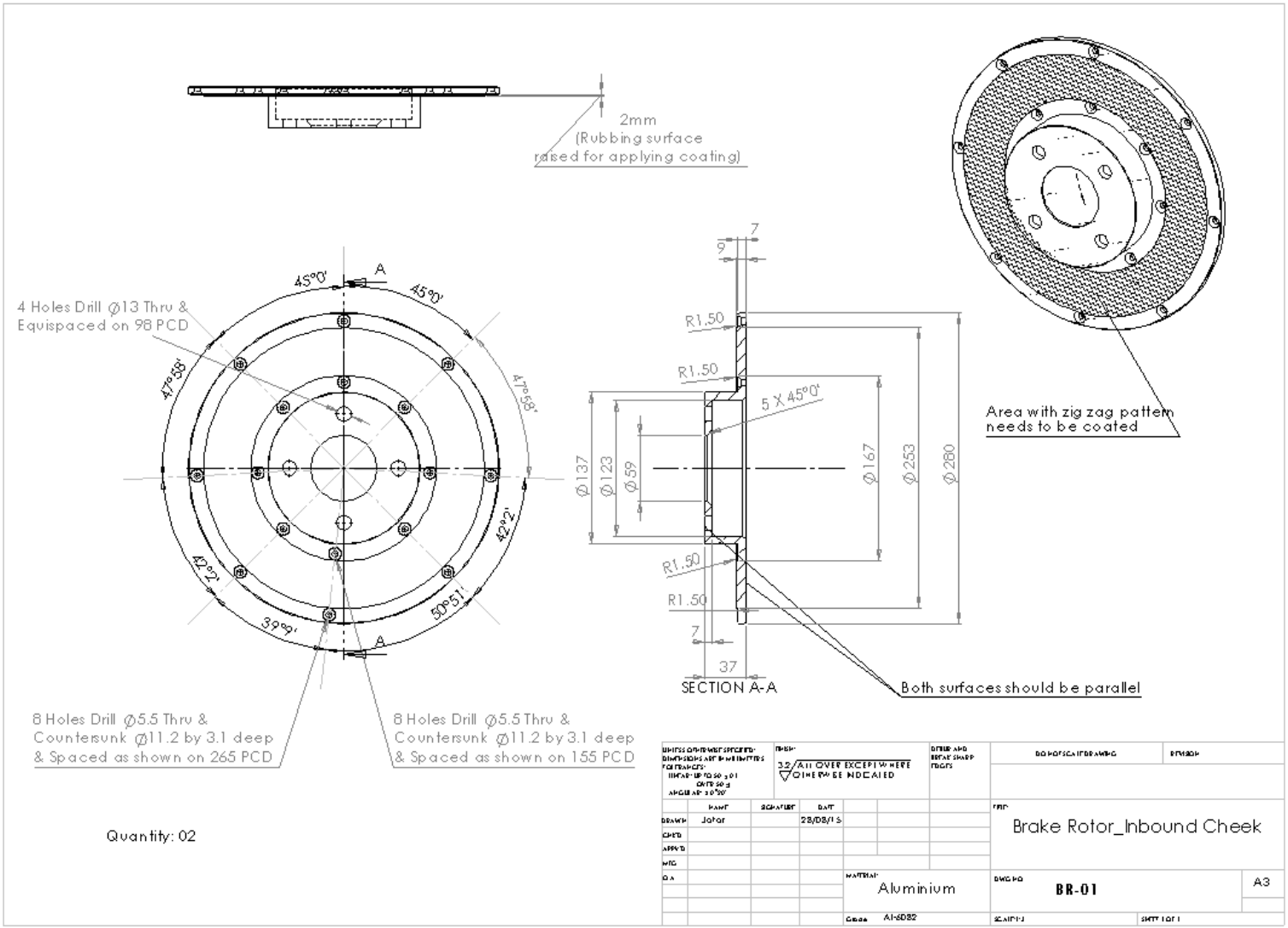

Figure 4-2: Brake rotor outboard cheek drawing

4.2.2 Inboard cheek

Figure 4-3 shows a CAD model of the inboard cheek whilst Figure 4-4 shows the corresponding engineering drawing. The rubbing surface has again been raised 2mm above the minimum rubbing cheek thickness of 7mm. The rectangular slots were provided to accommodate the hexagonal nuts used to clamp the three pieces of the disc together. This will ensure that the bolts and nuts do not work loose due to the mechanical vibrations during brake tests. A surface finish of 3.2 µm was again specified throughout. An 8mm sheet metal of Al-6082 was used for manufacturing the inboard cheek.

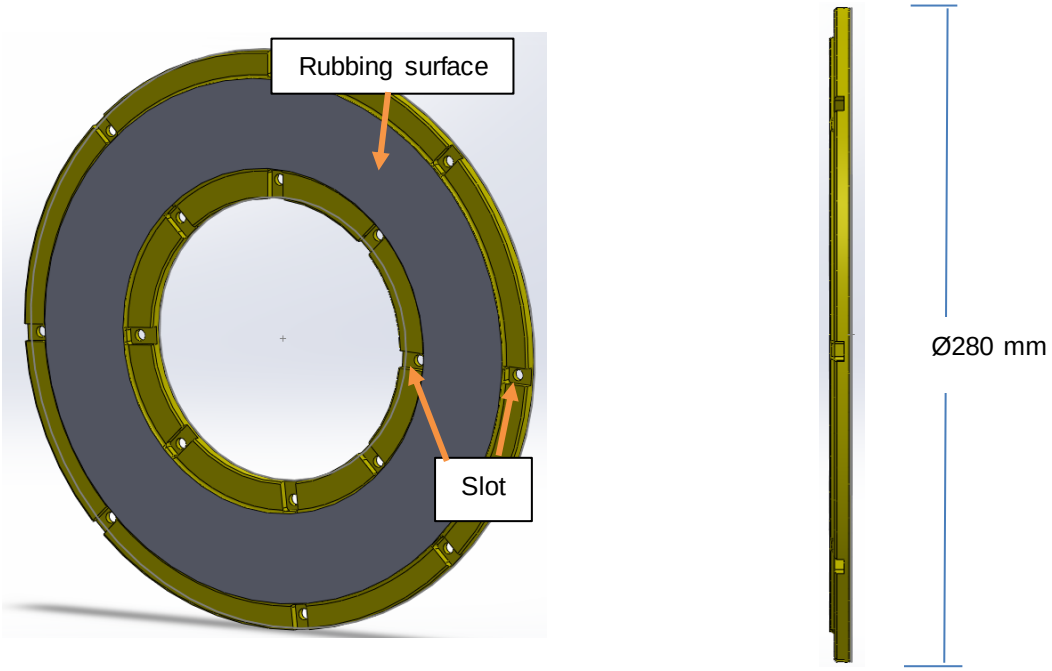

(a) Isometric view (b) Side view

(c) Elevated view

Figure 4-3: Inboard cheek

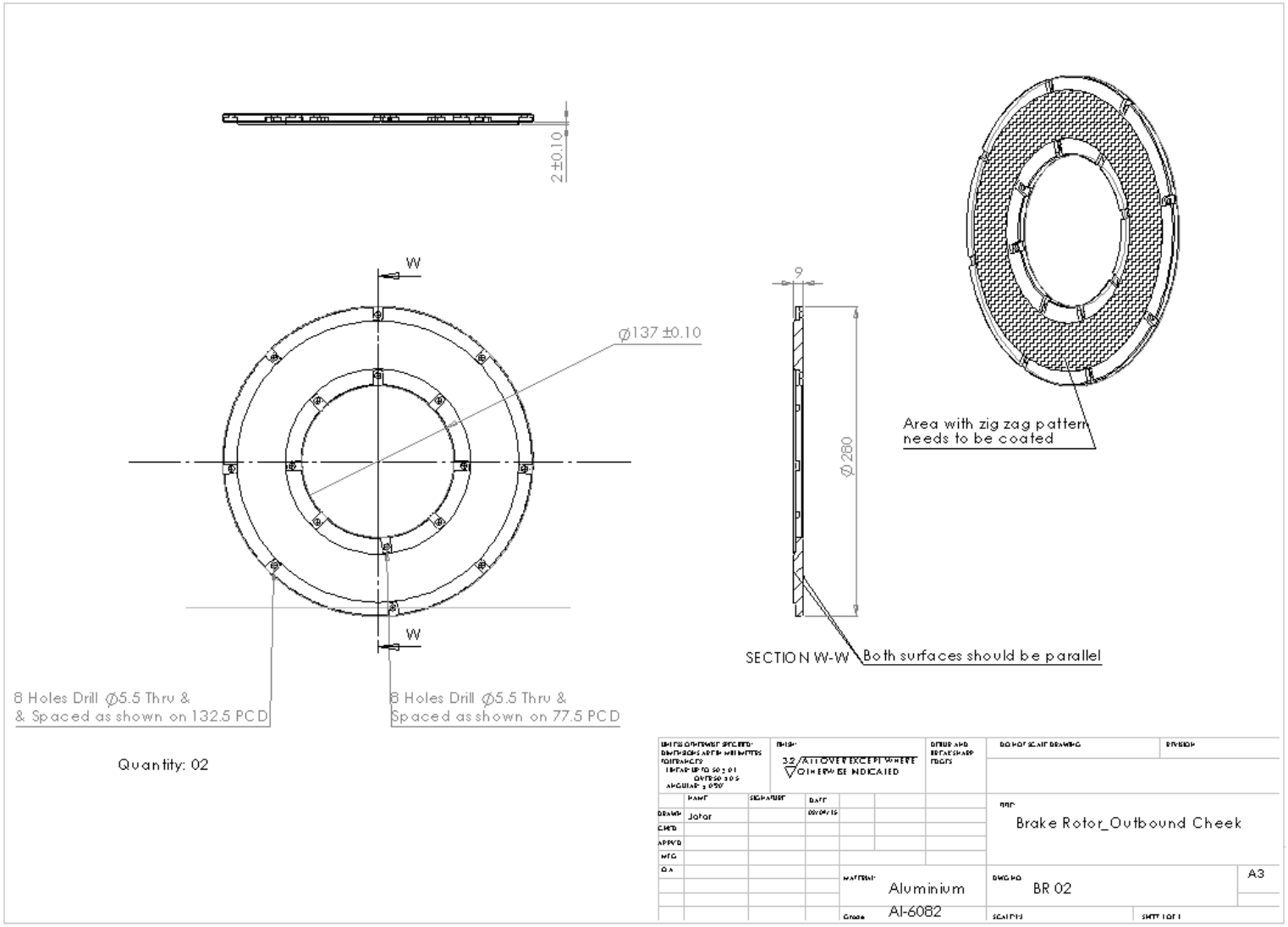

Figure 4-4: Brake rotor inboard cheek drawing

4.2.3 Inner ring containing vanes

Figure 4-5 and Figure 4-6 show the CAD model and the engineering drawing of the inner ring respectively. The total thickness of the inner ring was 7 mm of which the baseplate was 2 mm thick. 8 mm thick aluminium 6082 sheetwas used for the manufacturing of the inner ring. The inner ring was designed to provide vents for the passage of air flow. A simple radial vane configuration was selected as such vanes offer less resistance to airflow and they are also easy to manufacture and cost effective. The total number of vanes was 31. The prime number of vanes was chosen to minimise the vibrations and noise. However, the design of the inner ring is such that the number and shape of the vanes could be changed in a subsequent prototype. The selection of number of vanes depends on the heat transfer rate from the exposed surface area as well as the airflow through the vents. A large number of vanes would increase the surface area for heat dissipation but at the same time this would offer more resistance to the airflow. The vane extends from the inner radius of the ring to the outer radius. The vane width was 7.5 mm. The vane height was 5 mm.

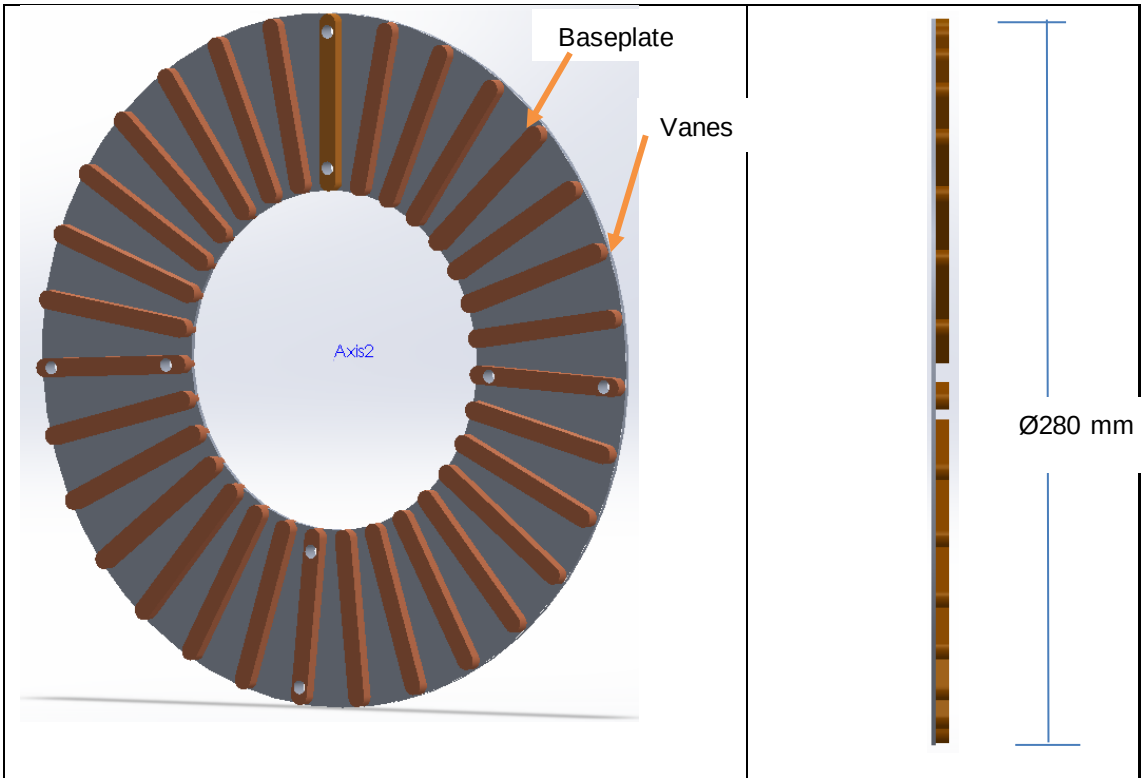

(a) Isometric view

(b) Side view

Figure 4-5: Inner ring

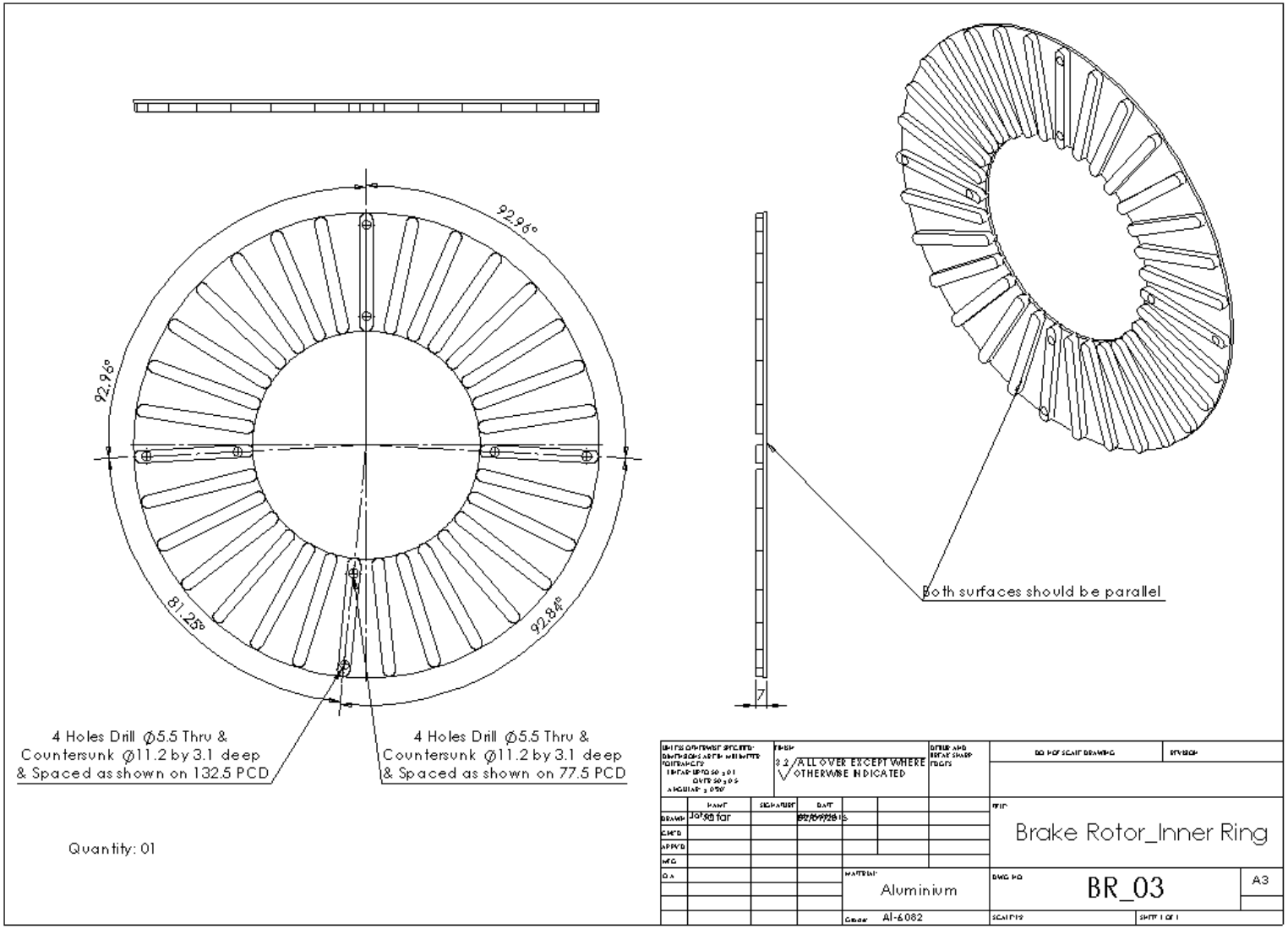

Figure 4-6: Brake rotor inner ring drawing

4.2.4 Number of pair of bolts for assembly of brake rotor

M5 steel bolts and nuts were used to fasten the three components of the brake rotor securely together. The full size brake dynamometer at the University of Leeds can apply a brake torque of up to 500 Nm. The selection of the number of bolt pairs has been made to withstand a maximum brake torque of 500 Nm.

Figure 4-7 shows the tangential forces acting on two pairs of bolts when the braking torque is applied to prototype disc brake. It is assumed in Figure 4-7 that the brake rotor is moving in the clockwise direction. The forces acting on the bolts in the outer ring are represented by F_1 and F_2 while the forces acting on the inner bolts are represented by f_1 and f_2. r_1 and r_2 are the pitch circle radii of the outer and inner bolts respectively.

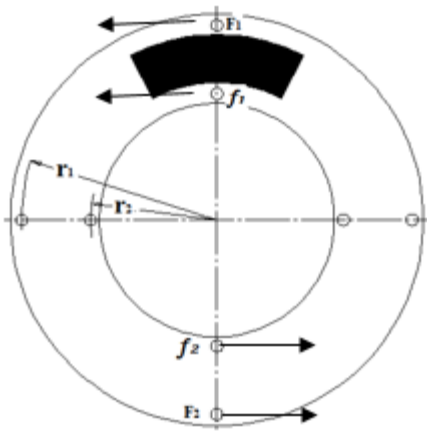

Figure 4-7: Forces action on bolts

Initially considering justtwo pair of bolts and applying equilibrium conditions:

$Maximum\ brake\ torque = 500$ Nm

$= (F_1 \times r_1 + F_2 \times r_1) + (f_1 \times r_2 + f_2 \times r_2)$ ……..…..…. (1)

$F_1 = F_2 = F_o = Forces\ on\ outer\ bolts$

$f_1 = f_2 = f_i = Forces\ on\ inner\ bolts$

We have, $r_1(F_1 + F_2) + r_2(f_1 + f_2) = 500$

or, $2r_1F_o + 2r_2f_i = 500$ ……..…..(2)

$If\ n = no.of\ pairs\ of\ bolt\ then\ above\ equation\ can\ be\ written\ as$

$n(r_1F_o + r_2f_i) = 500$

We have, $r_1 = 0.130m, r_2 = 0.065m$

Therefore, $n(0.130F_o + 0.065f_i) = 500$ ……...…….… (3)

Allowable shear stress for steel in bolts = $\tau = 70\ MPa$

The allowable shear stress was calculated according to distortion –energy theory i.e. 0.577 of the tensile yield strength of mild steel bolt plus for a factor of safety of 2. (Budynas et al., 2015)

For Outer bolts, $\tau = \frac{F_o}{A_o} = 70 \times 10^6\ Pa$

Therefore, $F_o = 70 \times 10^6 A_o$

For inner bolts, $\tau = \frac{f_i}{A_i} = 70 \times 10^6\ Pa$

Therefore, $f_i = 70 \times 10^6 A_i$

Simplifying and putting values of F_o and f_i in equation (3)results in:

$$n \times 10^6(9.1A_o + 4.6A_i) = 500$$

In terms of diameter of the bolts (d_o & d_i), the above equation becomes,

$$n = \frac{0.002}{\pi(9.1d_0^2 + 4.6d_i^2)}$$

Assuming M5 bolts are used throughout, $d_o = d_i = 4mm$

Then, $n \cong 3$

Therefore, four pairs of bolts are more than sufficient to resist the maximum braking torque.

Because of the geometry of the vanes, the bolt hole are not placed precisely 90° apart.

4.2.5 Coating of the rubbing surfaces of Inboard and outboard cheeks

PEO coating of the inboard and outboard rubbing surfaces was applied by the Keronite Company. The masking of the surfaces of the inboard and outboard cheeks and all other surfaces was carried out to ensure that only the rubbing surface were coated. The PEO coating has high thermal resistance and if applied to all surfaces then it will restrict heat convection from these surfaces. Figure 4-8 shows the masked inbound and outbound cheeks. The green Suprawax masking was applied as close as possible to the rubbing surfaces.

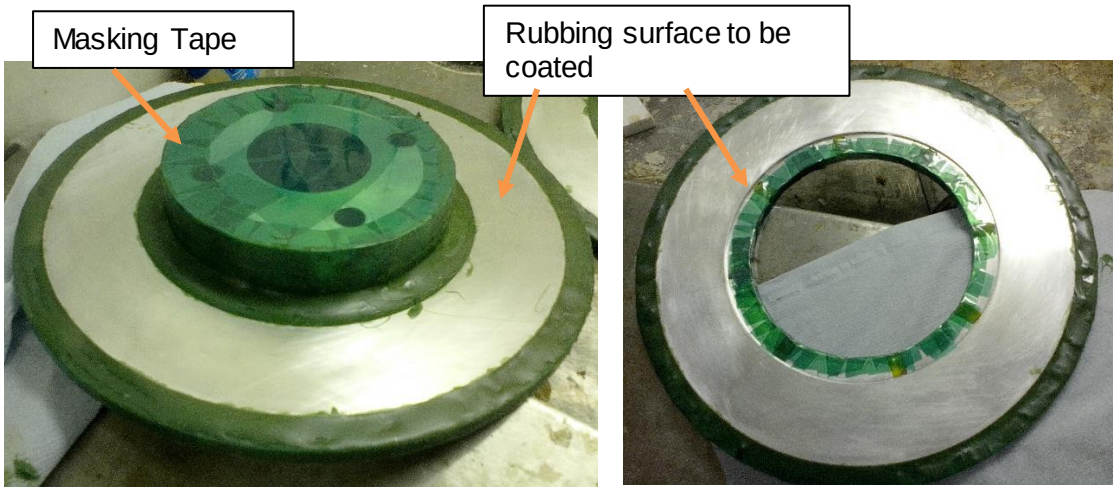

(a) Outboard cheek (b) Inboard cheek

Figure 4-8: Masking of Outboard and inboard Cheeks

A nominal 50 µm thick PEO coating was applied to each rubbing surface. Before the treatment, the cheeks were degreased by spraying acetone on the rubbing surface and then rinsing it with water. The apparatus for the PEO process consist of a water cooled electrolyte container with a low concentrated alkaline solution. The masked cheeks were immersed in the container and acted as an anode while the stainless steel container acts as a cathode. A potential difference of over 200 volts was applied during the process. This high anodic voltage triggers the micro discharge event at the electrolyte-cheek interface generating high instantaneous temperature and pressure. The occurrence of discharge resulted in plasma chemical reaction that contributed towards the formation of an oxide layer (alumina) on the surface of the Al-6082 aluminium alloy.

The PEO coated rubbing surfaces are shown in Figure 4-9.

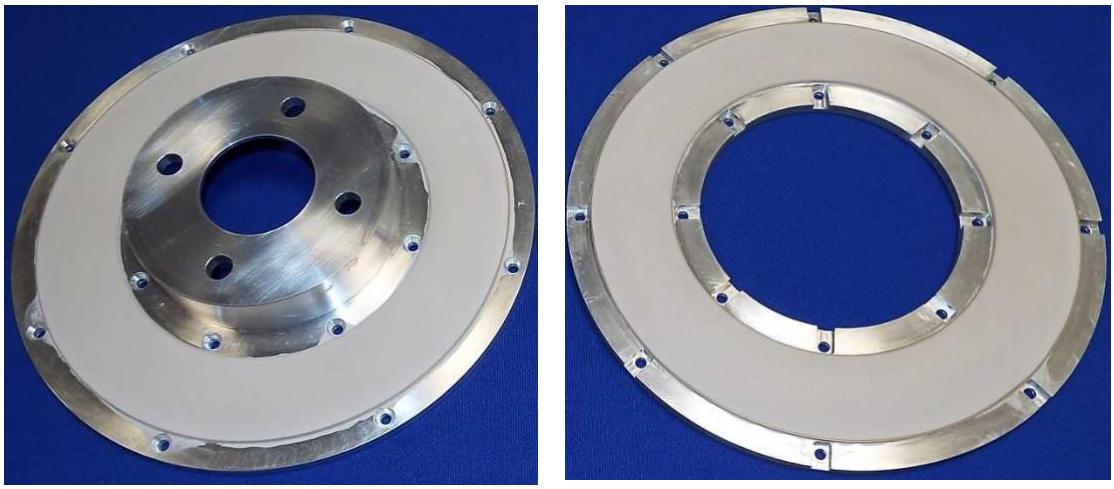

(a) Outboard Cheek (b) Inboard Cheek

Figure 4-9: PEO coated Inboard and outboard cheeks of aluminium Brake rotor

4.2.6 Assembly of brake Rotor

All three components of the brake rotor were manufactured in the workshop facility at the University of Leeds. Countersunk head M5 socket bolts of 20 mm in length were used for the assembly. Figure 4-10 shows the assembled brake rotor. Brake rotor were mounted on brake dynamometer which is discussed in next chapter along with the specially designed brake pads for working with coated rotor. The brake pads were provided by TMD Friction Inc.

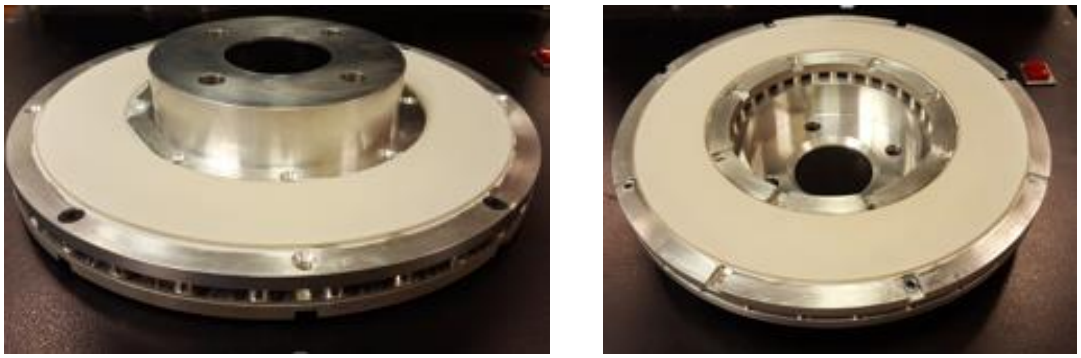

Figure 4-10: Assembled Brake rotor

4.3 Finite element model of a coated ventilated brake rotor

4.3.1 Development of finite element model

A three dimensional (3D) finite element model of a brake rotor was created using Abaqus software to predict the thermal performance of the novel PEO coated ventilated aluminium alloy brake rotor. Owing to the cyclic symmetry of the brake rotor, only a section of the brake rotor, containing one complete vane was model to save the computational time as shown in Figure 4-11. The main objective is to develop a model that can simulate the real braking events and validating the brake rotor model results against the experimental results. In this chapter, the development of the FE model is discussed along with the measurement of the effect of coating thickness and convective heat transfer coefficient.

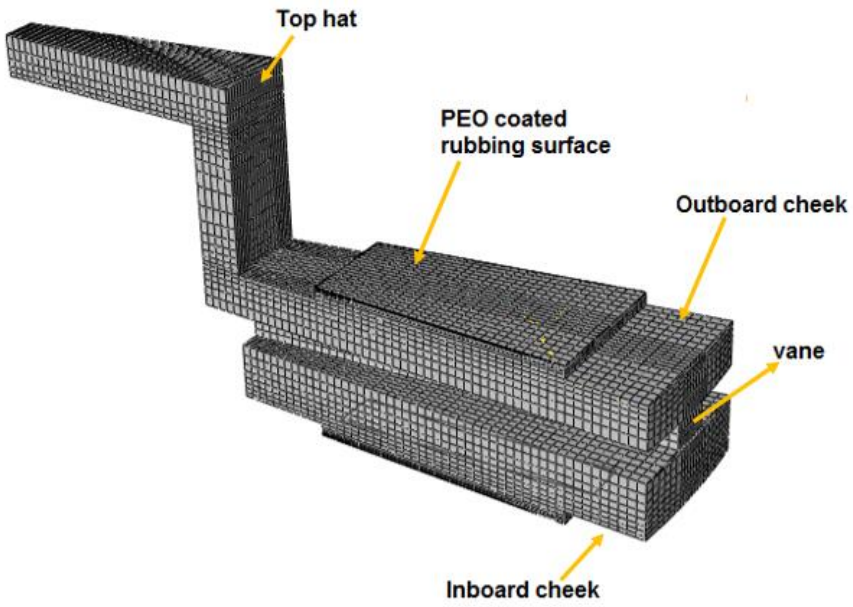

Figure 4-11: PEO coated ventilated brake rotor model

The FE model was used to simulate the drag brake conditions.

A 50µm thick PEO coated rubbing surface was specified in order to study the profile of heat transfer through the coating thickness. The heat flux applied to the rubbing surface was initially estimated by assuming a coefficient of friction value

of 0.5 between the friction pair and the brake rotor's rubbing surface. The heat flux was calculated as shown below:

$$q = T\,w$$

$$q = \frac{2\pi\mu NPAR_{eff}}{60A_{rubb}}$$

Where,

$q = heat\ flux, \frac{W}{m^2}$

$w = angular\ rotation, \quad {}^{rad}/_{S}$

$\mu = coefficient\ of\ Friction$

$N = rotational\ speed, \quad rpm$

$P = hydraulic\ pressure, \quad Pa$

$A = area\ of\ piston, m^2$

$R_{eff} = mean\ effective\ rubbing\ radius, m$

$A_{rubb} = surface\ area\ of\ mean\ rubbing\ surface, m^2$

The heat absorbed by the brake rotor was taken as 93% of the total heat dissipated during the braking event (Talati, 2009). Different coefficients of convective heat transfer were specified at the surfaces exposed to the surroundings which were assumed to be a constant temperature of 20℃.

Material properties applied to the FE model are indicated in Table 4-1. Material properties indicated in Table 4-1 were assumed to be isothermal and represent the typical values used in braking applications.

Material	Conductivity W/m²K	Density kg/m³	Elastic Modulus GPa	Specific Heat J/kgK	Expansion Coefficient K⁻¹
Al-6082 (Substrate)	180	2700	70	800	8.2E-06
PEO Coating	1.6	2700	212	800	2.4E-05

Table 4-1: Material properties of Al-6082 alloy and PEO coating

4.3.2 Mesh Sensitivity Study

Mesh sensitivity study (MSS) of a FE model is essential to obtain an accurate temperature distribution as well as for reducing the computational time. The model was meshed with 8-noded standard linear heat transfer brick elements (DC3D8). A sub-model was generated for carrying out the MSS as shown in Figure 4-12. Initially, various mesh configurations were assigned to the sub-model by altering the size of elements. The maximum temperature at certain nodes for each mesh density was compared. Figure 4-13 shows the maximum temperature obtained for various mesh densities of the sub-model. It can be seen that convergence in maximum temperature has taken place at a mesh density of 8525 elements.

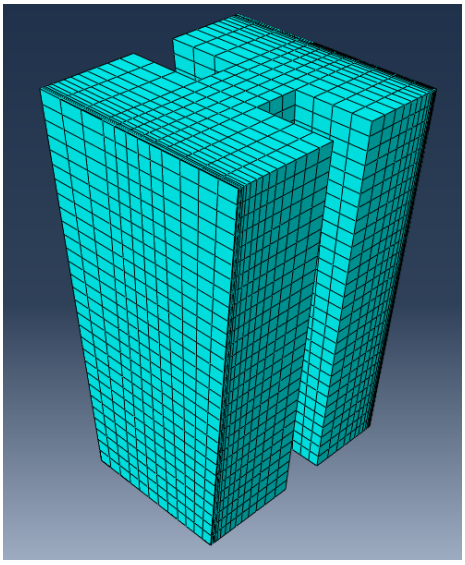

Figure 4-12: A sub-model for mesh sensitivity study

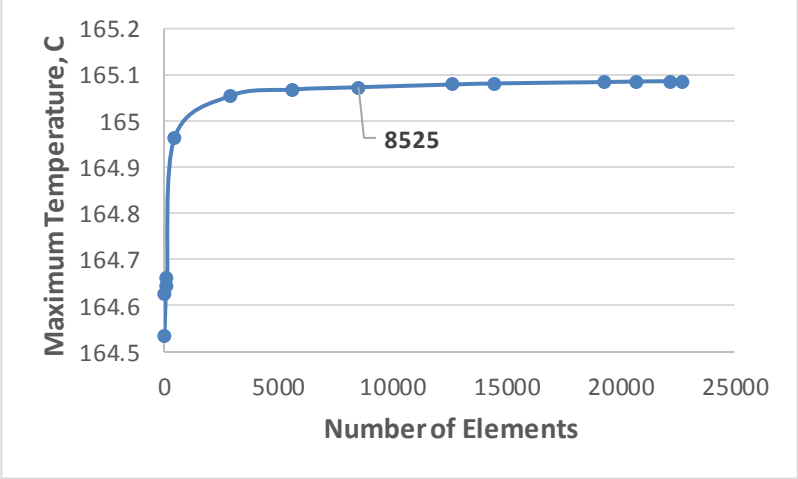

Figure 4-13: Maximum temperature for various mesh densities

In a similar manner, suitable mesh densities were determined for the individual components of the coated rotor such as along the coating thickness, inboard cheek, outboard cheek and the vanes. The model was run for various mesh densities and the following number of elements were found to be suitable along the thickness of the coated rotor:

1. Number of elements through the coating = 3
2. Number of elements through 2mm thick area = 10 (single biased 40)
3. Number of elements through 9mm thick area = 8 (single biased 2.5)
4. Number of elements through 7mm thick area = 6 (single biased 2.5)
5. Number of elements through 5mm vane = 8 (single biased 2.5)

The total number of elements for the whole model was 14355.

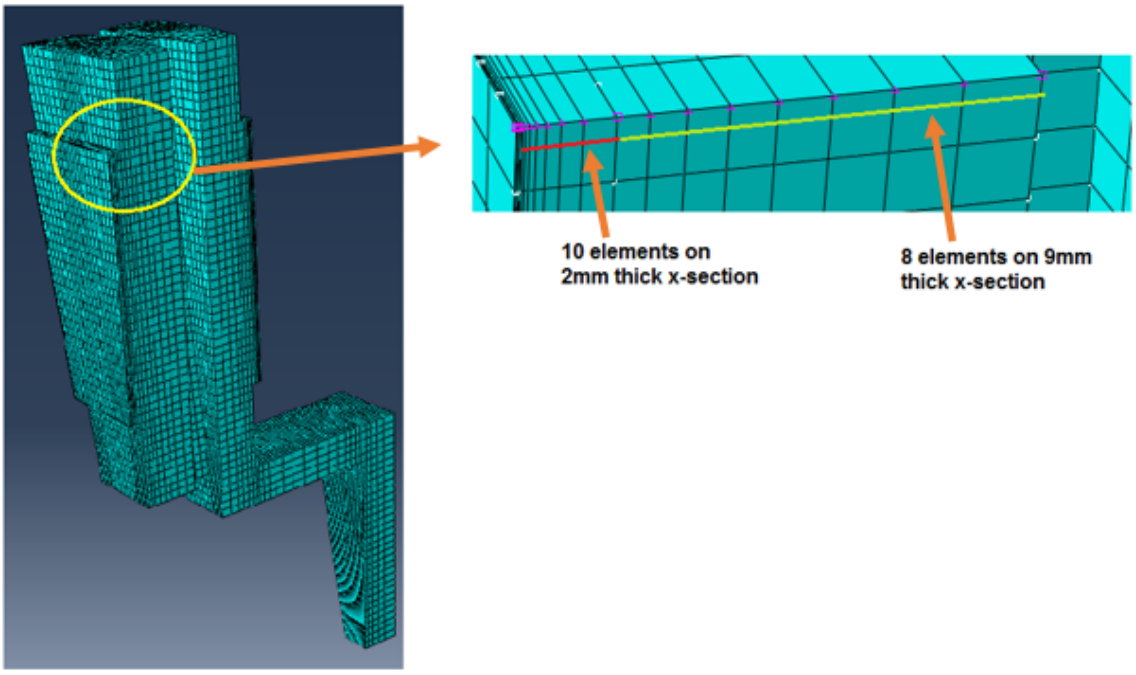

Figure 4-14: Elements configuration along the thickness of the coated rotor

Because of the difference in the thickness of the coating and the substrate, elements were arranged using a biasing ratio along the thickness of the rotor to apply uniformly increasing element size as shown in Figure 4-14.

4.3.3 Effect of coating thickness on heat transfer

A constant heat flux of 5×10^5 W/m^2 was applied on the rubbing surface to study the effect of various coating thicknesses on the heat transfer through the coating. The heat flux was calculated assuming a rotational speed of 440 rpm which corresponds to a vehicle speed of 100 Km/h.

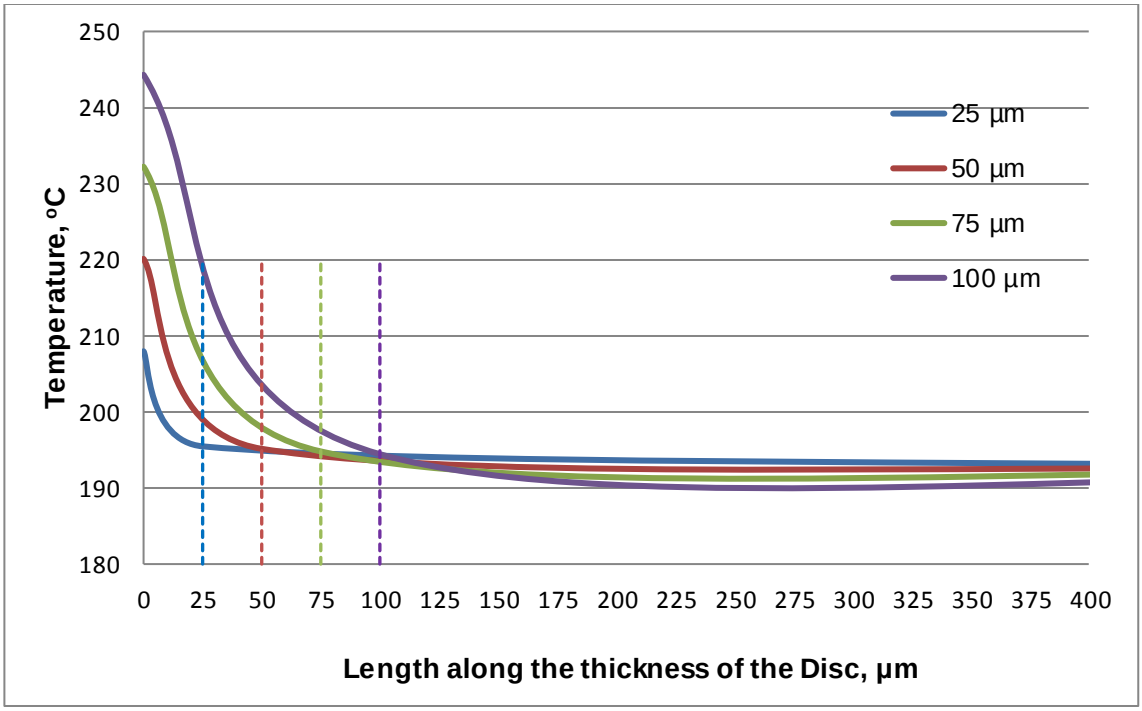

Figure 4-15: Effect of coating thickness on heat transfer

It can be seen from Figure 4-15 that the thickness of the coating has a very minimal effect on the temperature of the substrate which for this brake application was about 195℃ for all coating thickness. The higher the thickness, the higher will be the cost of the coating. Therefore, the chosen coating thickness of 50µm allows for a certain amount of wear which still acting as a sufficient thermal barrier.

4.3.4 Effect of convective heat transfer coefficient on temperature

The 3D FE model was run for different convective heat transfer coefficients. It was found that the convective heat transfer coefficient has a significant influence on the heat dissipation from the brake rotor as shown in Figure 4-16. The most suitable heat transfer rate coefficient was therefore chosen for simulating the dynamometer tests based on the result from these tests (see Chapter 5).

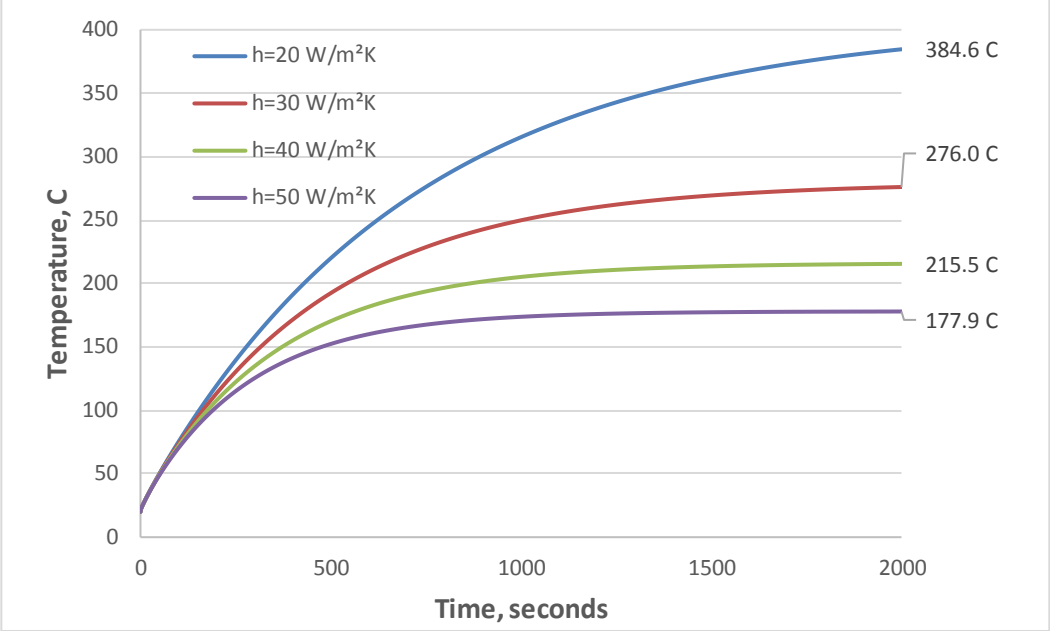

Figure 4-16: Effect of convective heat transfer coefficient on maximum temperature

4.4 Summary

In this chapter, a novel design of a PEO coated lightweight ventilated brake disc's rotor along with the development of the 3D FE model for numerical analysis of this rotor were discussed. The dimensions of the brake rotor were kept close to the conventional ventilated brake rotor of a small-medium passenger car. The brake rotor consists of three parts: outbound, inbound and inner ring. All these three parts were manufactured in the University of Leeds workshop from Al-6082 alloy. PEO coating was applied on the rubbing surfaces of the inbound and outbound cheeks. The experimental results of the dynamometer tests of this brake rotor are discussed in Chapter 5.

Chapter 5

Dynamometer testing and validation of finite element model of lightweight PEO coated ventilated brake disc

5.1 Introduction

In this chapter, the experimental procedures and results of the dynamometer tests on the lightweight PEO coated ventilated brake disc are presented. The tests were conducted on the Leeds 45 kW brake dynamometer. The main aim of the dynamometer testing is to evaluate the thermal performance of the coated brake rotor. A drag brake test condition was employed. A drag brake test assumes a condition in which a vehicle is descending a hill at a constant speed with a constant applied brake pressure. LabVIEW software was used for monitoring and controlling the test parameters. The pressure and torque transducers and the sliding thermocouple were calibrated prior to their use in the programme of testing.

Section 5.6 of this chapter discusses the numerical results. The 3D Finite Element model was developed using Abaqus software. Different assumptions based on the experimental results were applied to the FE model and the results were compared with the experimental findings to enable the validation of the FE model.

5.2 Brake dynamometer

Figure 5-1shows the layout of the Leeds full scale brake dynamometer. The brake dynamometer allows the user to apply different braking condition at various disc brake contact pressures and rotational speeds. The brake dynamometer consists of two main systems: the drive rig and the data acquisition and control system.

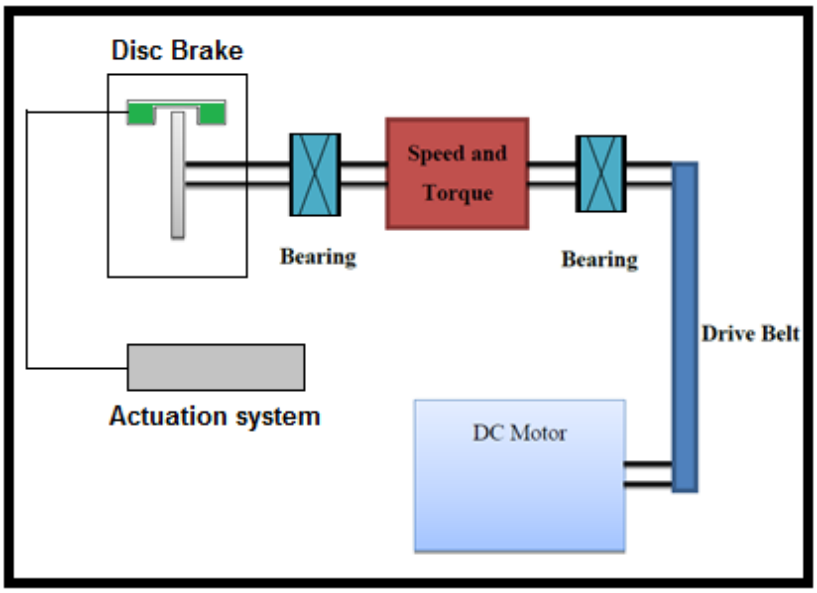

Figure 5-1: General layout of the Leeds full scale brake dynamometer

Figure 5-2 shows a photograph of the brake dynamometer at the University of Leeds. The Leeds dynamometer consist of the following components:

1. Electric motor (45 kW maximum power)
2. Torque transducer (able to measure up to 500 Nm of brake torque at a maximum rotating speed of 1500 rpm) (Torquemaster TM 213)
3. K-type sliding thermocouple
4. Hydraulic pressure system and pressure transducer (able to measure up to 50 bars of hydraulic pressure)
5. Data acquisition system (LabView software)

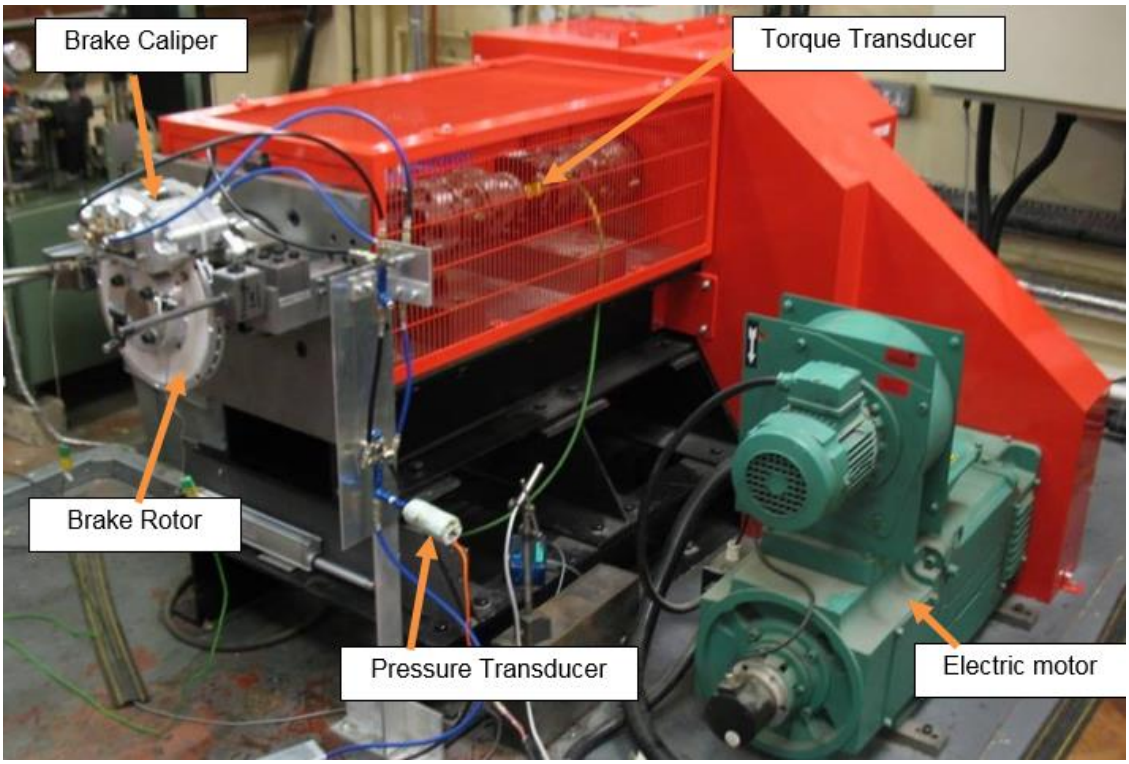

Figure 5-2: Leeds Brake Dynamometer

The Leeds dynamometer can be used for simulating vehicle braking conditions for both disc brakes and drum brakes. The disc brake contact pressure is applied by the actuation system shown in Figure 5-3. The actuation system is capable of applying different pressures on both trailing and leading edges of the brake pad although this feature was not used for the current tests. The hydraulic pressure for a specific brake test is set manually using a lever shown in Figure 5-3. A small adjustment screw beneath the lever is used to keep the pressure constant during a brake test. The maximum motor speed is 1500 rpm and this limits the variability of the test conditions that can be stimulated. Two sliding thermocouples as shown in Figure 5-4 were used to measure the temperatures on the mean rubbing surface of the coated disc just before and just after it contacts the brake pad during a brake test. The torque meter is used to measure the applied torque and this value of torque along with the known hydraulic pressure are used to evaluate the average coefficient of friction between the brake rotor and the friction pads assuming the centre of pressure is at the mean rubbing radius.

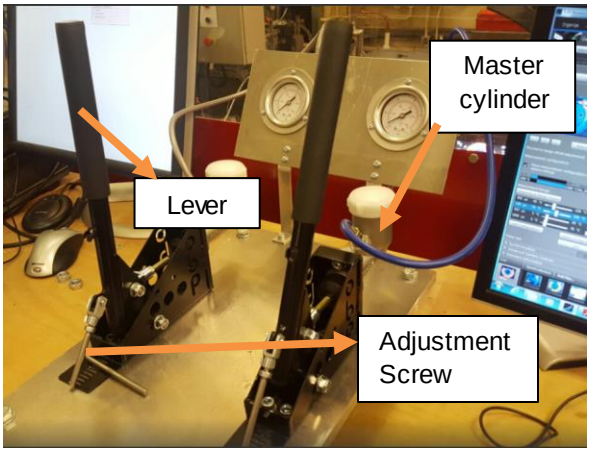

Figure 5-3: Actuation system

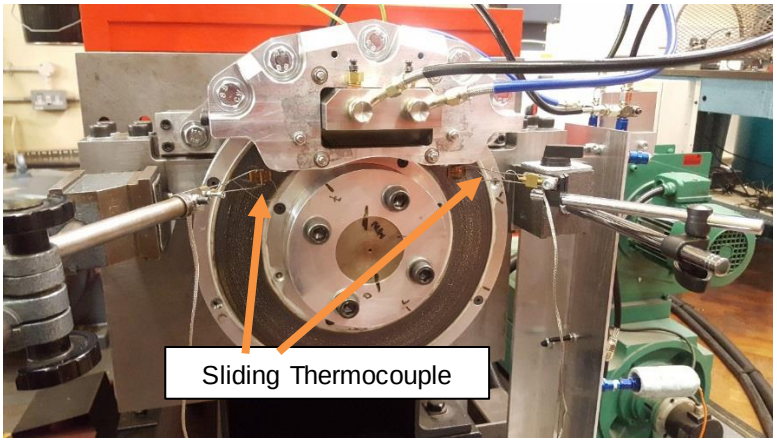

Figure 5-4: Sliding Thermocouples

An in-house developed LabView data acquisition program was used to monitor the test parameters. The user can control the hydraulic pressure and the rotating speed of the brake rotor independently. The software stores the measured surface temperature, brake torque, hydraulic pressure and motor speed in a single file that can be downloaded for further processing.

For safety purpose, the brake dynamometer is placed in a cage with a safety door which has to remain closed while running the tests. In addition, an emergency stop button is available for turning off the motor in case of emergency.

5.3 Transducer calibration

Calibration of the transducers was carried to ensure confidence in the test results from the brake dynamometer. The main goal was to remove uncertainty in the output from the transducer and establish linearity.

5.3.1 Calibration of thermocouples

K-type rubbing thermocouples were used to measure temperatures of the disc rubbing surface. A thermocouple works on a principle that when two different types of metallic wires are joined together and exposed to a temperature difference, a potential difference is generated. Figure 5-5 shows the K-type rubbing thermocouple (Type K standard version 401-130) used in these tests. This is a specially designed thermocouple for monitoring the rapidly changing temperatures in braking applications. The maximum temperature that can be measured is 850℃ with an accuracy of ±1.5℃.

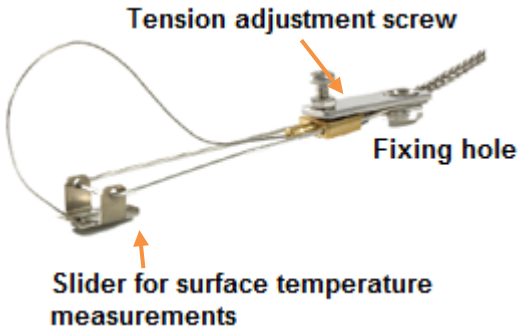

Figure 5-5: K-type rubbing thermocouple (TC direct Catalogue)

The in-house data acquisition system has a capability of measuring temperatures at four different locations at a time during the test. However, only two were used for the current tests. Each thermocouple was calibrated by placing the thermocouple in boiling water and in an ice tub. The values of temperatures from the LabView software and a hand-held infrared thermometer were compared with the expected values of 100℃ and 0℃. The necessary adjustments in gain and offset were made in LabView code to ensure an accurate calibration.

5.3.2 Calibration of pressure transducer

The pressure transducer (Druck PMP 317-2489) was calibrated using the Budenberg hydraulic dead-weight tester shown in Figure 5-6. This simple dead-weight tester consists of an oil reservoir, a weight connected to a piston to apply a known pressure and an external port for connecting the transducer to be calibrated. The weights are placed on the piston of known cross-sectional area. The screw pump is then used to adjust increase the pressure until the piston starts floating. After the system becomes stable, the pressure values are recorded and used in the calibration.

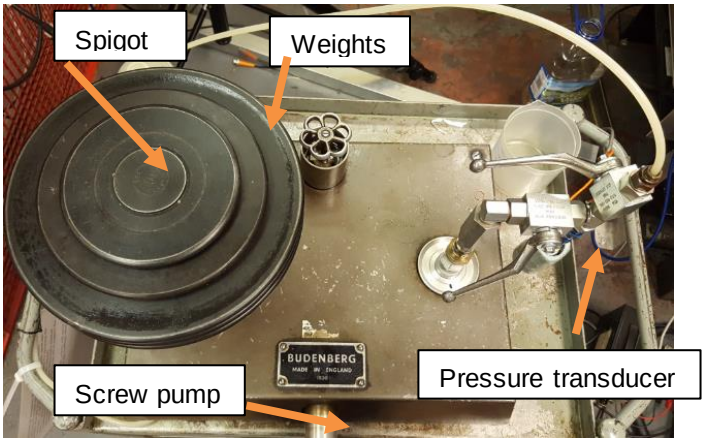

Figure 5-6: Hydraulic dead-weight Tester

The brake dynamometer's pressure transducer was mounted on the dead-weight tester. For each known hydraulic pressure applied on the tester, the output voltage values were recorded in the LabView program. The pressure transducer has an output voltage range from 7 to 30 volts according to the data sheet. The range of pressure applied is from 0 to 50 bars. The voltage values were recorded for a number of pressures both while adding and removing the weights. A linear regression was used to find the best fit relationship between the recorded voltage and hydraulic pressure as shown in Figure 5-7. The resulting linear equation was then used to convert the output voltage to line pressure during the brake tests. The pressure transducer has an accuracy of ±0.15% according to the equipment data sheet.

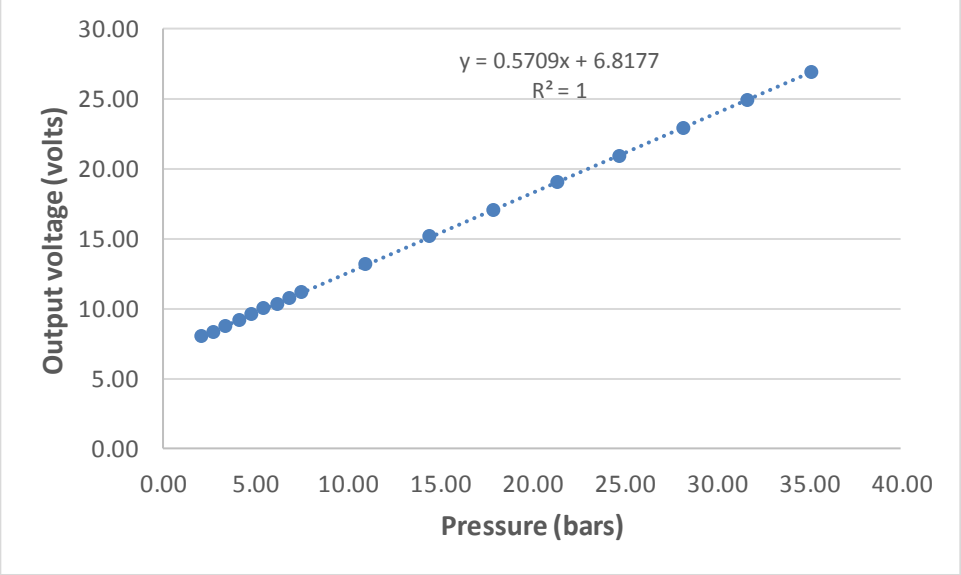

Figure 5-7: Linear regression between output voltage and hydraulic pressure for pressure transducer calibration

5.4 Disc thickness variation and brake rotor lateral runout

Disc thickness variation (DTV) and the brake rotor side runout (SRO) are the two main reasons behind cyclic torque fluctuations of a disc braking system. DTV and SRO are also responsible for increasing the non-uniformity of wear for both rotor and pad surfaces. DTV was measured with a micrometer along the mean disc rubbing surface. Shims were then used to minimize the DTV. The shims were placed in the middle of the vanes beneath the disc rubbing surface at the circumferential positions where minimum thickness was measured. In conventional disc brake systems, the rotor rubbing surfaces are ground to keep DTV to a minimum level. In the current coated rotor design, as the coated surface cannot be ground due to the small thickness of the coating so instead the rotor can be dissembled to allow the shims to be inserted.

SRO mainly arises due to the improper mounting of the top hat on the hub for example due to a rough or rusted hub surface. SRO was checked with a displacement dial indicator as shown in Figure 5-8. The probe of the dial indicator was placed against the outboard surface of the top hat of the rotor as a minute variation between the top hat and hub surface will lead to give a larger runout at the rubbing surface.

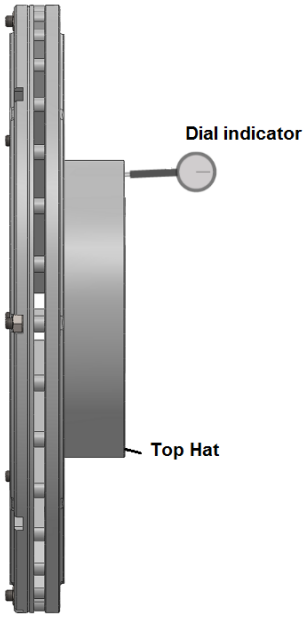

Figure 5-8: Rotor side runout measurement

Before measuring the SRO, the brake rotor was rotated multiple times to locate the position where the deviation of dial indictor is minimum. The dial indicator was set to zero on that location. The runout was recorded during one revolution of the rotor at fixed angular displacements of 22.5°. Positions were marked on the top hat where there was need for a shim to be placed for minimizing the SRO. Shims were then placed in between the top hat and the hub at the position of maximum SRO. Shims of different sizes were tried to keep the runout as low as possible. Figure 5-9 shows the measured values of runout at this position without a shim, with a 0.05 mm shim and with a 0.10 mm shim. The 0.10 mm shim gives a negligible amount of runout and so was used for all subsequent tests.

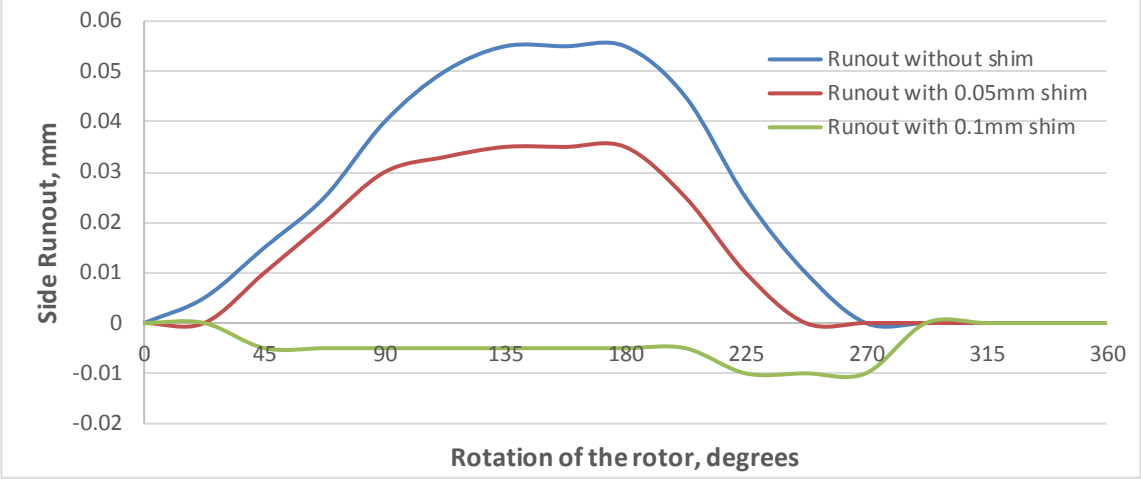

Figure 5-9: Side runout of coated rotor

5.5 Experimental procedures

The thermal performance of the novel PEO coated ventilated aluminium alloy brake rotor was evaluated against the custom friction pads supplied by TMD Friction Ltd. They were specially formulated pads designed to work with the coated alumina surfaces in the current research. The experimental investigations were carried out under drag brake conditions. The test matrix was derived from the guidelines of Society of the Automotive Engineer (SAE) J212 procedure as shown in Table 5-1. SAE J212 requires the bedding in test before the commencement of actual brake test using constant g stops. The coefficient of friction was monitored for all the tests and showed good consistency which gave the researchers confidence that this test matrix was appropriate even though the bedding-in test was carried out under drag tests. This was done because of unavailability of dynamometer to work under constant g stop condition.

All tests were repeated three times. Due to health and safety problems related to the release of fumes within the lab, the test matrix was designed to keep the maximum rubbing surface temperature under 300℃.

Bedding-in tests were carried out to establish a full contact between the new coated brake rotor and new friction pads and to burnish the pads as indicated in Table 5-1. During the bedding-in process, a uniform transfer layer of brake pad material was deposited on the brake rotor rubbing surface as shown in Figure 5-10. Initial tests during the bedding-in process were limited to a 100℃ rise in

disc surface temperature. However for the actual drag brake tests, the tests were continued until the temperature was stable and no more significant rise of temperature was monitored.

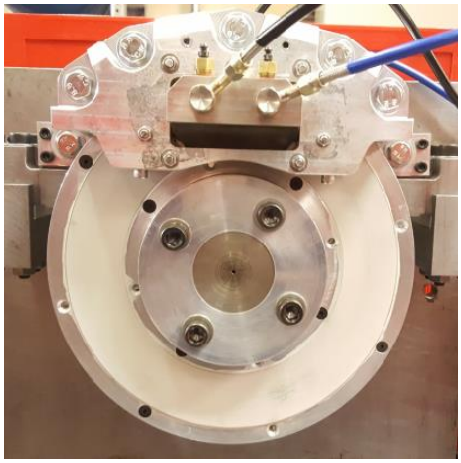

(a) Before Bedding-in test

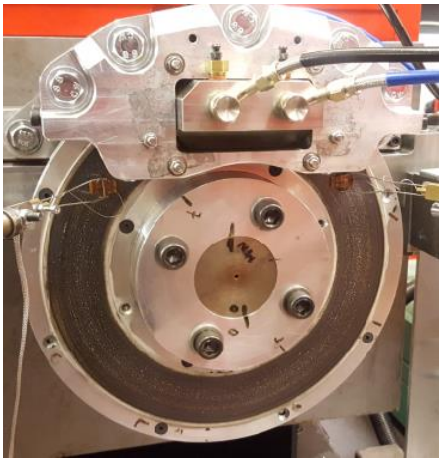

(b) After Bedding-in test (showing formation of transfer layer on disc rubbing surface)

Figure 5-10: Bedding-in process

Test No.	Test Name	Rotation speed (rpm)	Hydraulic Brake Pressure (bar)	Mean Sliding Speed (m/s)	Mean Contact Pressure (MPa)
1	Bedding-in	100	5	1.1	0.2
2	Bedding-in	200	5	2.2	0.2
3	Bedding-in	300	5	3.29	0.2
4	Bedding-in	300	5	3.29	0.2
5*	Drag Brake	90	5	0.99	0.2
6*	Drag Brake	90	7.5	0.99	0.3
7*	Drag Brake	90	10	0.99	0.4
8*	Drag Brake	270	10	2.97	0.4
9**	Drag Brake	90	10	0.90	0.4

Table 5-1: Test matrix

* test conducted on PEO coated Al-6082 rotor

** test conducted on GCI (grade 220)

The test parameters were chosen in view of the limitations imposed by the dynamometer motor power, measuring range of the torque meter and pressure transducer and the imposed maximum temperature limit as discussed above. Initial calculations were carried out based on the assumption that the maximum coefficient of friction between the brake rotor and the friction pads was 0.6. Table 5-2 summarises the calculation of brake power required for various combinations of hydraulic pressure and rotational speed of the dynamometer. The mean rubbing radius of the disc was assumed to be 105 mm and friction pad area was 1267 mm^2. It can be seen that the maximum hydraulic pressure and the rotational speed that can be applied during the test to remain within the 45 kW motor power limit were 30 bar and 900 rpm respectively. The extent of the test range further decreased due to the imposed limitations on the maximum rotor surface temperature during a test of not more than 300℃.

The conventional solid Fiat Punto GCI brake rotor was also tested (Test 9) with the same friction material as used for the coated rotor for the purpose of comparison under the same conditions as for Test 7 in Table 5-1.

Pressure (Bars) / RPM	**5**	**10**	**15**	**20**	**25**	**30**
90	0.8	1.5	2.3	3.0	3.8	4.5
180	1.5	3.0	4.5	6.0	7.5	9.0
270	2.3	4.5	6.8	9.0	11.3	13.5
360	3.0	6.0	9.0	12.0	15.0	18.1
450	3.8	7.5	11.3	15.0	18.8	22.6
540	4.5	9.0	13.5	18.1	22.6	27.1
630	5.3	10.5	15.8	21.1	26.3	31.6
720	6.0	12.0	18.1	24.1	30.1	36.1
810	6.8	13.5	20.3	27.1	33.9	40.6
900	7.5	15.0	22.6	30.1	37.6	45.1

Table 5-2: Estimated brake power in kW for different combinations of rotational speed and applied pressure

5.6 Experimental results

5.6.1 Coefficient of friction

Figure 5-11 shows the variation of the measured coefficient of friction with time during Test 5, Test 6 and Test 7 as defined in Table 5-1. Due to the high frequency fluctuations in the torque data, the moving average trendline option in Excel was used to clearly show the trend for coefficient of friction. The hydraulic pressure was manually controlled to keep the pressure to specified values shown in Table 5-1 for each test. This is the main reason in the fluctuation of coefficient of friction value. It can be seen that all three tests showed the same trend. In the initial stages of test, the coefficient of friction varied significantly and as the test progressed, it reached a stable value of about 0.5. The applied hydraulic pressure had a significant effect on the rate of change in coefficient of friction during the test. At an applied pressure of 5 bars, the coefficient of friction attained a stable value after approximately 1700 seconds. However, in the subsequent tests with higher pressures, the coefficient of friction took less time to attain a stable value. This was primarily due to the partial removal of the transfer layer at the start of each test. The thermal fade phenomena which usually occurs at elevated temperature was not as significant as for the conventional GCI brake rotor. The coefficient of friction- time history plot for which is shown in Figure 5-12. The test was conducted under same conditions as defined in Table 5-1 for Test 7. The effect of thermal fade on friction coefficient is quite evident in this test.

By comparison of Figure 5-12 with Figure 5-11c, it can be seen that the coefficient of friction for the PEO coated ventilated aluminium alloy brake was found to be higher and more stable than for the conventional GCI rotor under the same conditions. Both PEO coated and GCI discs attained the maximum coefficient of friction of almost 0.5 during the test nearly at the same time. It was noticed that the PEO coated disc maintained nearly the constant coefficient of friction profile till the end of the Test. On the other hand, the GCI disc has shown an appreciable change in coefficient of friction as shown in Figure 5-12.

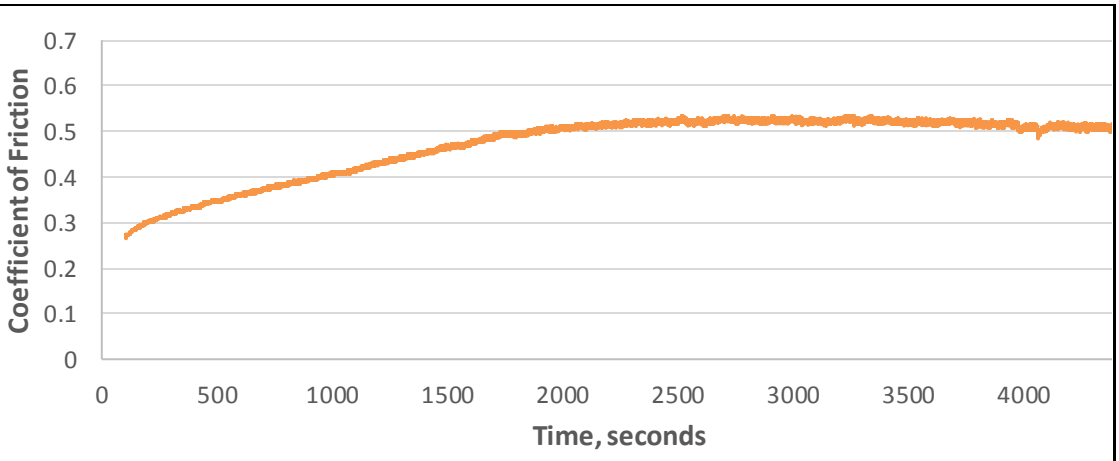

(a) Test 5 (90rpm & 5 Bars)

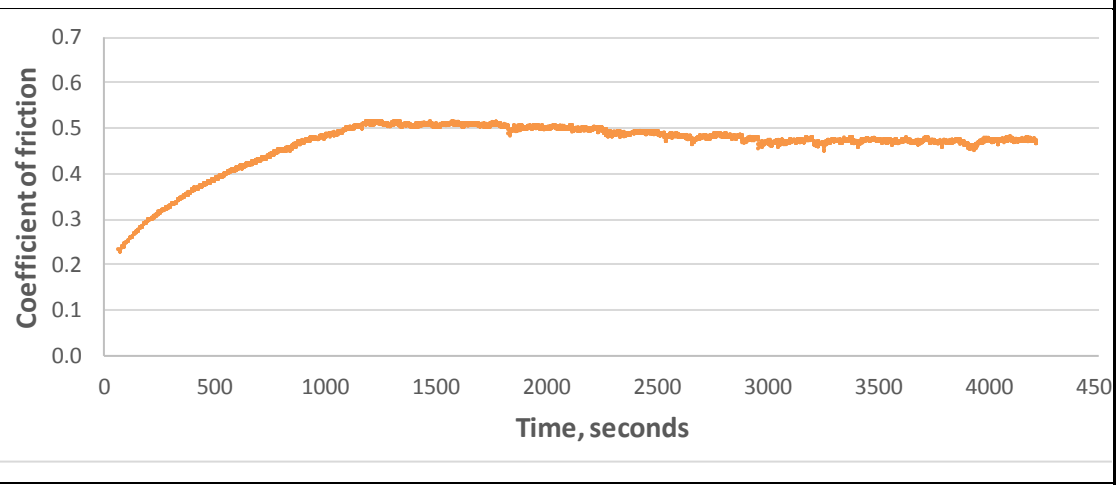

(b) Test 6 (90rpm & 7.5 Bars)

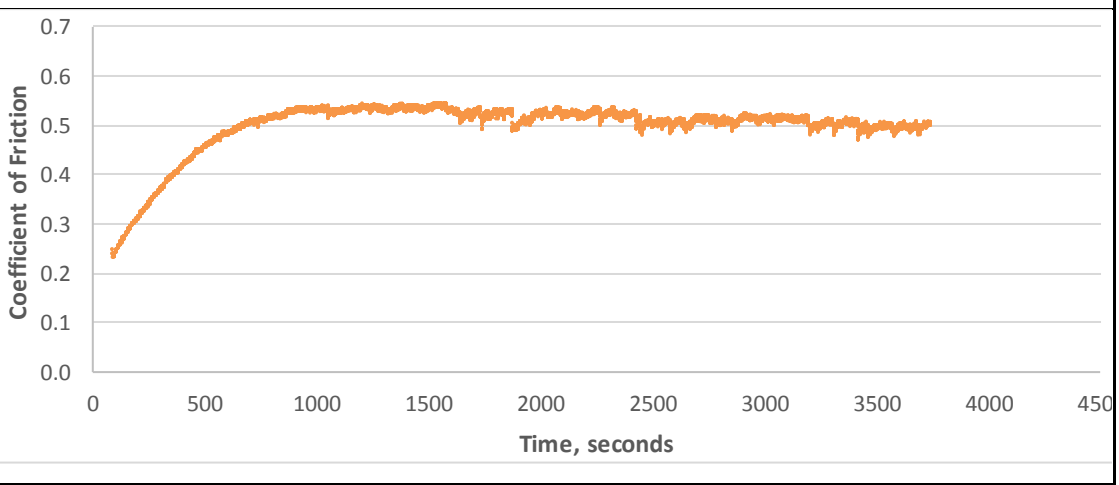

(c) Test 7 (90rpm & 10 Bars)

Figure 5-11: Coefficient of Friction-time history plot for coated ventilated brake rotor

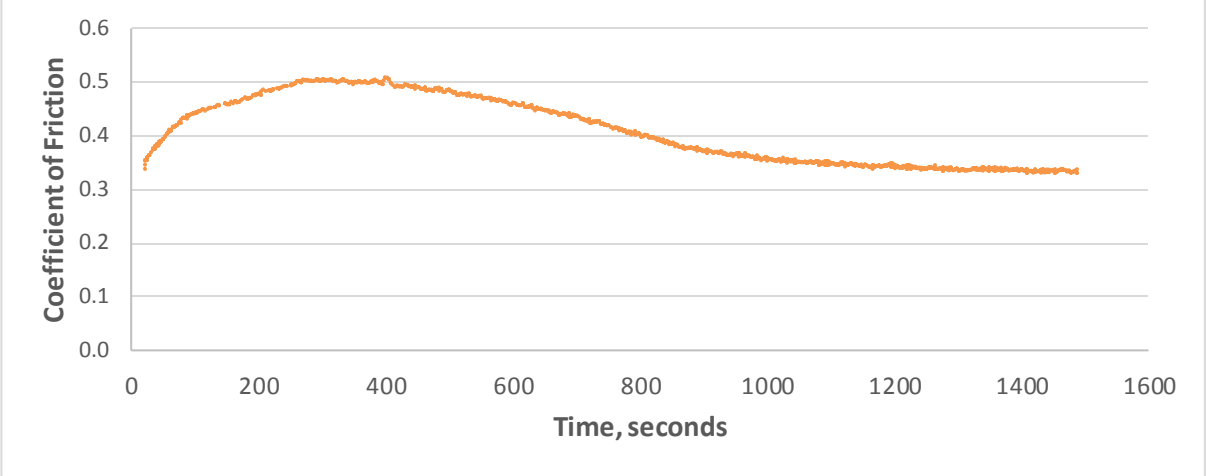

Figure 5-12: Coefficient of Friction-time history plot for GCI brake rotor (90rpm & 10 bar)

5.6.2 Thermal performance

Figure 5-13 shows the temperature-time history plot for Test 7. Test 7 was repeated three times. The results showed good consistency which gave confidence in the repeatability of the results. The maximum temperature reached during the test was around 280℃. Although, temperatures were measured at both trailing and leading edges of the brake rotor but only temperatures measured at trailing edge are shown as difference in temperature is negligible. Also, the temperature was measured only on outboard rotor rubbing surface. Due to space constraints, it was not possible to use thermocouples on inboard.

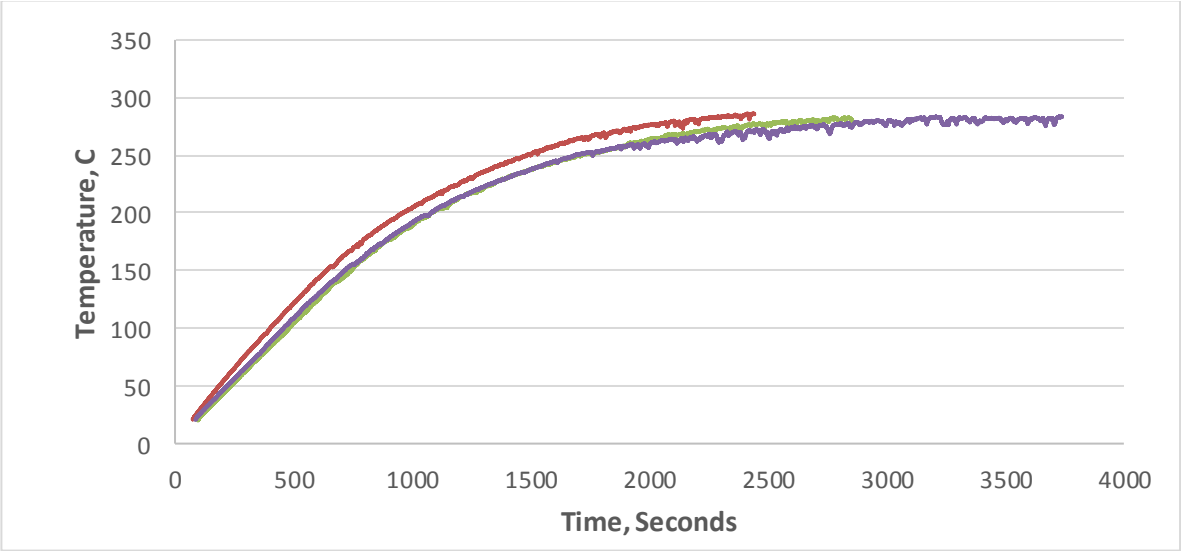

Figure 5-13: Test 7

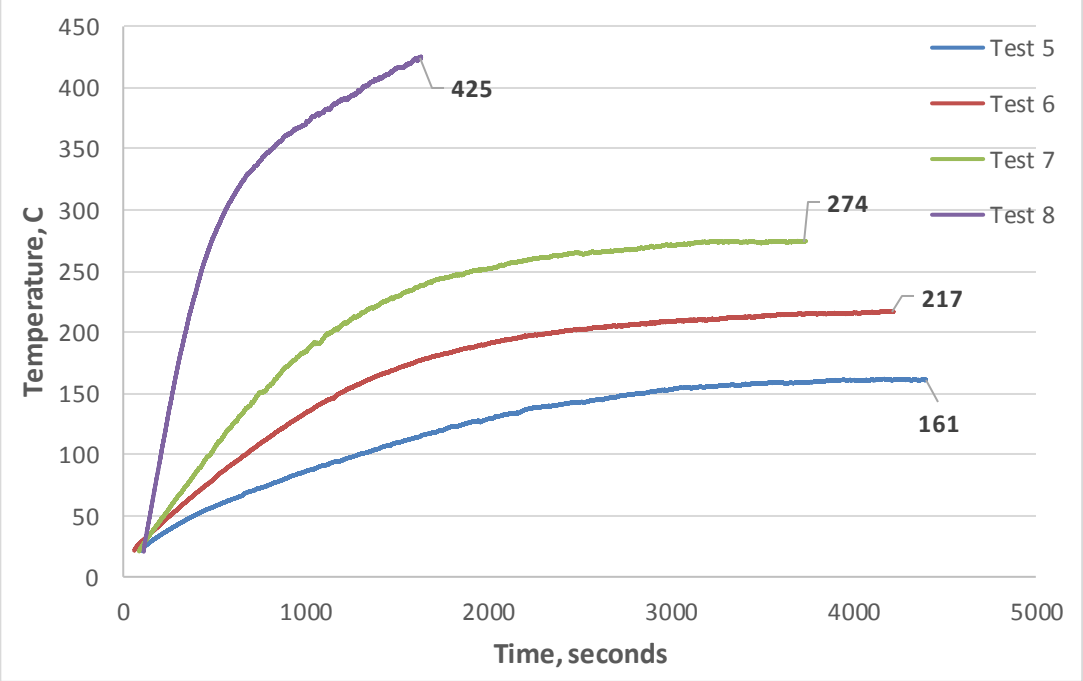

Figure 5-14: Temperature-time history plot for Test 5, Test 6, Test 7 and Test 8

Figure 5-14 shows a comparison of temperature rise with time for the PEO coated rotor for the different tests as defined in Table 5-1.

It was observed that the difference in the maximum temperatures at steady state condition for all the tests were quite consistent. Test 8 could not be completed to a steady state temperature due to safety concerns. The brake power during Test 8 was six times more than that of Test 5. The difference in maximum temperature at stable condition was almost constant between Test 5 and Test 6 and between Test 6 and Test 7 at around 55 to 60 C. Therefore, it was predicted that maximum temperature for Test 8 could reached 500℃ if wasn't stopped.

Figure 5-15 shows the relationship between coefficient of friction and temperature for Test 5, Test 6 and Test 7. The coefficient of friction increased with the increase in temperature until the temperature reached about 150℃ for all tests. After 150℃, the coefficient of friction attained a stable value of around 0.5. There was very little indication of thermal fade in these tests.

Figure 5-16 shows the variation in coefficient of friction of GCI rotor with the rise in temperature during Test 9. It can be seen that there is an appreciable decrease in coefficient of friction after 180℃. Also, the maximum temperature attained by the GCI disc was nearly 270℃ at steady state condition. The steady state

condition was reached in 1200 sec which is far less than the steady state condition obtained with tests conducted with PEO coated aluminium discs. But this is not comparable as solid disc was used for testing GCI disc.

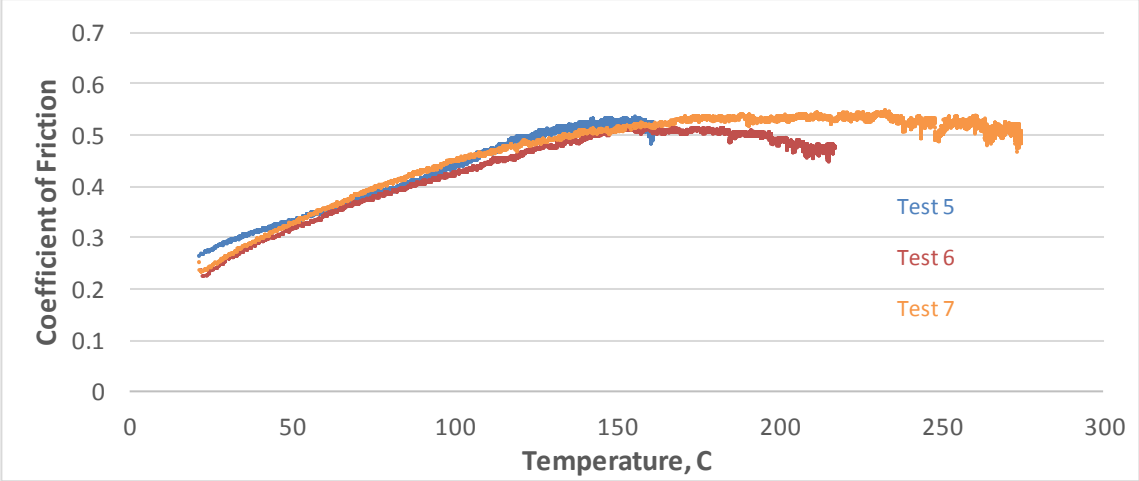

Figure 5-15: Relationship between CoF and rubbing surface temperature for coated rotor tests

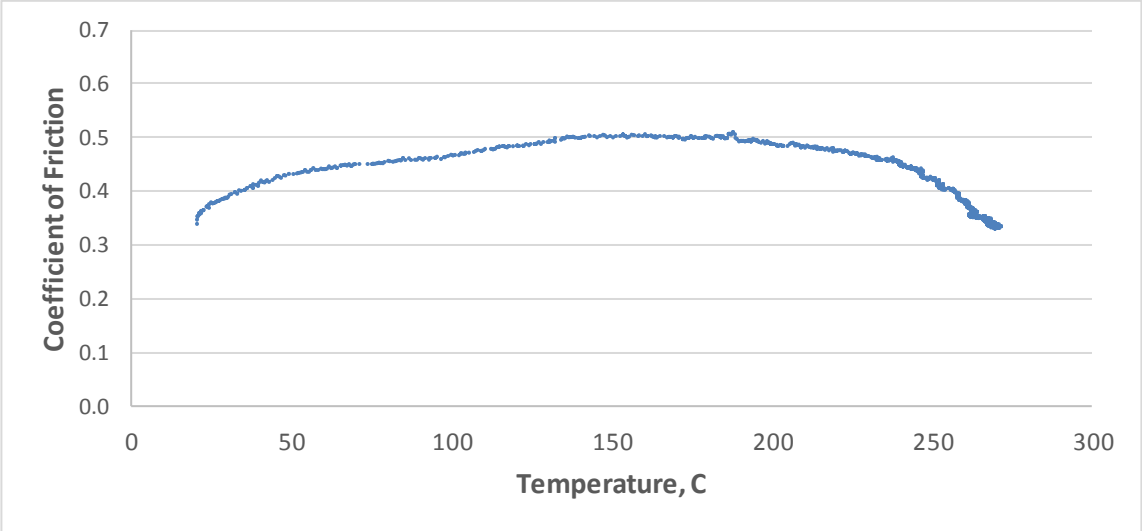

Figure 5-16: Relationship between CoF and rubbing surface temperature for GCI rotor (Test 9)

5.7 Numerical results

The thermal performance of the full scale coated ventilated disc brake was investigated using a 3D finite element heat transfer model developed in Abaqus/CAE 6.14-1 as explained in Chapter 4.

The following assumptions were used for the simulation:

1. It was observed from the experimental results that the coefficient of friction at the start of all of the tests was around 0.25 and this gradually increases to a stable value of around 0.5. All tests followed almost the same trend for the coefficient of friction and the only difference was the time taken during each test to reach the stable value of 0.5. The higher the brake power applied, the sooner the coefficient of friction value reached a stable value. Therefore, the heat flux applied to the rubbing surface in the FE model was determined based on the idealised variation of coefficient of friction for Test 7 as shown in Figure 5-17 for Test 7. It can be seen that idealised coefficient of friction varies linearly from 0.25 to .50 for the first 1000 seconds of the drag brake duration and then stays at a constant value of 0.5 until the end of the braking application.

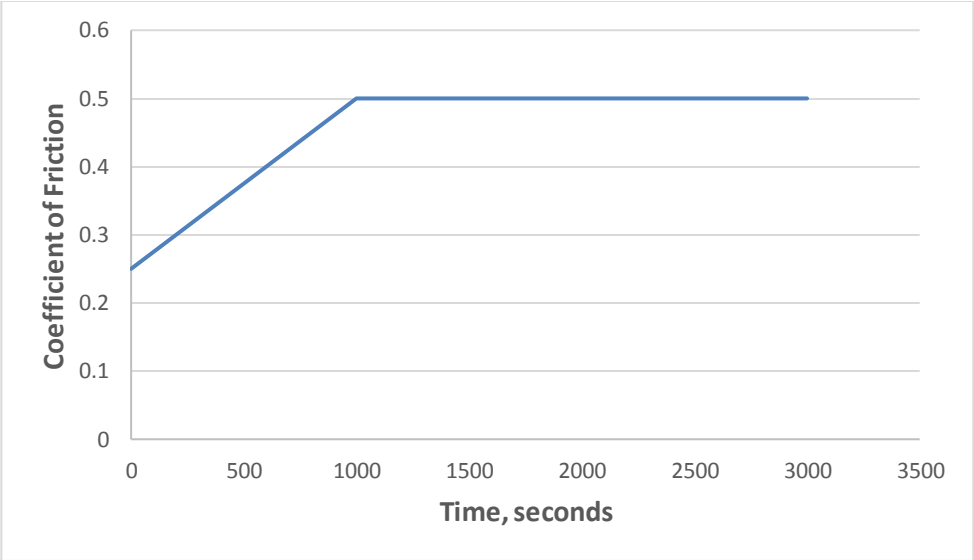

Figure 5-17: Assumed variation in CoF with braking time for FE simulations

2. The total rate of heat generation during the drag application was calculated from Equation 5.1. However, only a certain amount of this heat is transferred to the brake rotor and the rest transferred to the brake pad material. A typical

heat partitioning factor of 0.90 to 0.95 has been used by different researchers. In the current research, it was observed that a partitioning ratio of 0.93 gives a good agreement with the experimental results. Hence the heat flux to be applied on each rubbing surface is given by equation (5.2):

$$Total\ rate\ of\ heat\ generation, \quad Q_T = T.w = \left(2\mu P A_{piston} R_{eff}\right).2\pi N/60 \quad \text{…. ……..……..……} \quad (5.1)$$

$$Heat\ flux\ per\ unit\ rubbing\ surface,\ q_{RS} = \frac{0.93 Q_T}{A_{total\ rubbing\ surface}} \quad \text{……...…….. } (5.2)$$

where,

T	= Brake torque, Nm
ω	= rotational speed, rad/s
A_{piston}	= area of piston, m^2 = 0.001267m^2
R_{eff}	= effective mean rubbing radius = 0.105m
P	$=$ hydraulic pressure, MPa
N	= rotational speed, rpm
$A_{total\ rubbing\ surface}$	= total area of disc rubbing surfaces = 0.048 m^2
μ	= coefficient of friction

Figure 5-18 shows the resulting heat flux applied to the rubbing surfaces of the model to replicate the experiment performed with parameters for Test 7 as shown in Table 5-1. Similar calculations were performed for tests 5 and 6.

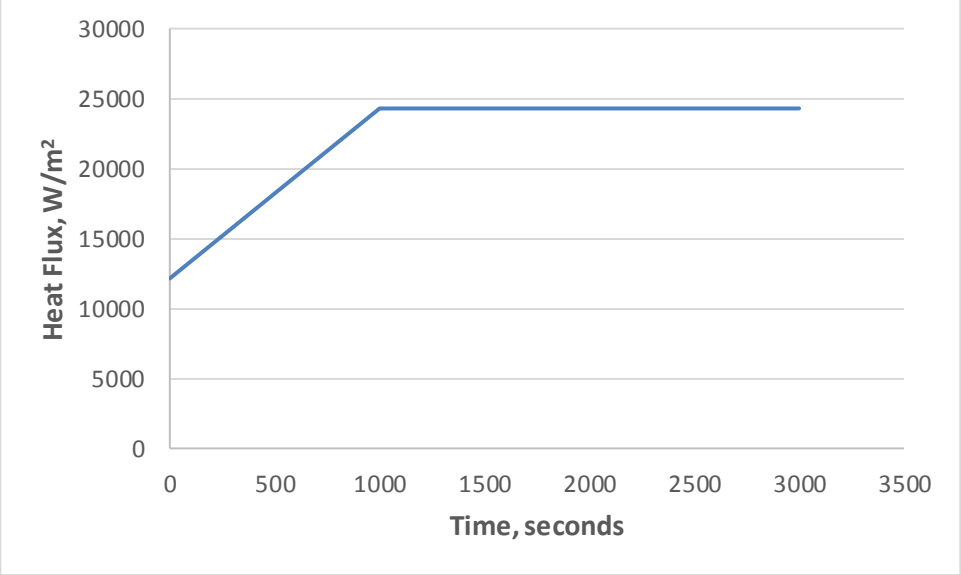

Figure 5-18: Heat flux applied to the FE simulation of Test 7

The numerical results were compared with the experimental results for the different values of convective heat transfer coefficient defined in chapter 4. Each test condition for PEO coated disc in Table 5-1 was simulated for various values of convective heat transfer coefficient. Figure 5-19, Figure 5-20 and Figure 5-21 show the temperature profile of both the experimental and numerical results with respect to time for Test 5, 6 and 7 as defined in Table 5-1. These results shows generally good agreement between the experimental and FE model results for a convective heat transfer coefficient of 30 W/m^2K. Hence the validated FE model can be used for future parametric studies.

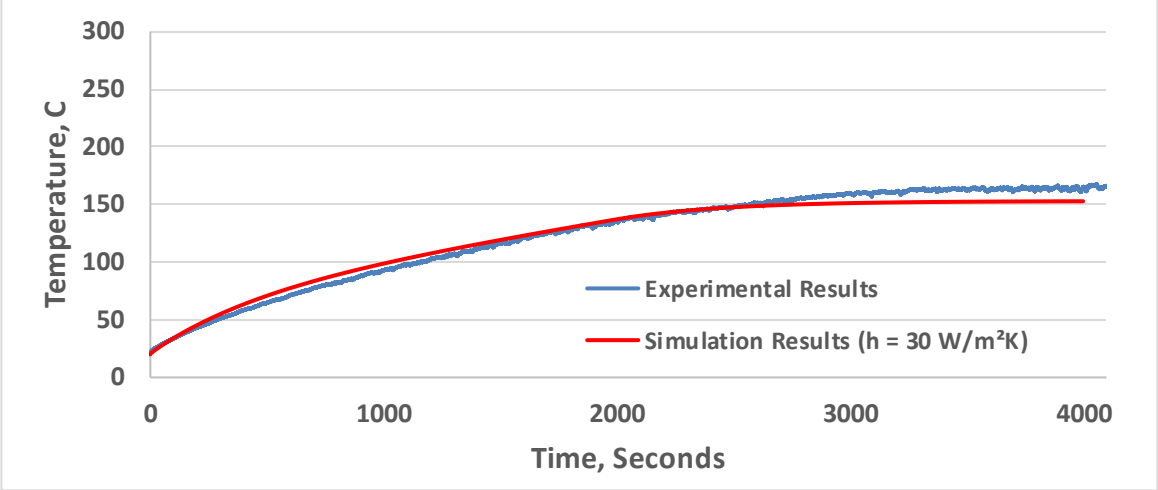

Figure 5-19: Experimental and simulation rubbing surface temperatures for brake test 5 (05 bars & 90 rpm)

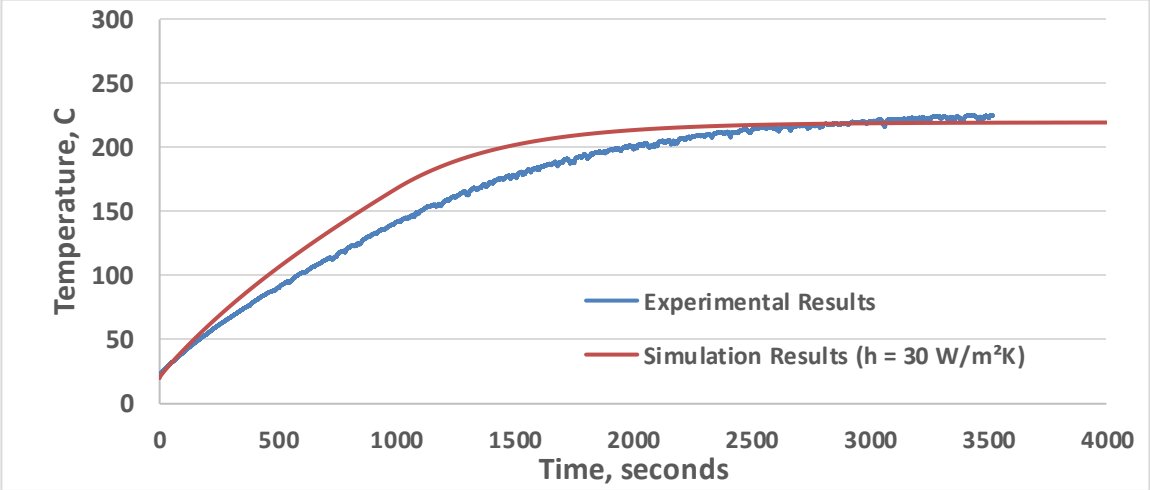

Figure 5-20: Experimental and simulation rubbing surface temperatures for brake test 6 (7.5 bars & 90 rpm)

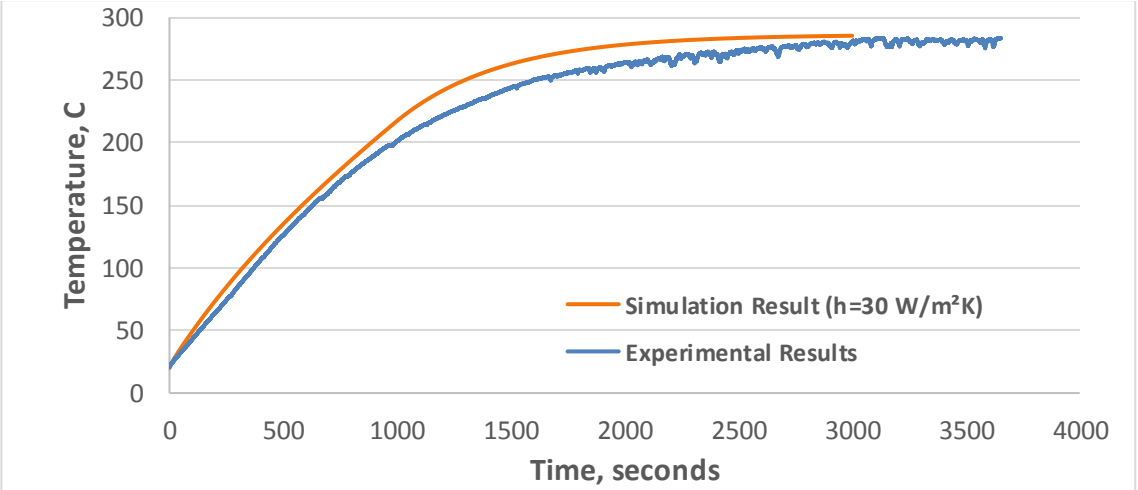

Figure 5-21: Experimental and simulation rubbing surface temperatures for brake test 7 (10 bars & 90 rpm)

5.8 Summary

In this chapter, the experimental procedures and results for investigating the thermal performance of a novel lightweight PEO coated ventilated aluminium alloy brake rotor have been described. A drag brake test matrix was developed according to the SAE standards. The tests were conducted at different hydraulic pressures applied to the pads and rotational speeds of the brake rotor. It was observed that the coefficient of friction was initially quite low in each test but attained a stable value once the disc surface temperature reached at about 150℃. The average coefficient of friction for coated rotor was found to be about 0.5 under these steady state. The thermal performance of the coated disc was also studied using a brake rotor FE model of the coated rotor. The analysis was carried out on Abaqus software and a good agreement between the experimental and simulation results was found. For a convective heat transfer coefficient of 30 W/m^2K applied to all the free surfaces of the rotor.

Chapter 6

Discussion

6.1 Introduction

One of the primary goals of present day researcher into automotive engineering is to maximise the fuel economy of the vehicles and lower its emissions. Over the years, steel and cast iron has been used in automobile industry as the primary material in manufacturing due to its low cost, ease of manufacture and higher strength. The advancement of industrial technology and manufacturing processes in the 21st century has opened up a new horizon to use lightweight materials. This thesis has investigated the potential of using a lightweight aluminium alloy with a PEO coating on the rubbing surface as an alternative material to a conventional cast iron disc.

The main objective of this chapter is to discuss the key findings and to analyse the possible significance of the findings which were presented in the previous chapters of the thesis.

6.1.1 Importance of friction and wear rate of a disc brake

Friction plays a vital role in slowing down a vehicle. Therefore, it is very important that the lightweight coated aluminium alloy brake rotor exhibits the same or even better friction performance than that associated with conventional grey cast iron brake rotors. Pin-on-disc testing was used to evaluate the sliding behaviour of the friction material over the small coated aluminium alloy disc under different sliding parameters as discussed in Chapter 3. The coefficient of friction for the coated disc from pin-on-disc tests was of the order of 0.6 whereas the coefficient of friction for grey cast iron using the same friction material was of the order of 0.5. These values of coefficient of friction were recorded during steady state sliding conditions. It was noticed from the results of the pin-on-disc tests that there is a variation in coefficient of friction for both the coated aluminium alloy brake discs

and the grey cast iron brake discs when the test repeated under the same conditions. This is due to the fact that frictional material pins used in the pin-on-disc tests were only 5mm in diameter. The friction material is a composite material therefore each disc may have been exposed to slightly different combination of composition of friction material at the small sliding interface during each pin-on-disc test.

Both disc and pad undergo wear during braking. The wear rate affects the lifespan of both disc and pad and more importantly the wear particle become airborne causing environmental issues. In current research, the wear rate were determined and compared for both PEO coated aluminium alloy and grey cast iron surfaces using pin-on-disc testing. The same friction material was used with both types of the disc material. Each disc and friction material were weighed before and after each test. The test were performed for two contact pressures (0.5 & 1.0 MPa and a student T-test was carried out to determine the effect of different contact pressures. It was found that there was no significant change in the specific wear rate at the two contact pressures. However, the grey cast iron disc wore significantly more when compared to the coated aluminium alloy disc. This indicates an increase in the lifespan of the coated aluminium brake rotor as shown in Figure 3-27. The grey cast iron rotor wore more than its partnering friction material and for the PEO coated aluminium disc, the friction material wore less when compared to coated disc. This shows the higher hardness of the coated disc surface in comparison to that of the grey cast iron disc.

The relationship between the coefficient of friction and the wear rate was also explored. It was observed that the higher the coefficient of friction, generally gives the higher wear rate of the grey cast iron disc and friction material. In the case of the coated disc, the wear rate of the friction material increases with increase in coefficient of friction but the effect of coefficient of friction on the wear rate of the coated disc was found to be relatively insignificant.

The lifespan of PEO coated aluminium alloy rotor depends on the wear rate of the coating. The specific wear rate of PEO coated disc measured from pin-on-disc test were used to find out lifespan of coating as shown in Table 6-1. The above values are based on a PEO coating thickness of 50 µm. Although the

variation in coating thickness has no effect on the thermal performance of the brake rotor, this greatly affects the lifespan of the rotor even though the wear rate is very less as compared to conventional GCI rotors. A 50µm of coating would completely erode away in 1325 km of braking for a contact pressure of 0.2 and rotational speed of 90 rpm. To increase the braking distance, thickness should be increased. There is a need to find the equivalent coating thickness that could give the same lifespan comparable to GCI rotor.

Mean hydraulic Pressure (bar)	5	7.5	10
Mean contact Pressure (MPa)	0.2	0.3	0.4
Mean sliding speed (rpm)	90	90	270
Lifespan of 50 µm coating (hours)	372	248	62
Braking distance (km) before 50 µm coating completely wears out	1325	884	662

Table 6-1: Lifespan of PEO coated brake rotor

6.1.2 Experimental and numerical analysis of the PEO coated aluminium alloy disc

The use of lightweight aluminium alloy materials in the braking system, for reducing the fuel consumption of a passenger car and cutting down the non-exhaust emissions, is a great challenge. To address this challenge, an experimental and numerical analysis was carried out for a light weight PEO coated aluminium alloy to investigate its thermal and tribological performance. An extensive literature review was carried out to identify the key factors for the design of a prototype of a full scale aluminium alloy brake rotor. It was found that the use of aluminium alloys in braking system is limited due to their low surface hardness and relatively low maximum operating temperature. In order to overcome the

limitations of the aluminium alloy, a prototype lightweight brake rotor was designed to be a ventilated rotor to keep the temperature below the maximum operating temperature and secondly, the alumina coating was generated over the brake rubbing surface to offer a higher wear resistance due to the increase in surface hardness. The prototype consisted of three components as discussed in Chapter 4. The advantage of three components especially for the laboratory testing is that the inner ring can be manufactured separately with a different vane configuration for comparison purpose. Straight radial vanes were used in the current research but, in the future, more complex vane configurations could be readily incorporated in the prototype.

A moderately onerous drag brake test matrix was developed and recognises the limitations of the dynamometer and safety protocols in the laboratory. It was not possible with the current dynamometer set-up to simulate constant g brake applications. Also, due to inadequate ventilation of the laboratory, the maximum temperature was limited to 300℃. However, under strict supervision, a few tests were run until the temperature reached 425℃; the brake rotor remained intact and no failure of the rotor was observed. Overall, the lightweight PEO coated demonstrated good thermal performance. The coating showed a good adhesion with substrate (aluminium alloy) and remained intact during all tests.

A three dimensional thermal finite element model was developed using Abaqus. Due to symmetry and to save computational time, only a section of the rotor model was used to investigate the thermal performance of the coated disc brake. Satisfactory agreement between experimental and numerical results were obtained using a convective heat transfer coefficient of 30 W/m^2K. Different coating thicknesses were employed in the model and no significant change in substrate temperature was observed as shown in Figure 4-15. Therefore, the optimum value of thickness could possibly be obtained by considering the cost of manufacturing the PEO coated brake disc rather than its thermal performance. Also, any small reduction in coating thickness due to wear over the life of the rotor should not cause safety concerns.

6.1.3 Impact of current research on industry

As previously stated, European OEMs are looking for more cost effective and light weight cars to compete with the global automobile producers in order to achieve global emissions standards and low fuel consumption (GALM Europe, 2018).

The potential of using the lightweight PEO coated ventilated aluminium alloy disc brake as an alternative to conventional grey iron disc brake is apparent from the results of this current research. Both thermal and tribological performances of the coated rotor are very promising. The main concerns with the PEO coating is the slow growth rate of the oxide layer and the relatively high manufacturing costs involved in the process (Matykina et al., 2017). In the current research, only the brake rubbing surfaces were coated. This was done partly to reduce the cost of coating but also, to use the higher thermal conductivity of the substrate to allow heat to be conducted to non-coated surfaces in order to achieve rapid cooling of the rubbing surfaces and also to limit the build-up of temperature with in the substrate.

Furthermore, this current research has contributed towards further strengthening the relationship between the University of Leeds and Kernoite International in the field of PEO coating. This research has also enhanced the partnership between the University of Leeds and TMD Friction and lead to the development of new types of friction material including the use of copper free pads to run against the PEO surface and to reduce the release of harmful wear debris into the environment.

Chapter 7

Conclusions and Future work

7.1 Conclusions

Thermal and tribological performance of a lightweight ventilated aluminium alloy (Al-6082) brake disc with an alumina coating applied using a plasma electrolytic oxidation coating process have been investigated. Such a disc could be a viable option in order to reduce the upsprung mass of the vehicle. This would also lead to better fuel economy and lower wear particle emissions from the friction brake. The performance of the coated aluminium disc was compared with the performance of a conventional grey cast iron disc brake for both small scale pin-on-disc testing and on a full scale dynamometer.

The research findings can be summarised as follows:

- The coefficient of friction prevailing between the PEO coated brake disc and the brake pad material during pin-on-disc testing was found to be higher at about 0.6 as compared to the conventional grey cast iron (μ = 0.5). Also, the coefficient of friction for full scale PEO coated brake disc was found to be around 0.5 on the dynamometer testing.
- At higher temperatures during braking, the change in coefficient of friction was observed to be uniform and stable for the coated aluminium disc. Moreover, the effect of thermal fade was not significant up to a temperature of 300℃.
- A three dimensional finite element model were developed and the experimental results were used to optimise the convective heat transfer coefficient specified in the model. The good agreement between the model and experimental results gave the confidence to use the model to further investigate the thermal performance of the lightweight coated disc brake.
- The model was used to show numerically that the substrate temperature was not affected greatly by the thickness of the coating. This is an

important finding because the actual thickness of the coating may vary due to manufacturing variabilities and also wear during the service life of the disc.

- The wear rate of the coated disc brake surface in pin-on-disc testing was found to be significantly lower around 15 times than that for the conventional grey cast disc brake surface under the same conditions. This suggests a much higher service life for the lightweight coated disc brake. Also, the wear rate of the custom friction material was 5 times lower when run against the PEO coating than when the same friction material was run against the cast iron.

Therefore, the main significance of this research is in demonstrating both experimentally and numerically the thermal performance of a full scale PEO coated lightweight aluminium alloy disc brake. The good agreement between the dynamometer testing and numerical results and the outcome of the pin-on-disc study of tribology characteristics presented in the thesis give a wide range of information for the automotive braking industry to seriously consider the potential of using lightweight disc brake rotors.

7.2 Future work

The recommendations for further improving the current research work are discussed below:

- Further experiment should be done using the brake dynamometer for harsh braking conditions (including repeated constant g stops) to study the PEO coated brake rotor response at more elevated temperatures.
- Further studies should be carried out using a validated three dimension finite element model to optimise rotor parameters such as cheek thickness, coating thickness and number of vanes and vane configuration.

- Corrosion studies should be carried out for onerous conditions such as salt water and compared with the results for conventional grey cast iron disc brake.
- Different vane configuration should be investigated in order to improve the heat dissipation from the disc brake by convection. The advantage of the prototype ventilated disc used in the current study is that instead of manufacturing the whole brake rotor, only the inner ring (see section 4.2.3) needs to be manufactured with different vane configurations.
- Although the current research has shown the potential benefits of the using coated aluminium disc in terms of less non-exhaust vehicle emissions, further studies are required to quantify the different size and nature of particulate matter emitted during braking from the PEO coated disc-friction pair.

References

ADEBISI, A. A., M. A. MALEQUE and M. M. RAHMAN. 2011. Metal matrix composite brake rotor: Historical development and product life cycle analysis. *International Journal of Automotive and Mechanical Engineering (IJAME),* Volume 4, pp.471-480.

AHMAD, F., S. H. J. LO, M. ASLAM and A. HAZIQ. 2013. *Tribology Behaviour of Alumina Particles Reinforced Aluminium Matrix Composites and Brake Disc Materials*. *Procedia Engineering.*

ALNAQI, A., S. SHRESTHA, P. BROOKS and D. BARTON. 2014. Thermal Performance Of Peo Coated Lightweight Brake Rotors Compared With Grey Cast Iron. *In: EuroBrake 2014,* Lille, France. FISITA (UK) Limited.

ALNAQI, A. A., KOSARIEH, SHAHRIAR, BARTON, DAVID C., BROOKS, PETER C., and S. SHRESTHA. 2016. Material characterisation of lightweight disc brake rotors. *Proceedings of the Institution of Mechanical Engineers, Part L: Journal of Materials Design and Applications*.

Band Brakes. 2004. *Clutches and Brakes.* CRC Press.

BARTON, D. C. 2012. Materials Design for Disc Brakes. *In:* A. J. DAY, J. KLAPS and C. F. ROSS, eds. *Braking of Road Vehicles 2012.* 2012 ed. Bradford, UK: University of Bradford, pp.p193-205.

BATAKIS, A. P. and J. W. VOGAN. 1985. NASA Contract Report 1750222. *Rocket thrust chamber thermal barrier coatings*.

BELHOCINE, A. and M. BOUCHETARA. 2011. Thermal Behavior of Dry Contacts in the Brake Discs.

BLAU, P. J., B. C. JOLLY, J. QU, W. H. PETER and C. A. BLUE. 2007. Tribological investigation of titanium-based materials for brakes. *Wear,* **263**(7–12), pp.1202-1211.

BUDYNAS, R. G., R. G. BUDYNAS and J. K. NISBETT. 2015. *Shigley's Mechanical Engineering Design.* McGraw-Hill Education.

CHAN, D. and G. STACHOWIAK. 2004. Review of automotive brake friction materials. *Proceedings of the Institution of Mechanical Engineers, Part D: Journal of Automobile Engineering,* **218**(9), pp.953-966.

CHANDRA VERMA, P., L. MENAPACE, A. BONFANTI, R. CIUDIN, S. GIALANELLA and G. STRAFFELINI. 2015. Braking pad-disc system: Wear mechanisms and formation of wear fragments. *Wear,* **322-323**, pp.251-258.

CHI, Z. 2008. *Thermal Performance Analysis and Geometrical Optimization of Automotive Brake Rotors* Master of Applied Sciences thesis, University of Ontario Institute of Technology , Canada.

CHILDS, P. R. N. 2014. *Mechanical Design Engineering Handbook.* Elsevier.

CUEVA, G., A. SINATORA, W. L. GUESSER and A. P. TSCHIPTSCHIN. 2003a. Wear resistance of cast irons used in brake disc rotors. *Wear,* **255**(7–12), pp.1256-1260.

CUEVA, G., A. SINATORA, W. L. GUESSER and A. P. TSCHIPTSCHIN. 2003b. Wear resistance of cast irons used in brake disc rotors. *Wear,* 255(7), pp.1256-1260.

CUI, S., J. HAN, Y. DU and W. LI. 2007. Corrosion resistance and wear resistance of plasma electrolytic oxidation coatings on metal matrix composites. *Surface and Coatings Technology,* **201**(9–11), pp.5306-5309.

CURRAN, J. A. and T. W. CLYNE. 2005. The thermal conductivity of plasma electrolytic oxide coatings on aluminium and magnesium. *Surface and Coatings Technology,* 199(2), pp.177-183.

CURRY, E. 2012. Design, Installation and Production of Brake Rotors. *In:* A. J. DAY, J. KLAPS and C. F. ROSS, eds. *Braking of Road Vehicles.* Bradford, UK: University of Bradford, .

DAHM, K. L., A. J. BLACK, S. SHRESTHA and P. A. DEARNLEY. 2009. Plasma Electrolytic Oxidation treatment of aluminium alloys for lightweight disc brake rotors, York (UK)

DAY, A., M. TIROVIC and T. NEWCOMB. 1991. Thermal effects and pressure distributions in brakes. *Proceedings of the Institution of Mechanical Engineers, Part D: Journal of Automobile Engineering,* 205(3), pp.199-205.

DECC. 2014. *Department of energy and climate change, 2012 UK Greenhouse Gas Emissions, Final Figures*

DEMIR, A., R. SAMUR and I. KILICASLAN. 2009. Investigation of the coatings applied onto brake discs on disc-brake pad pair. *Metalurgija*.

ENCYCLOPÆDIA. 2014. *Friction Brake* [online]. [Accessed]. Available from: http://kids.britannica.com/comptons/article-9273329/brake.

ERIKSSON, M., F. BERGMAN and S. JACOBSON. 1999. Surface characterisation of brake pads after running under silent and squealing conditions. *Wear,* 232(2), pp.163-167.

GREAT BRITAIN. 2009. *Regulation (EC) No 443/2009 of the European Parliament and of the Council of 23 April 2009 setting emission performance standards for new passenger cars as part of the Community's integrated*

approach to reduce CO 2 emissions from light-duty vehicles. Official Journal of the European Union.

GREAT BRITAIN. 2014. *Amending Regulation (EC) No 443/2009 to define the modalities for reaching the 2020 target to reduce CO2 emissions from new passenger cars*. Official Journal of the European Union.

FARAG, M. M. 2006. *Chapter 14: Quantitative Methods of Materials Selection in Mechanical Engineers' Handbook: Materials and Mechanical Design.* 3rd ed.

GALM Europe. *7th Annual Global Automotive Lightweight Materials Europe 2018* [online]. [Accessed]. Available from: http://www.global-automotive-lightweight-materials-europe.com/.

GÉRARD, B. 2006. Application of thermal spraying in the automobile industry. *Surface and Coatings Technology,* 201(5), pp.2028-2031.

GRIEVE, D., D. BARTON, D. CROLLA and J. BUCKINGHAM. 1998. Design of a lightweight automotive brake disc using finite element and Taguchi techniques. *Proceedings of the Institution of Mechanical Engineers, Part D: Journal of Automobile Engineering,* 212(4), pp.245-254.

HALDERMAN, J. D. and C. D. J. MITCHELL. 2000. *Automotive Brake Systems.* 2nd ed. Upper Saddle River, New Jersey: Prentice-Hall.

HARA, Y., M. INOUE, T. MIBE, H. NAKANISHI and T. OYAMA. 2003. *Non-asbestos disc brake pad for automobiles*. Patent number: EP0959262 B1.

HASSAN, M. Z., P. C. BROOKS and D. C. BARTON. 2013. The evaluation of disc brake squeal propensity through a fully coupled transient thermomechanical model. *Proceedings of the Institution of Mechanical Engineers, Part D: Journal of Automobile Engineering,* 227(3), pp.361-375.

HENDRICKSON, S. A. B., GERRY. 2001. *Hot Rodder's Bible : The Ultimate Guide to Building Your Dream Machine.* MBI Publishing Company, USA.

HTTP://WWW.LOCARSOS.COM/. 2013. [online]. [Accessed].

HTTPS://WWW.CCG.MSM.CAM.AC.UK/RESEARCH-AREAS/THE-PLASMA-ELECTROLYTIC-OXIDATION-PEO-PROCESS. [online]. [Accessed]. Available from: https://www.ccg.msm.cam.ac.uk/research-areas/the-plasma-electrolytic-oxidation-peo-process.

IOANNIDIS, P., BARTON, D., AND BROOKS, P. 1999. Noise and Vibration Characterisation of Cast Iron and Siliconised Carbon Composite Brake Rotors. *SAE Technical Paper 2005-01-2313*.

JACKO, M. G. 1978. Physical and chemical changes of organic disc pads in service. *Wear,* 46(1), pp.163-175.

JIMBO, Y., T. MIBE, K. AKIYAMA, H. MATSUI, M. YOSHIDA and A. OZAWA. 1990. *Development of high thermal conductivity cast iron for brake disk rotors*. SAE Technical Paper.

KERMC, M., M. KALIN and J. VIŽINTIN. 2005. Development and use of an apparatus for tribological evaluation of ceramic-based brake materials. *Wear,* 259(7–12), pp.1079-1087.

LEE, Y. S., P. C. BROOKS and D. C. BARTON. 2003a. A predictive tool to evaluate disc brake squeal propensity. Part 1: The model philosophy and the contact problem. *International Journal of Vehicle Design,* 31(3), pp.289-307.

LILES, G. D. 1989. *Analysis of disc brake squeal using finite element methods*. SAE Technical Paper.

LIMPERT, R. 1975. The thermal performance of automotive disc brake squeal. *SAE Technical Paper 750873*.

KERONITE INTERNATIONAL LTD, [online]. 2017. [online]. Available from: https://blog.keronite.com/what-is-plasma-electrolytic-oxidation-article.

MATYKINA, E., R. ARRABAL, M. MOHEDANO, B. MINGO, J. GONZALEZ, A. PARDO and M. C. MERINO. 2017. Recent advances in energy efficient PEO processing of aluminium alloys. Transactions of Nonferrous Metals Society of China, 27(7), pp.1439-1454.

MCPHEE, A. D. and D. A. JOHNSON. 2008. Experimental heat transfer and flow analysis of a vented brake rotor. *International Journal of Thermal Sciences,* 47(4), pp.458-467.

NEWCOMB, T. P. 1959. Transient temperatures attained in disk brakes. *Brit. J. Appl. Phys.,* 10, p339.

NEWCOMB, T. P. 1960. Temperatures reached in disc brakes. *J. Mech. Engng Sci,* 2, pp.167-177.

NEWCOMB, T. P. and R. T. SPURR. 1989. *A Technical History Of The Motor Car.* Adam Hilger, New York.

NICHOLSON, G. 1995. *Facts about Friction: A Friction Material Manual Almost All You Need to Know about Manufacturing.* Gedoran.

ORTHWEIN, W. C. 2004. Band Brakes. *Clutches and Brakes.* CRC Press.

OUYANG, H., W. NACK, Y. YUAN and F. CHEN. 2005. Numerical analysis of automotive disc brake squeal: a review. *International Journal of Vehicle Noise and Vibration,* 1(3), pp.207-231.

PAPINNIEMI, A., J. C. S. LAI, J. ZHAO and L. LOADER. 2002. Brake squeal: a literature review. *Applied Acoustics,* 63(4), pp.391-400.

PAWŁOWSKI, L. 2008. *The science and engineering of thermal spray coatings.* Chichester: Wiley.

PEVEC, M., G. ODER, I. POTRČ and M. ŠRAML. 2014. Elevated temperature low cycle fatigue of grey cast iron used for automotive brake discs. *Engineering Failure Analysis,* 42(0), pp.221-230.

QU, J., P. J. BLAU and B. C. JOLLY. 2009. Oxygen-diffused titanium as a candidate brake rotor material. *Wear,* 267(5–8), pp.818-822.

RAJ, K. T. R., R. RAMSAI, J. MATHEW and G. SONIYA. 2014. Numerical investigation of fluid flow and heat transfer characteristics on the aerodynamics of ventilated disc brake rotor using CFD. *Thermal Science,* (00), pp.204-204.

SAE. 2000. *Society of Mechanical Engineers, Brake system dynomometer test procedures-passenger car-SAE J212 JAN98*. SAE Inc., Warrendale, PA.

SANDERS, P. G., T. M. DALKA and R. H. BASCH. 2001. A reduced-scale brake dynamometer for friction characterization. *Tribology International,* 34(9), pp.609-615.

SASAKI, Y., M. YANAGI, Y. TODANI and T. MITA. 2000. *Friction material composition*. Patent number: US6080230 A.

SMMT. 2014. *New Car CO2 Report 2014: The 13th report* [online]. [Accessed]. Available from: http://www.smmt.co.uk/co2report

Talati, F., Jalalifar, S. 2009. Analysis of heat induction in a disk brake system. *Heat and Mass Transfer, 45(8):1047-1059.*

TCDIRECT. *TC for Temperature Sensing, Measurement and Control*. [Accessed 10/12/2017]. Available from: http://www.tc.co.uk/thermocouples/thermocouples.html.

TOLSTOI, D. M. 1967. Significance of the normal degree of freedom and natural normal vibrations in contact friction. *Wear,* 10(3), pp.199-213.

TORRES, B., M. CAMPO, M. LIEBLICH and J. RAMS. 2013. Oxy-acetylene flame thermal sprayed coatings of aluminium matrix composites reinforced with MoSi2 intermetallic particles. *Surface and Coatings Technology,* 236(0), pp.274-283.

WAHLSTRÖM, J., D. GVENTSADZE, L. OLANDER, E. KUTELIA, L. GVENTSADZE, O. TSURTSUMIA and U. OLOFSSON. 2011. A pin-on-disc investigation of novel nanoporous composite-based and conventional brake pad materials focussing on airborne wear particles. *Tribology International,* 44(12), pp.1838-1843.

YANO, M. A. M., M. 1993. Heat Flow on Disc Brakes. *SAE Technical Paper 931084*, pp.119-124.

YEROKHIN, A. L., X. NIE, A. LEYLAND, A. MATTHEWS and S. J. DOWEY. 1999. Plasma electrolysis for surface engineering. *Surface and Coatings Technology,* 122(2–3), pp.73-93.

ZHANG, P., X. NIE and H. HU. 2010. *Wear Protection of Al383/SiO2 Metal Matrix Composites by Plasma Electrolytic Oxidation (PEO) Process*. SAE Technical Paper.